

The University of Manitoba

THE DESIGN OF A
SIMPLE PRIME FOCUS FEED FOR PARABOLOID REFLECTORS
USING GRAPHIC CAD TECHNIQUES

BY

© Michael I. Borgford

A Thesis

Submitted to the Faculty of Graduated Studies
In Partial Fulfillment of the Requirements

For the Degree of Master of Science

DEPARTMENT OF ELECTRICAL ENGINEERING

Winnipeg, Manitoba

Canada

Permission has been granted to the National Library of Canada to microfilm this thesis and to lend or sell copies of the film.

The author (copyright owner) has reserved other publication rights, and neither the thesis nor extensive extracts from it may be printed or otherwise reproduced without his/her written permission.

L'autorisation a été accordée à la Bibliothèque nationale du Canada de microfilmer cette thèse et de prêter ou de vendre des exemplaires du film.

L'auteur (titulaire du droit d'auteur) se réserve les autres droits de publication; ni la thèse ni de longs extraits de celle-ci ne doivent être imprimés ou autrement reproduits sans son autorisation écrite.

ISBN 0-315-42338-2

THE UNIVERSITY OF MANITOBA
FACULTY OF GRADUATE STUDIES

The undersigned certify that they have read, and recommend to
the Faculty of Graduate Studies for acceptance, a Master's thesis
entitled: ..The Design of a Simple Prime Focus Feed for.....
..Paraboloid Reflectors using Graphic CAD Techniques.....
.....
submitted byMichael I. Borgford.....
in partial fulfilment of the requirements for the degree of
Master of Science
.....

L. Shafai
.....

Advisor L. Shafai

.....
M. Barakat
.....

E. Bridges
.....
E. Bridges
.....

M. Barakat
.....

External Examiner

Date ..July 3, 1985.....
.....

Oral Examination is:

Satisfactory

Not Required

[Unless otherwise specified by the major Department, thesis students
must pass an oral examination on the subject of the thesis and matters
relating thereto.]

THE DESIGN OF A SIMPLE PRIME FOCUS FEED FOR PARABOLOID REFLECTORS
USING GRAPHIC CAD TECHNIQUES

BY

MICHAEL IAN BORGFORD

A thesis submitted to the Faculty of Graduate Studies of
the University of Manitoba in partial fulfillment of the requirements
of the degree of

MASTER OF SCIENCE

© 1985

Permission has been granted to the LIBRARY OF THE UNIVER-
SITY OF MANITOBA to lend or sell copies of this thesis, to
the NATIONAL LIBRARY OF CANADA to microfilm this
thesis and to lend or sell copies of the film, and UNIVERSITY
MICROFILMS to publish an abstract of this thesis.

The author reserves other publication rights, and neither the
thesis nor extensive extracts from it may be printed or other-
wise reproduced without the author's written permission.

ABSTRACT

The following thesis presents the design and implementation of the Interactive Graphic Antenna Design Package (IGAD), and describes a paraboloid prime focus feed design example using graphic computing methods. IGAD-ROT2 is a graphic pre and post-processor that was created to merge the ROT2 antenna analysis program with the Calma Corporation's CAD/CAM Computer. It was written in Calma's design analysis language to provide a user oriented interface to an antenna design system. IGAD-ROT2 provides a graphic medium to relieve the menial tasks of computer assisted antenna modelling and design. It enables high precision production drawings to be generated, is useful as a learning device, and provides the database for future antenna CAD development.

Two paraboloid prime focus feeds were designed using the graphic techniques associated with IGAD-ROT2. The design process was initiated with a basic microstrip disk configuration and evolved into a flanged disk antenna geometry. Two flanged disk geometries resulted. Both flanged disk antennas failed to meet the prime focus feed standards established by corrugated horns. Alterations on the disk geometry and modifications

to the flange choke were effected with IGAD-ROT2, and were unable to alter the H-plane field. This restricted the maximum aperture efficiency, maintained high sidelobe levels, and resulted in a low paraboloid aperture angle.

Possible enhancements to the IGAD-ROT2 package are plentiful and should be undertaken upon completion of this paper. Future work must also be implemented on the flanged disk antenna design, it's bandwidth, input impedance, and feed structure to determine the optimum performance, since they are not covered in this thesis.

ACKNOWLEDGEMENTS

Sincere thanks and appreciation are extended to Dr. L. Shafai of the Department of Electrical Engineering, University of Manitoba for his technical guidance, to G. Neilson of the Department of Electrical Engineering, University of Manitoba for his many hours of assistance, and to S. Johnson for her invaluable help and support preparing this document.

TABLE OF CONTENTS

	Page No.
ABSTRACT	i
ACKNOWLEDGEMENTS	iii
TABLE OF CONTENTS	iv
LIST OF FIGURES	vii
LIST OF TABLES	xii
LIST OF VARIABLES	xiii
INTRODUCTION	xiv
CHAPTER I GRAPHIC COMPUTER AIDED ANTENNA DESIGN	1
1.1 CAD/CAM Systems	1
1.1.1 CAD/CAM Equipment	2
1.1.2 Advantages of CAD/CAM	3
1.2 Calma CAD System and the IGAD Package	5
1.3 ROT2	8
CHAPTER II IGAD-ROT2	11
2.1 Introduction	11
2.2 Merging Calma and ROT2	12
2.2.1 Construction Mode	13
2.2.2 Plot Mode	16
2.2.3 Drawing Mode	18
2.3 Connectivity	20
2.4 Submodels	22

	Page No.
CHAPTER III FEED CHARACTERISTICS OF PARABOLOID REFLECTORS	30
3.1 Introduction	30
3.2 Paraboloid Reflector - Feed Relationship	31
3.2.1 Calculation of Paraboloid Reflector Efficiency and Gain Factor	32
3.2.2 Cross-Polarization	35
3.2.3 Summary of Feed Parameters	36
3.3 Development of Paraboloid Reflector Feeds	38
3.4 Microstrip Disk Radiator	42
CHAPTER IV DESIGN OF SIMPLE PRIME FOCUS FEED	51
4.1 Introduction	51
4.2 Initial Geometry	52
4.3 Optimization of Antenna Geometry	54
4.3.1 Disk Scatterer Optimization	56
4.3.2 Flange Optimization	58
4.4 Modification to Flanged Disk Antenna	60
4.4.1 Disk Modifications	60
4.4.2 Choke Modifications	66
4.5 Flanged Disk With Maximized Gain Factor	69
4.6 Modifying the Feed Structure	70
4.7 Summary of Geometry Modifications	72
CHAPTER V CONCLUDING REMARKS AND FUTURE ENHANCEMENTS	101
5.1 IGAD-ROT2	101
5.2 Disk Antenna	103

	Page No
REFERENCES	107
APPENDIX A The GE Engineering System	108
APPENDIX B List of IGAD-ROT2 Subroutines	109
APPENDIX C Calculation of Paraboloid Efficiencies	114

LIST OF FIGURES

	Page No.
CHAPTER I	
Figure 1 - ROT2 Program Structure	10
CHAPTER II	
Figure 1 - IGAD-ROT2 Program Structure	24
Figure 2a - Construction Screen Layout and Menu	25
Figure 2b - Plot Screen Layout and Menu	26
Figure 2c - Drawing Screen Layout and Menu	27
Figure 3 - The Method Used to Create Multiple Contour Geometries Illustrated with a Circular Metal Ground Plane	28
Figure 4 - The Method Used to Insert Contours Illustrated with a Circular Metal Ground Plane	29
CHAPTER III	
Figure 1 - Geometry of a Paraboloid Reflector	44
Figure 2a - Optimum Illumination Feed Pattern	45
Figure 2b - Relative Field Intensity of Optimum Illumination at Paraboloid Rim for Differing Feed Pattern Numbers	45
Figure 3 - Polarization Characteristics of Reflector Antennas	46
Figure 4 - Superimposed Magnetic and Electric Aperture Fields Produce Huygen's Source with Linear Polarization	46
Figure 5 - The Dual Mode Conical Horn and Radiation Characteristics	47

	Page No.
Figure 6 - The Scalar Horn and Corrugated Feed	47
Figure 7a - Rotationally Symmetric Trapezoidally Corrugated Horn	48
Figure 7b - Rotationally Symmetric Sinusoidally Corrugated Horn	48
Figure 8 - Microstrip Disk Geometry	49
Figure 9 - Comparison of First Order Mode Approximation with an Ideal Feed and a Good Feed	50
 CHAPTER IV	
Figure 1 - Disk Antenna Modelled using IGAD-ROT2	73
Figure 2 - Radiation and Efficiency characteristics of Disk Antenna (Refer to Figure IV-1)	74
Figure 3 - Optimization Variables for Disk Antennas	75
Figure 4 - Optimization Program Structure	76
Figure 5a - Constrained Optimization of Non-Flanged Disk Antenna Cross-Polarization < -20 dB, Disk Height > 0.1	77
Figure 5b - Constrained Optimization of Non-Flanged Disk Antenna Radiation and Efficiency Characteristics Cross-Polarization < -20 dB, Disk Height > 0.1	78
Figure 6a - Constrained Optimization of Non-Flanged Disk Antenna Cross-Polarization < -20 dB, Disk Radius > 0.25 , Disk Height > 0.1	79

	Page No.
Figure 6b - Constrained Optimization of Non-Flanged Disk Antenna Radiation and Efficiency Characteristics Cross-Polarization ≤ -20 dB, Disk Radius > 0.25 , Disk Height > 0.1	80
Figure 7a - Constrained Optimization of Flanged Disk Antenna Cross-Polarization ≤ -20 dB, Disk Radius > 0.25 , Disk Height > 0.1	81
Figure 7b - Constrained Optimization of Flanged Disk Antenna Radiation and Efficiency Characteristics Cross-Polarization ≤ -20 dB, Disk Radius > 0.25 , Disk Height > 0.1	82
Figure 8a - Conic Disk Antenna Radiation Characteristics Peak Directed Away From Ground Plane	83
Figure 8b - Conic Disk Antenna Radiation Characteristics Peak Directed Away From Ground Plane (Refer to Figure IV-8a)	84
Figure 8c - Conic Disk Antenna Radiation Characteristics Peak Directed Away From Ground Plane (Refer to Figure IV-8a)	85
Figure 9a - Conic Disk Antenna Radiation Characteristics Peak Directed Towards Ground Plane	86
Figure 9b - Conic Disk Antenna Radiation Characteristics Peak Directed Towards Ground Plane (Refer to Figure IV-9a)	87
Figure 9c - Conic Disk Antenna Radiation Characteristics Peak Directed Towards Ground Plane (Refer to Figure IV-9a)	88

	Page No.
Figure 10a - Disk Antenna with External Post Radiation Characteristics	89
Figure 10b - Disk Antenna with External Post Radiation Characteristics (Refer to Figure IV-10a)	90
Figure 10c - Disk Antenna with External Post Radiation Characteristics (Refer to Figure IV-10a)	91
Figure 11 - Modification Parameters for the Normal and External Choke Types	92
Figure 12a - Constrained Optimization of the Flanged Disk Antenna Flange Length \leq 1.0, Disk Radius $>$ 0.25, Disk Length \leq 0.1	93
Figure 12b - Constrained Optimization of the Flanged Disk Antenna Radiation and Efficiency Characteristics Flange Length 1.0, Disk Radius $>$ 0.25, Disk Length $>$ 0.1	94
Figure 13b - Flanged Disk Antenna with External Post	95
Figure 13b - Flanged Disk Antenna with External Post Radiation and Efficiency Characteristics (Refer to Figure IV-13a)	96
Figure 14a - Single Dipole Fed Flanged Disk Antenna	97
Figure 14b - Single Dipole Fed Flanged Disk Antenna Radiation and Efficiency Characteristics (Refer to Figure IV-14a)	98

	Page No.
Figure 15a - Single Dipole Fed Flanged Disk Antenna with External Post	99
Figure 15a - Single Dipole Fed Flanged Disk Antenna with External Post Radiation and Efficiency Characteristics (Refer to Figure IV-15a)	100
Appendix A - The General Electric Engineering System	109

LIST OF TABLES

	Page No.
TABLE I - Conic Scatter Modification Results Conic point Directed Away From the Ground Plane	64
TABLE II - Conic Scatter Modification Results Conic peak is directed towards the ground plane	64
TABLE III - Disk Scatterer with External Post Modification Results	65
TABLE IV - Flange Rim Choke Wall Modification Results	67
TABLE V - Flange Rim Choke Slit Width Modification Results	67
TABLE VI - Flange Rim Choke Slit Depth Modification Results	68
TABLE VII - Flange Rim External Choke Slit Width Modification Results	68
TABLE VIII - Comparison of Flanged Antennas	103

LIST OF SYMBOLS

\hat{a}_r	Unit vector in r direction
\hat{a}_ϕ	Unit vector in ϕ direction
\hat{a}_θ	Unit vector in θ direction
a	Microstrip disk patch radius
d	Paraboloid aperture diameter
D	Directivity
\bar{E}_θ	θ component of the electric field
\bar{E}_ϕ	ϕ component of the electric field
η	Aperture efficiency (gain factor)
η_s	Spillover efficiency
η_I	Illumination efficiency
f	Paraboloid focal length
$G_f(\theta)$	Gain function of paraboloid feed
J_s	surface current density
J	$\sqrt{-1}$
k_0	Freespace wave number
λ	Wavelength
Pt	Total power
π	3.14159265
μ	Relative permeability
ϵ	Relative permittivity
u	Power intensity
ω	Angular frequency

Note - Unless otherwise specified, all units of measure will be given with respect to the resonant wavelength.

INTRODUCTION

The development of the electronic revolution over the past 20 years has brought with it an engineering tool of significant importance, that being the "Computer Aided Engineering" (CAE) or "Computer Aided Design/Computer Aided Manufacture" (CAD/CAM) systems. In electrical engineering both graphic printed circuit board and integrated circuit design have been supported by CAD/CAM techniques for a number of years. More recently, microwave circuit CAD systems have become available, but little emphasis has been placed on graphic antenna design. Traditionally antenna design has been performed in one of two ways, either by a trial-and-error experimental procedure or using an analytical approach. Both of these methods are limited in their applications: the analytic method is restricted to simple geometries and cannot easily be generalized and the latter is time consuming, usually labor intensive, and often very expensive.

Several routines have been written to numerically predict radiation characteristics for families of antenna geometries [1-3]. One such routine (ROT2) calculates the field radiation patterns for antennas which exhibit rotational symmetry about one axis. An interactive graphic antenna design (IGAD) package was developed by the author as a pre and post processor for ROT2 by integrating it with the Calma CAD/CAM system. The IGAD package is

composed of three major components. The analysis routine is needed to predict the antenna radiation characteristics, the CAD/CAM system provides the graphics processing, and an interface is required to merge the two. Graphic antenna design techniques are useful in reducing time and cost of production and design, while improving antenna detail.

The IGAD package is not limited to only rotationally symmetric antenna geometries. Concurrent with the authors work, G. Neilson is developing two additional graphic interface processors to be used in conjunction with analysis routines [2,3] for wire and surface patch modelled antenna geometries. The three programs and associated graphics combine to form the IGAD package. Only ROT2 portion (IGAD-ROT2) is relevant in this text, and therefore no further consideration will be extended to the wire and surface model sections of IGAD.

The remainder of this paper presents a discussion of the work involved developing a graphic interface for ROT2 and a design example illustrating the system performance. The first two chapters deal exclusively with the IGAD-ROT2 package development, while the final three chapters examine the design considerations of a paraboloid reflector feed using the graphic techniques. The topics covered include the following: CAD systems and the benefits, and preliminary information on the graphic antenna design package (Chapter 1); the design and development of IGAD (Chapter 2); background on paraboloid reflector feed design

(Chapter 3); the design of a prime focus feed (Chapter 4); and finally the conclusions and future developments (Chapter 5).

CHAPTER I

GRAPHIC COMPUTER AIDED ANTENNA DESIGN

1.1) CAD/CAM Systems

Computer aided engineering, which now touches virtually all bases of engineering, began with the computer revolution in the early 1950's. At that time computers were little more than large programmable calculators capable of the iterative and trial-and-error type calculations that were necessary in mechanical and electrical design optimizations [4,5]. The closing of the 1950's and the beginning of the 1960's saw a dramatic increase in computer processing power, as well as the emergence of multitasking systems. This era witnessed the development of numerous generalized engineering algorithms (such as finite element analysis) and specialized application routines. Computing costs were very high and affordable only by large corporations. This lasted until the early 1970's when the advent of powerful mini computers brought the in-house computing costs within the range of the more abundant, smaller firms. Concurrently technology had developed to the point where the processing of screen graphics had become cost effective. Merging powerful interactive computing methods with high speed graphics was the

next logical step. These Computer Aided Engineering (CAE) systems were first introduced as bundled hardware and software (turnkey) packages. As microprocessors, mini computers, and CAE equipment decreased in cost and standardization became more prevalent, the systems became more dissociated. The different components associated with CAE tended towards more specialized and localized functions.

Today, CAE systems possess much greater computing power and speed. Software, for many systems, has been available for up to 10 years allowing for significant development and often high reliability. Computer Aided Engineering spans almost every facet of engineering. Appendix A elucidates the extent of General Electric Corporation's [6] CAE environment which covers computer assisted product development from the initial concept through to manufacturing and quality control.

1.1.1) CAD/CAM Equipment

Most CAD configurations consist of a central computer (with resident graphic software) networked with 1 or more specialized workstations. A typical workstation includes a high resolution graphics screen, an alphanumeric screen for nongraphic display, a keyboard for command and data entry, and an electronic graphics tablet and "digitizing" pen. Computer Aided Design systems are not limited to the centralized architecture described above.

Stand-alone workstations are available complete with graphics and primary processing functions. It is also possible, in many cases, to network these workstations with a central processing unit. In such cases, data transfer is handled in a standard format, usually IGES (International Graphic Exchange Standard)

1.1.2) Advantages of CAD/CAM

Extensive capital is required to purchase the above equipment. To justify such expenditures, the benefits of graphic CAD techniques when applied to antenna design must be established. The advantages of Computer Aided Design related to the engineering field are well documented and in many instances apply to antenna theory as well, as is illustrated below:

- Computer graphics provide a medium through which antenna models may be quickly created and modified. Menial, time consuming tasks such as spacial coordinate generation are handled by the software, and not the designer. Design time is therefore significantly reduced.
- The antenna is, in most cases, modelled as three dimensional geometries with corresponding mass properties. These properties can be extracted and used to drive computer numerically controlled (CNC) machines or used to analyse the structural qualities of the antenna under diverse load conditions such as high winds. Wind loading is a

particularly important performance characteristic of paraboloid reflector antennas.

- Electromagnetic theory is a particularly abstract subject that students often have trouble comprehending. Graphically depicting antenna models in space with the corresponding radiation characteristics would help increase the fundamental understanding of antenna theory. Also, animation of these models would illustrate how various antenna components affect the radiated field. This should enhance the comprehension of electromagnetic basics and thus lead to more creative and improved designs.

- Production drawings can be easily generated from the antenna model.

Generally speaking then, it may be concluded that CAD: (1) improves design time and detail, (2) integrates design and engineering and, (3) reduces production time and costs.

1.2) Calma CAD System and the IGAD Package

All software developed for the Interactive Graphic Antenna Design (IGAD) system has been accomplished at the Manitoba Research Council's (MRC) Industrial Technology Center (ITC) in conjunction with the University of Manitoba. ITC currently operates a VAX 11/780 minicomputer with the following application packages:

- General Electric's Calma CAD [7-9] system features a three dimensional data base for wire frame models and 4 workstations.
- Structural Dynamics Research Corporation (SDRC) CAD system is a solid modelling software package used mostly for static and dynamic structural analysis. SDRC is owned by General Electric.

The development of IGAD is limited to only the Calma system. Future work should ideally see the incorporation of SDRC software to analyse the mechanical and structural properties of the antenna models

Calma's Design, Drafting and Manufacturing language (DDM) is an interactive graphic language used to build items of geometry via the digitizing tablet or keyboard. Calma also includes a Design Analysis Language (DAL) to assist the user with software development. DAL is a high level programable graphics language

composed of virtually all the DDM commands plus several "Fortran-like" mathematical and input/output (I/O) functions. In addition, DAL interfaces to Fortran. This leaves an ideal environment to address the two areas of software development associated with IGAD: (1) the generation and display of antenna geometries and performance characteristics (using DAL), and (2) the calculation of radiation patterns exhibited by these geometries (using Fortran).

It is possible using the DAL/Fortran interface driver to pass more than just scalars between the languages. Virtually all data base representations of screen geometry that can be generated by DAL (or DDM) may be passed to and from Fortran. Since DAL is written in Fortran, the software execution time may be decreased by bypassing DAL and writing the graphics code in Fortran. This would lead to fast, but unfortunately, extremely complex and long algorithms. Instead only the mathematical and I/O subroutines are programmed in Fortran.

Calma uses a three dimensional data base representation to store screen models. Any number of model viewing windows may be defined using a "flying eye" to select the window orientation. Windows are displayed in user defined viewports. Up to six viewports are supported per screen layout, therefore six different model images may be displayed simultaneously. Geometries Calma supports include points, arcs, lines, splines, surfaces, B-surfaces, labels, notes and dimensions. Non-graphic text and

data may be stored with the model using entities called text-data items.

1.3) ROT2

Given below is background information on the analysis routine that was integrated within IGAD-ROT2 to the Calma CAD/CAM. ROT2 is a Fortran computer program that utilizes the Electric Field Integral Equation (EFIE) approach to predict the scattered field from a perfect conducting body of rotational symmetry. The solution to EFIE is effected by the method of moments technique. An in-depth look at the modelling and computational aspects of ROT2 may be found by referring to Ole Rydhal's thesis on "Scattering From Small Bodies" [10].

ROT2 was written to treat a large variety of rotational scatterers. Up to 10 separate scattering bodies may be modelled using the program. Each body is composed of 1 or more basic geometry contours that are present within the main program. Geometry segmentation must be defined by the user to determine how tightly the contour curve is modelled as a series of straight line doublets. The designer specifies the minimum and maximum number of segments per wavelength and the minimum deviation of the contour curve from the straight line approximation. Incident field definition is restricted to four different types: dipoles, monopoles, plane waves, and conical horns. Calculation of the scattered far field is accomplished via one of two methods. The approximate solution determines the far field radiation without the contribution of the near field terms. The more precise

solution utilizes the near field radiation but requires significantly more computer time.

The chart given in Fig. I-1 illustrates the ROT2 program structure. An input program consisting of command cards and specification cards is used to model the antenna geometry, define the incident field, and determine the output. Following each command card may be a series of specification card(s) which summarize the parameters of the instruction being executed. The commands are divided up into 4 sections. The Interpreter section is a collection of miscellaneous functions that control the program flow, determine the degree of output and label the different models. The Geometry section uses a base of six primary shapes (each rotationally symmetric) to model the antenna geometry. The Incident Field is composed of a plane wave, a conical horn, or a series of dipoles. The desired field calculations are specified via the Output section commands.

The computational methods of ROT2 are not important in this text, but the modelling techniques used by the antenna designer must be considered if the ROT2 input/output is to be emulated by the graphics system. The following chapter will discuss the author's task of combining the CAD system with ROT2.

Main Program

Subroutines

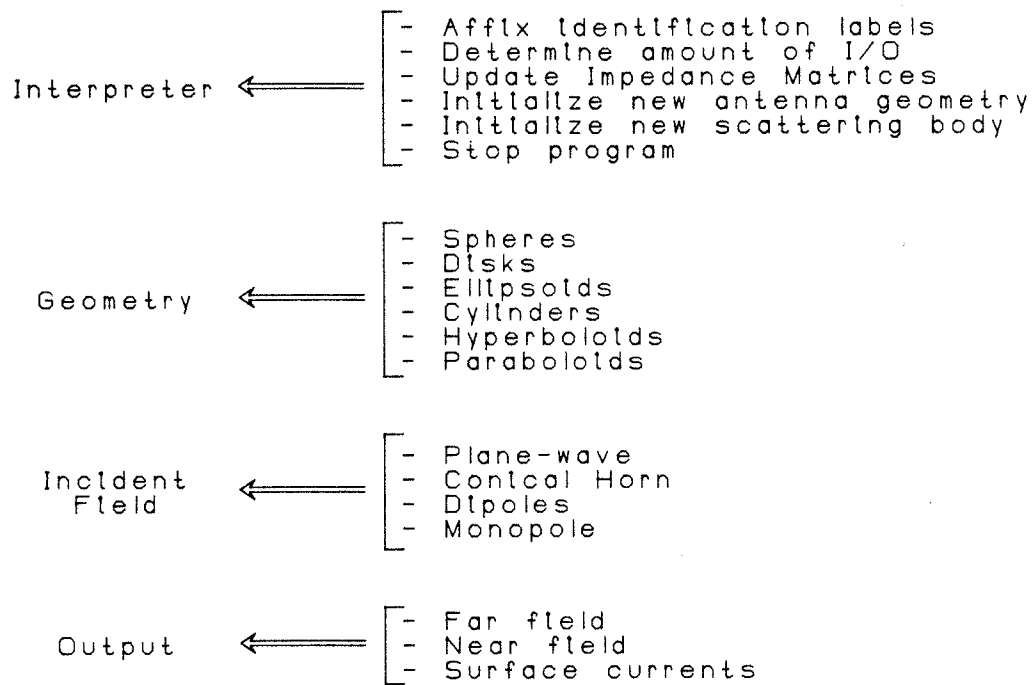


FIGURE 1-1 ROT2 Program Structure

CHAPTER II

IGAD-ROT2

2.1) Introduction

The previous chapter provided some preliminary information on the Calma CAD/CAM and the ROT2 analysis program. The actual work accomplished to perform the Calma-ROT2 merger is detailed in subsequent sections of this chapter. Initially an explanation of the pre and post-processing software functions written by the author in Calma's Design Analysis Language (DAL) will be given. Included within these functions are the construction, plot and drawing modes of operation. As well, a couple of additional attributes included with the graphics code and not found in ROT2 are expounded upon. IGAD-ROT2 incorporates a submodel feature that enables the designer to work concurrently on several different antenna submodels, and also maintains connectivity data to ensure proper modelling of the antenna geometry is accomplished.

2.2) Merging Calma and ROT2

The initial IGAD-ROT2 concept was developed to integrate graphic computing techniques with available Fortran antenna analysis programs. At the outset of the project, the two main package components were available: (1) a copy of ROT2 was obtained from the University of Manitoba and implemented on (2) the Manitoba Research Council's CAD facilities. The analysis routine and the graphic computing methods form the basis of the IGAD-ROT2 package. DAL interface routines were written by the author to interactively integrate the two.

The Calma-ROT2 interface software was developed to serve two basic functions:

- 1 - To act as a pre-processor for the analysis routine.

This includes properly modelling the antenna with screen graphics, and using this data to generate the ROT2 input file. The pre-processor must also be capable of emulating all ROT2 commands and performing the model management and display modification functions.

- 2 - To act as a post-processor which is initiated after the antenna analysis calculations are complete. This software is responsible for displaying the radiation characteristics on the screen (or paper) in a manner that is readily understood by the designer. It must also be capable of model management and display modification functions.

The graphic processors described above are driven through user-friendly screen menus that enable command and data entry. Included with the Calma source code is a tablet function used for the creation, calibration, and editing of the tablet or on-screen menus. Associated with each menu pick is a series of DAL subroutines that were written specifically to perform all data acquisition, screen geometry construction, and archiving. The screen menus were designed by the author using the Calma tablet functions. Appendix B lists and briefly describes the DAL interface programs that were developed specifically to accomplish the Calma-ROT2 merger.

2.2.1) Construction Mode

Figure II-1 illustrates the overall IGAD-ROT2 program structure. The chart shows how the program flows naturally through the construction, execution, plotting, and drawing modes of operation. The post and pre-processing sections of the software are divided at the ROT2 execution point.

Three screen menus have been created for the construction, plot, and drawing modes and are individually illustrated in Figures II-2a to II-2c. The screen layout for the construction mode handles all of the pre-processing functions and is given in Figure II-2a. All antenna construction and editing must be performed in this mode via the menu. Plan, right side, and

isometric views are displayed in the three viewports. Changes to the displayed information are automatically reflected through all viewports (a result of the three-dimensional data base). The windows contained in each viewport may be relocated or redefined through graphic menu picks. Interactive modifications may be performed in any displayed window, regardless of its orientation.

The previously discussed ROT2 input command groups are located along the top two rows of processor buttons in Figure II-2a. The graphic symbols under the Geometry heading are used to build the antenna contour from a base of primary shapes. Cylinders, spheres, ellipsoids, paraboloids, hyperboloids, and disks are among the contours included. Each contour pick is a series of DAL subroutines, each capable of the following:

- Prompting the designer for geometrical parameters.
- Constructing the contour on the graphics screen using DAL spline, line, and surface commands.
- Prompting for the contour segmentation deviation parameters.
- Storing acquired information as a text-data item with the antenna model. This data is later accessed to write the ROT2 input file.

Excitation of the antenna is restricted to the dipole, monopole, vectored plane wave, and conical horn commands displayed under the Incident Field heading in Figure II-2a. Current listing and field specification commands (with or without field approximations) specify the analysis program output. Again, as with the geometry subroutines, DAL programs are written to perform all information retrieval, construction (where applicable), and archiving for the Incident Field and Calculation command groups. Also included along the top rows are a series of command modifier buttons that are used in conjunction with the processor buttons to modify, add, or delete the above construction elements.

To perform menu picks using the on-screen menu, it is necessary to disable the tablet associated with the digitizing pad. This allows Design, Drafting and Manufacturing (DDM) commands to be entered by the keyboard only. Since most users will have a very limited knowledge of DDM, several useful functions such as screen magnification and grid selection have been incorporated into the graphic tablet as display modification commands. These functions are located in the bottom half of the vertical command column along with the window modification buttons (very bottom). The top half of the column contains the general model commands. These DAL subroutines enable the designer to retrieve and file models, execute the ROT2 input file translation program, exit back to DDM, display information associated with an item, and alter the working submodel set and model pointers (the

purpose of these functions will be expanded on later). The translation program is used to convert the stored screen geometry into the ROT2 input command file

The two rows of buttons located in the middle of the screen allow numeric data entry from the graphics tablet (the keyboard may also be used). Toggling between construction, plot, and drawing modes is accomplished via the "SLO" commands. The model, display, and window commands are common for most modes of operation and have been included with all screen menus.

2.2.2) Plot Mode

The plot screen layout is shown in Figure II-2b. This screen layout consists of 1 plot and 2 geometry viewports. Again, any orientation may be displayed in the geometry windows, but model modifications should only be performed in the construction mode. The plot window has a fixed alignment and should not be altered.

Several DAL routines have been written to help facilitate plotting of field information. User definable options such as axes length, plot location, plot type, and number of plots (no limit) have been integrated into the software. The plot software also reads and scales field data and generates all axes, labels, and plot lines. Currently 4 plot types are supported:

1. User Defined - Allows the designer to plot up to 4

sets of data for each ϕ plane: the E-plane magnitude, the E-plane phase, the H-plane magnitude, and the H-plane phase. Often it is necessary to display magnitude and phase information on the same plot. This option is included. Two or three plot axes are created depending on the number of different data set types.

2. Cross and Co-polar - The cross-polar and co-polar field intensities, as defined by C. Ludwig, [11] are displayed in plot form. The formulation of cross and co-polar will be investigated in Chapter 3.
3. Gain - The gain is plotted for a given ϕ plane.
4. Parabolic Reflector Feed Efficiency and Gain Factor - Three important performance characteristics of an ideal paraboloid reflector feed are the spillover efficiency, illumination efficiency and gain factor. These three parameters are plotted together. Calculation of paraboloid reflector design parameters are covered later in Chapter 3.

Many of the mathematic intensive calculations such as cross and co-polar, gain, reflector feed efficiency, gain factor, data scaling, and point list generation are written in Fortran and utilize Calma's DAL/Fortran interface.

The "PLOT DEL" and "PLOT MOVE" commands are self explanatory. Editing of screen text is accomplished through the DAL function "TED". The commands to the left of the "TED" button are standard DDM dimensioning functions. A command button that is especially useful with dimensioning is "ACC" which allows the number of decimal places to be altered on subsequently displayed dimension numbers.

2.2.3) Drawing Mode

The drawing mode screen menu (Fig. II-2c) was developed to facilitate the creation of production drawings. It is usually activated upon completion of work in either the construction or plot modes. A drawing is defined in this text as a composition of one or more geometry or plot screen windows placed together by the designer within the drawing mode. The drawing mode contains only one viewport. A typical command sequence needed to produce a drawing of an antenna or its radiation characteristics illustrates the flexibility of the drawing mode. Using the command buttons listed on the top of the screen menu, the designer first determines which windows are to be included; then composes the drawing by adding and/or deleting window(s); if necessary, edits the window(s); and finally submits the drawing to the plotter. All windows in the plot and construction modes are available to be placed within a drawing. This enables both design and production drawings to be extracted from the antenna model.

The drawing may be one of several standard paper sizes or may be user defined.

The "WIN" functions shown in Fig. II-2c pertain to adding, deleting, or moving of the drawing windows, while the "DRW" commands are used to add, delete, or move entire drawings. "DRW OFF" turns off the drawing mode and disables the "PLOT"ting function. The user may also list the available drawings and windows through the "LST" functions.

Several of the model, numeric, and display commands discussed previously have been included with this menu and are located within the lefthand column of buttons. As well, toggling between either of the remaining modes of operation isaccommodated via the "SLO" functions.

2.3) Connectivity

Antenna geometries composed of multiple contours must be created in a structured fashion to enable the computer to properly model the connected segments. Geometries should therefore be created such that the conductor path is continuous and closes upon itself. The sheet metal ground plane shown in Figure II-3 is modelled using 3 cylinders. The properly modelled disk in the top drawing has a conductor path shaped from a continuous string of cylinders that start and end on the axis of rotation, whereas the remaining two scatterers are incorrectly formed.

IGAD-ROT2 handles the problems associated with multiple contours by imposing connectivity restrictions on each shape. This ensures that each contour is "built" from an existing one, unless of course, it is an initial scatterer geometry. A base contour is determined either from the designer selecting an existing item or by defaulting to the previously created one. The antenna creation process continues in this fashion, building contours from the preceding one, until the antenna model is complete. Each contour has associated with it a unique geometry identification number. This number is stored along with the geometry numbers of connected items in the contour text-data item. Access of this data when the translation routine is executed ensures the command card sequence is correctly ordered. Connectivity violations are detected during translation and the

user is notified with a warning message and an abort option.

Deletions and modifications may be performed on connected items. Modifying these items automatically updates the connected contours. Both displayed and stored information is affected. Contour holes left as a result of geometry deletion should be filled with additional items before translation. Figure II-4 highlights this point. The middle cylinder of the top ground plane is deleted (connectivity broken) and a choke composed of 5 cylinders is inserted to re-establish connectivity.

2.4) Submodels

An additional useful and time saving submodel feature has been incorporated into the IGAD-ROT2 structure. One Calma model may store up to 10 antenna submodels. The working submodel set ("WRKNG SET") command shown in Figures II-2a to II-2c is used to activate any number of submodels. All of the geometry, incident field, field calculation, deletion, and addition commands only act upon the activated submodel set. This enables the designer to perform construction additions and deletions on groups of antennas, rather than on an individual basis.

Often the designer is interested in determining how the modification of an antenna part (for example a ground plane) will affect its radiation characteristics. Instead of creating 5 antenna models, each with a different ground plane, he/she could model the antenna minus the ground plane once and have it reflected through five antennas with the submodel option. Following this, a different ground plane could be created for each of the 5 antenna geometries. Normal procedures would then be used to translate the models, execute ROT2, and generate the desired plots. Caution must be exercised to ensure connectivity is maintained throughout all of the submodels since only one antenna is displayed at a time. The computer and engineering time saved as a result of this approach is obvious

The working submodel set also determines the list of models submitted for translation. DAL software controls all "book keeping" associated with writing the proper command and specification card sequences. This ensures that the models are submitted in required order. To increase the computing efficiency and command usage of ROT2 input cards, submodels are user definable as either a geometrical variation or an incident field variation of the preceding submodel. An incident field variation model maintains the same geometry as the previous submodel but is excited with a different source. Consequently the antenna impedance matrix of the previous submodel is stored within ROT2 and reused to significantly reduce the program execution time. Geometrically varied models have a different geometry from the previous submodel but may be excited with the same source.

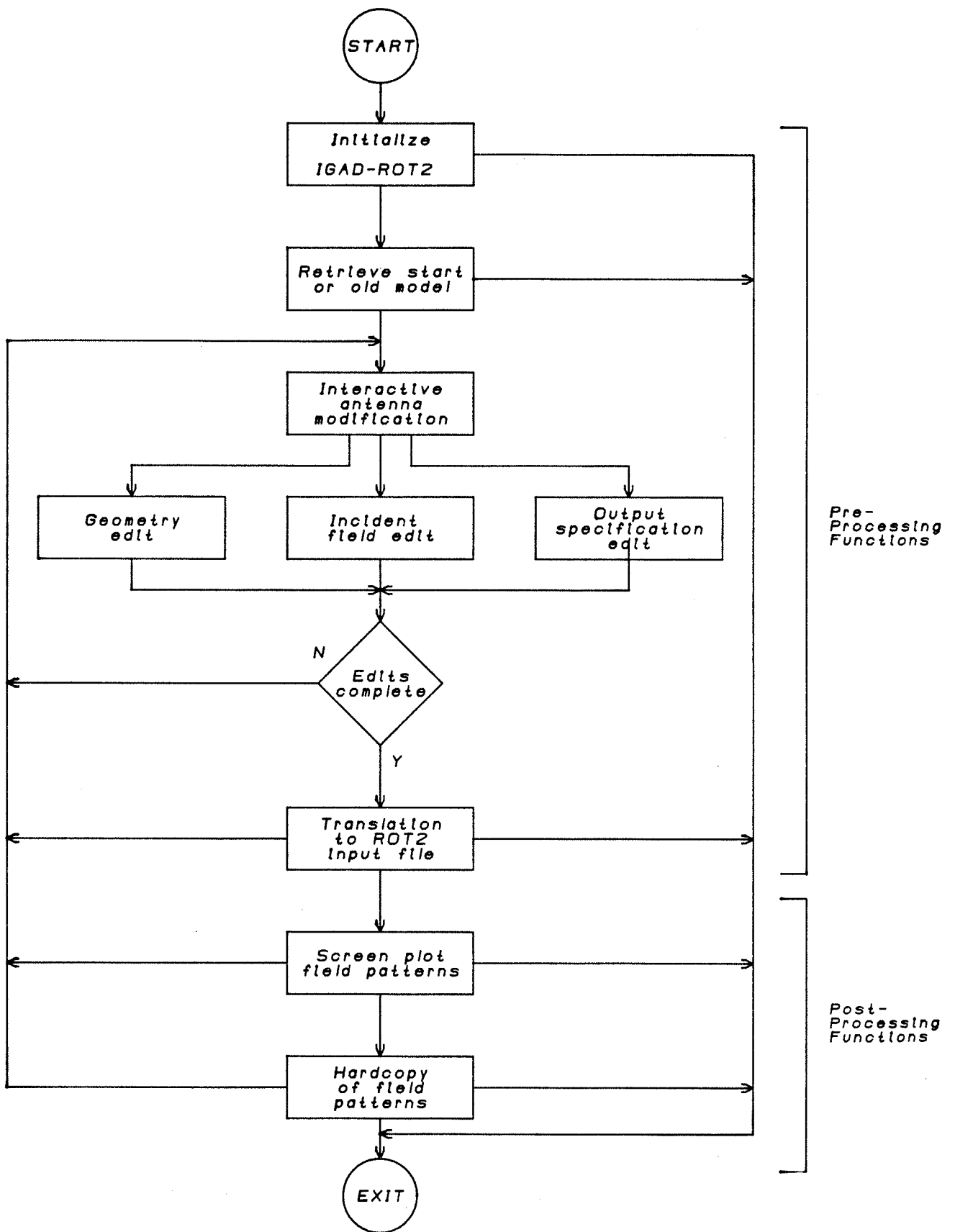


FIGURE II-1 IGAD-ROT2 Program Structure

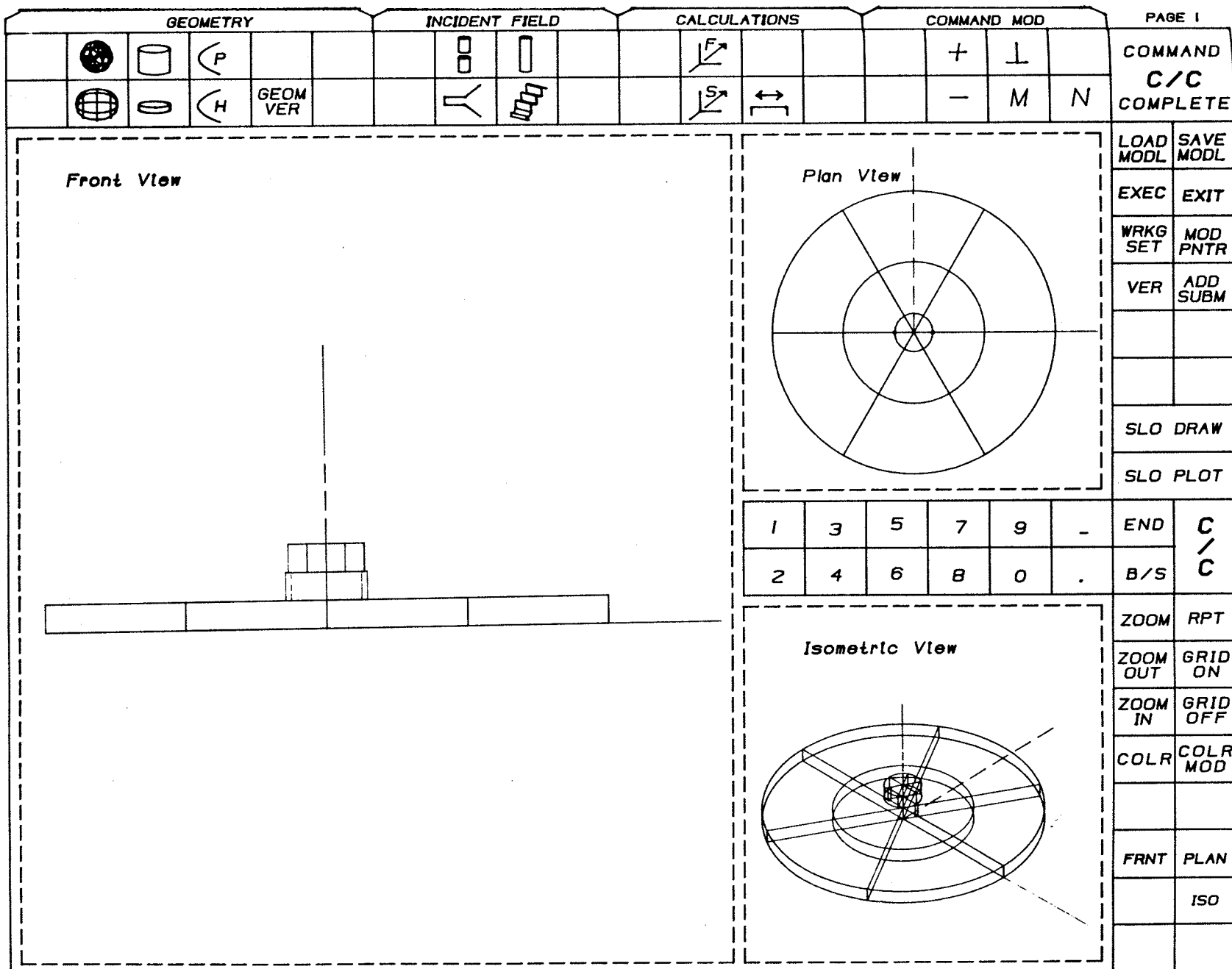


FIGURE II-2a Construction Screen Layout and Menu

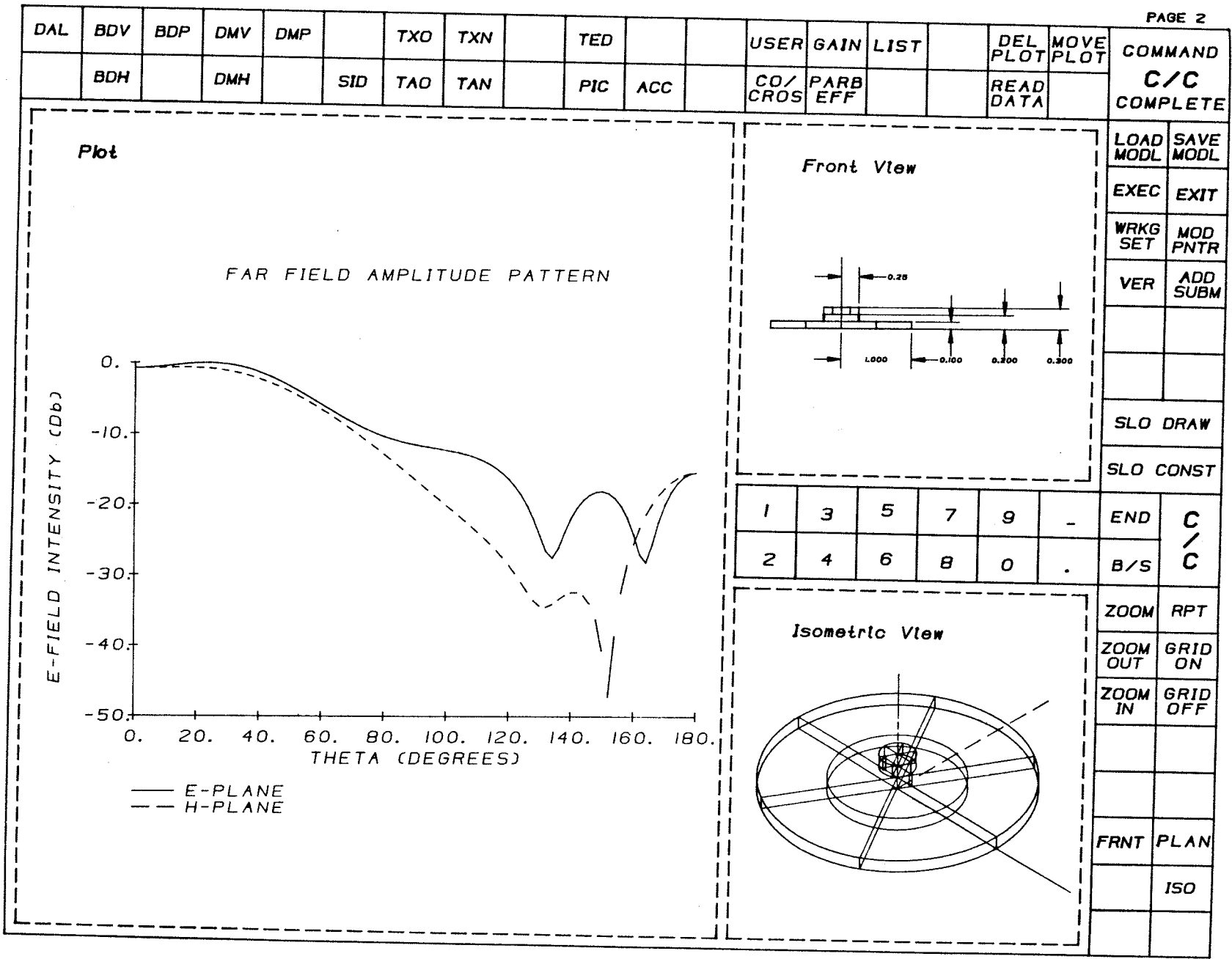


FIGURE II-2b Plot Screen Layout and Menu

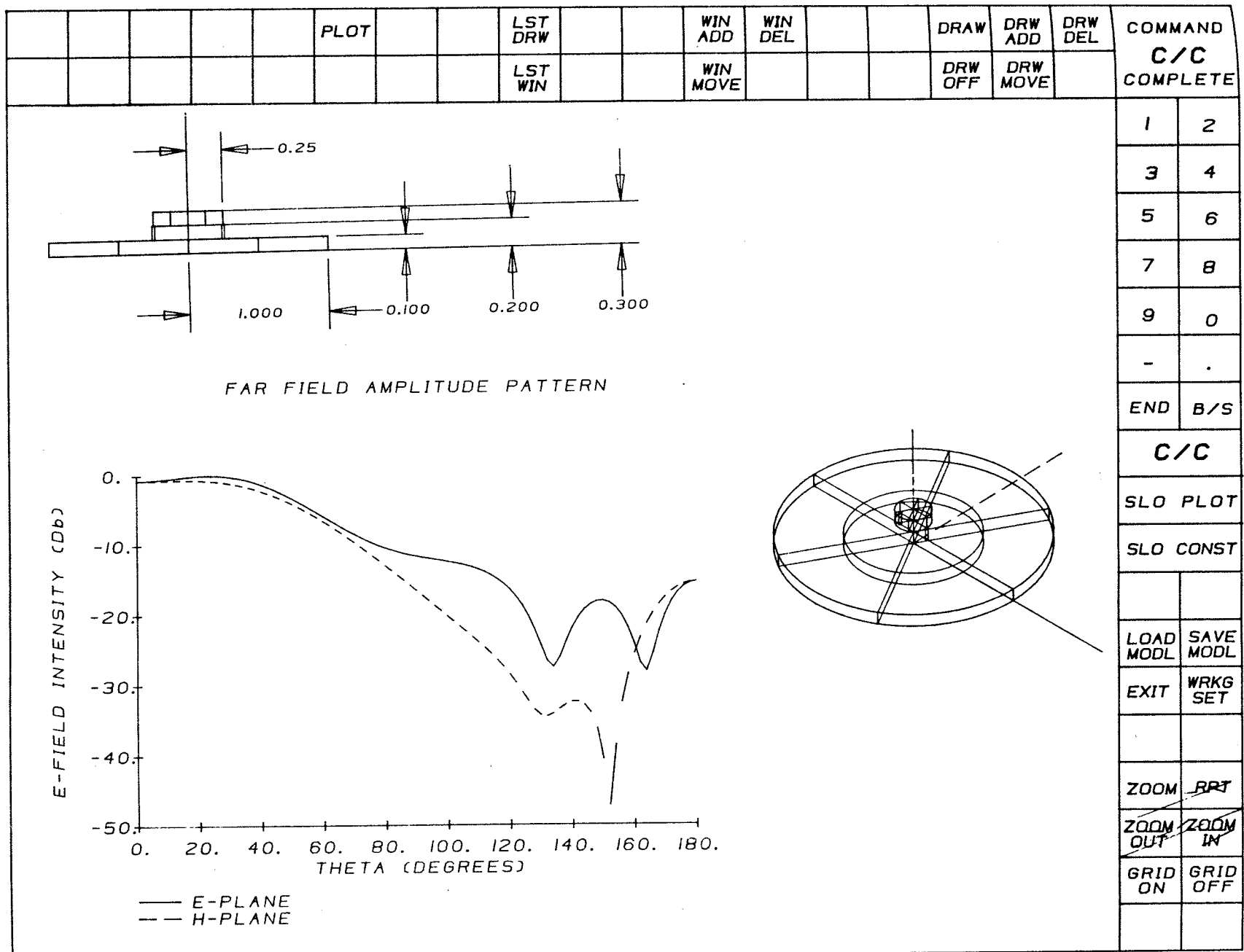


FIGURE II-2c Drawing Screen Layout and Menu

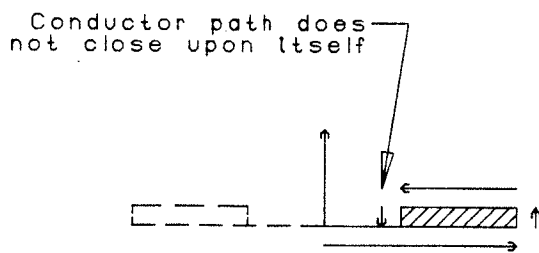
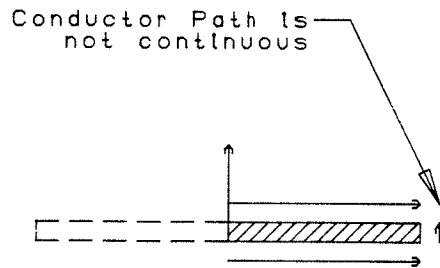
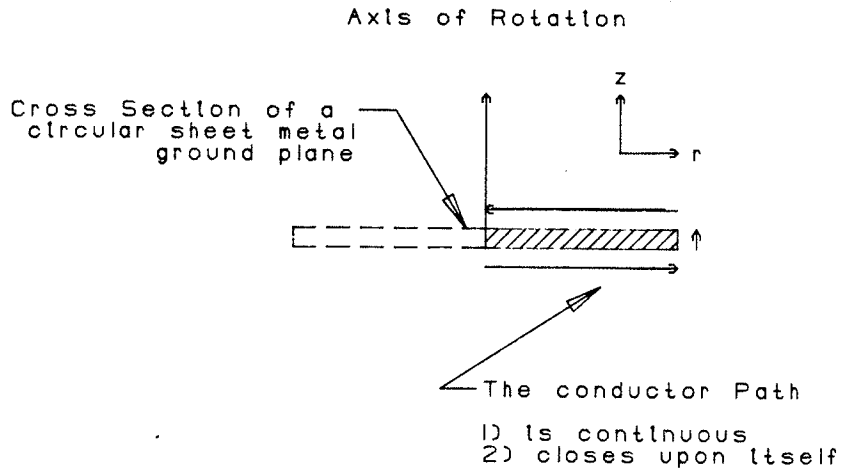
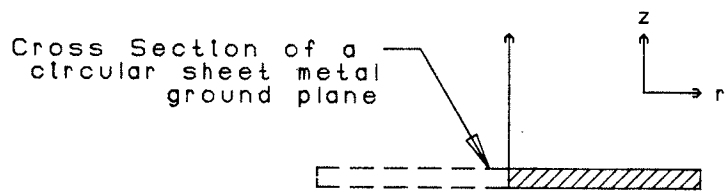


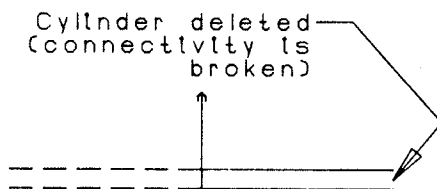
FIGURE II-3 The Method used to Create Multiple Contour Geometries Is Illustrated with a Circular Sheet Metal Ground Plane

Axle of Rotation

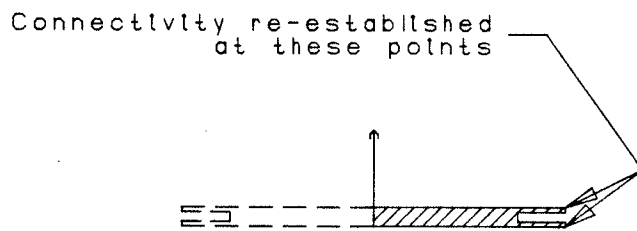


Normal circular ground plane

(A)



(B)



Choke inserted along disk rim (composed of 5 cylinders)

(C)

FIGURE II-4 The Method used to Insert Contours is Illustrated with a Circular Metal Ground Plane

CHAPTER III

FEED CHARACTERISTICS OF PARABOLOID REFLECTORS

3.1) Introduction

The second chapter discussed the IGAD-ROT2 package that has been completed to date. The following chapter presents material on ideal paraboloid reflector performance characteristics and background information on the more traditional prime focus feeds. A relatively new antenna type, the microstrip disk, is also discussed. This antenna, upon initial investigation, appears to approach the standards of established prime focus feed horns. The electrical performance of the microstrip disk antenna is briefly investigated at the conclusion of this chapter. The fundamentals associated with microstrip disk antenna operation will form the basis from which an original antenna, the flanged disk radiator will be developed.

3.2) Paraboloid Reflector - Feed Relationship

To understand the considerations that must be taken when initiating a new feed design we must first discuss the relationships governing the reflector performance. Figure III-1 illustrates a paraboloid reflecting surface illuminated by a feed located at the focal, the coordinates of a point on the reflector, and an observation point in the far field. Two methods are commonly used to analyze the radiation characteristics from the reflector surface. The "aperture distribution" method uses geometric ray optics to determine the scattered field over a projected reflector area normal to the axis of rotation [12]. Standard techniques are then applied to the aperture to determine the far field radiation.

The second technique, titled the "current distribution" method, utilizes the physical optics approximation to determine the current density (J_s) induced on the reflector surface from the feed antenna. This current is integrated over the reflector surface to obtain the secondary field. The gain follows from the secondary field calculation. The performance of the reflector may be more readily understood from its gain and is detailed in the following section.

3.2.1) Calculation of Paraboloid Reflector Efficiency and Gain Factor

The current distribution technique is applied by Balanis [12] to calculate the fields radiated from a paraboloid. The radiation integrals and auxiliary vector potentials are used to calculate the scattered fields in both E and H planes:

$$\bar{E}_\theta = -j \frac{\omega \mu}{4\pi r} e^{-jkr} \iint \hat{a}_\theta \cdot J_s e^{jkr \cdot \hat{a}_r} ds \quad (1a)$$

$$\bar{E}_\phi = -j \frac{\omega \mu}{4\pi r} e^{-jkr} \iint \hat{a}_\phi \cdot J_s e^{jkr \cdot \hat{a}_r} ds \quad (1b)$$

where

- ω = angular frequency
- μ = relative permeability
- k = freespace wave number
- \hat{a}_r = unit vector in the r direction
- \hat{a}_θ = unit vector in the θ direction
- \hat{a}_ϕ = unit vector in the ϕ direction
- J_s = surface current on the reflector

The derivation of the above field equations is based on several simplifying assumptions:

- the scattering reflector is a smooth closed surface
- $J_s=0$ over the shadowed surfaces and scattering occurs only from the illuminated face.
- direct radiation from the feed is ignored.
- edge diffraction is neglected.
- blockage from the feed and support structure is ignored

The calculation of the antenna directivity follows from Equation (1) above. By restricting the source to a linearly polarized and circularly symmetric field with no cross-polar components, the scattered field equations reduce to [12]

$$E_{\theta}(r, \theta=0) = -j \frac{2\omega\mu f}{r} \left[\sqrt{\frac{\epsilon}{\mu}} \frac{P_t}{2\pi} \right]^{\frac{1}{2}} e^{-jk(r+2f)} \int_0^{\theta_0} \sqrt{G_f(\theta')} \tan\left(\frac{\theta'}{2}\right) d\theta' \quad (2)$$

where

- f = focal length
- P_t = total power
- ε = relative permittivity
- θ₀ = the paraboloid rim angle
- G_f(θ₀) = antenna feed gain function

The power intensity may then be determined

$$U = 16 \frac{\pi^2}{\lambda^2} f^2 \frac{P_t}{4\pi} \left| \int_0^{\theta_0} \sqrt{G_f(\theta')} \tan\left(\frac{\theta'}{2}\right) d\theta' \right|^2 \quad (3)$$

where λ = wavelength

and the directivity follows as

$$D = \left(\pi \frac{d}{\lambda} \right)^2 \left\{ \cot^2 \frac{\theta_0}{2} \left| \int_0^{\theta_0} \sqrt{G_f(\theta')} \tan\left(\frac{\theta'}{2}\right) d\theta' \right|^2 \right\} \quad (4)$$

where d = aperture diameter

Term 1 of the directivity expression above corresponds to the gain of a uniform constant phase aperture field. This value is modified by the aperture efficiency (term 2) to yield the reflector directivity. The aperture efficiency (or gain factor) is composed of the following components

$$\eta = \eta_S \eta_I \eta_X \eta_D \eta_B \quad (5)$$

where

- η_S = Spillover efficiency
- η_I = Illumination efficiency
- η_X = Cross-polarization efficiency
- η_D = Phase error efficiency
- η_B = Feed blockage efficiency

Assuming the phase error and blockage efficiencies are insignificant, the gain factor then becomes a function of the spillover, illumination and cross-polarization efficiencies. The calculation of these parameters, shown in Appendix C, is included with IGAD-ROT2 and has been incorporated within the plot routines

To attain a uniform, constant phase aperture distribution, it can be shown that the feed pattern must satisfy the following equation [12]:

$$G_f(\theta) = \begin{cases} \sec^n\left(\frac{\theta}{2}\right) & 0 \leq \theta \leq \theta_o \\ 0 & \theta > \theta_o \end{cases} \quad (6)$$

where n = the feed pattern number

Of course this is impossible to achieve. Consequently the feed pattern must be approximated by compromising the spillover and illumination efficiencies. Figure III-2a illustrates approximated and ideal field patterns. The relative field strengths necessary at point A (on Fig. III-2a) to attain optimum illumination for different feed pattern numbers are compared in Fig. III-2b. For typical feed structures ($n=2-4$) the edge illumination should be 8-10 dB below the maximum intensity.

2.2.2) Cross-Polarization

In the preceding section the gain factor was calculated based on the assumption that the cross-polarization was 0. This generally is not possible to achieve since components of the orthogonal field are always present to some degree. It may be shown, however, that restrictions placed on the source field can minimize the cross-polarization. To determine the cross-polar and co-polar expressions we start with a generalized expression for the feed far field

$$\bar{E}(\theta, \phi) = \hat{a}_\theta [f(\theta) \cos\phi] + \hat{a}_\phi [g(\theta) \sin\phi] \quad (7)$$

Ludwig's [11] third definition of cross-polarization can be applied to the above expression to yield the following

$$Co-pol = f(\theta) \cos^2\phi + g(\theta) \sin^2\phi \quad (8)$$

$$Cross-pol = \sin\phi \cos\phi [f(\theta) - g(\theta)]$$

where \hat{a}_θ = unit vector in the θ direction
 \hat{a}_ϕ = unit vector in the ϕ direction
 $f(\theta)$ = E-Plane field
 $g(\theta)$ = H-Plane field

It can be seen from the above equations that elimination of the unwanted cross-polar components will result if the E-plane and H-plane fields are equal. This will also equate the co-polar field to either the H-plane or the E-plane electric field. A Fortran subprogram used to calculate the cross-polar and co-polar intensities has been written and incorporated into IGAD-ROT2.

3.2.3) Summary of Feed Parameters

The previous two sections have highlighted the considerations associated with paraboloid reflector feed design. To achieve the optimum design, a nearly uniform aperture distribution is required with little edge illumination. The spillover content should be minimized to reduce unwanted power loss. Random fields in the

spillover region contribute to the signal-noise strength degradation and are represented by an increased antenna noise temperature. Finally the cross-polarization should be kept to a minimum. This will be possible if the feed is circularly symmetric.

The parameters associated with paraboloid feed design have now been introduced. Before proceeding with the discussion of the design example, a review of past feed structures will be briefly presented and compared to printed circuit disk antennas.

3.3) Development of Paraboloid Reflectors

Large paraboloid reflector development evolved from the need to explore deep space radio emissions with high gain antennas. Two important historical events during the 1930's initiated the research efforts of these antennas. Jansky [13] detected the first extraterrestrial radio emissions in 1931, and Reber [14] constructed the first large parabolic reflector for radio astronomy use in 1937. This initial work had hardly begun when World War II started. Further developments remained dormant during the fighting years, but a rekindled interest in astronomy during the post war era lead to the construction of several large radio telescopes throughout the world. The means of excitation for these early antennas were simple structures, usually folded dipole elements.

The aperture field polarization generated by dipole feeds was shown by Cutler [15] to contain a strong cross-polar field component. Figure III-3 illustrates the spherical field distribution necessary to radiate a linearly polarized secondary field. The remaining two sketches in Fig. III-3 show the polarization characteristics of a dipole element and its corresponding aperture distribution. In 1954 Jones [16] discovered it was possible to superimpose magnetic and electric dipole field components, to produce a parabolic reflector Huygens source with linear polarization. Figure III-4 highlights the

aperture fields of the two dipole elements and the resultant linearly polarized field.

During the 1950s, the first feed horns arose out of the need for increased antenna gain necessary in deep space communications. The first conical horns operated in the dominant mode and exhibited poor circular symmetry. In 1963 Potter [17] introduced a step discontinuity in the horn throat. This resulted in a transfer of energy from the dominant TE₁₁ mode to the TM₁₁ mode. Figure III-5 shows the field intensities and aperture distributions associated with each modal component and the combined field. Proper design of the step discontinuity allowed equal excitation of the E and H planes field intensities and suppressed the sidelobes. This idea was extended by Potter and Ludwig [18] to include the higher order modal components. Consequently an antenna with better prime focus feed characteristics at the resonant frequency resulted. However, the bandwidth was restricted due to a distorted aperture distribution caused by different modal phase velocities.

The problems associated with multimode conical horns were later solved concurrently by Minnett and Thomas [19] of Australia, and Kay [20] of the U.S.A. They independently discovered that properly introducing $\lambda/4 - \lambda/2$ deep corrugations into the inner diameter of the horn, enabled similar boundary conditions to be impressed on the E and H fields inside the horn. Thus the phase velocities associated with TE_{mn} and TM_{mn} were made to be

identical. A new hybrid mode HE_{mn} resulted from the combined TM_{mn} and TE_{mn} modes. The corrugated feed and scalar horn are sketched in Fig. III-6. The performance of the corrugated horn as a paraboloid reflector feed may be summarized as follows:

- identical E and H plane patterns and low cross-polarization
- low sidelobe levels
- large bandwidth
- shaped main beam to fit prime focus feed requirements

More recently the ideas associated with corrugated horns were taken one step further by Kishk [21] and extended to rotationally symmetric trapezoidally and sinusoidally corrugated horns (see Fig. III-7). The radiation characteristics were determined numerically and found to effectively satisfy the paraboloid design parameters. The advantage of these circular horns over the more classical types was not attributed to the electrical performance, but rather to the improved cost and ease of manufacturing.

The basic design of feeds has remained relatively unchanged over the past 15-20 years. These antennas, although very efficient electrically (approximately an 80% aperture efficiency), suffer due to expensive production costs and a large mass (thus requiring rigid support structures). Printed antennas, however, are very inexpensive to fabricate and extremely lightweight, but cannot match the electrical performance of horn feeds. It is anticipated that the basic microstrip patch antenna can be modified such that its radiation characteristics fit the prime

focus feed requirements while maintaining the inexpensive manufacturing techniques. The radiation properties of microstrip patches will therefore be investigated prior to the initiation of the design process.

3.4) Microstrip Disk Radiator

Figure III-8 shows the basic microstrip disk geometry. A thin dielectric substrate is sandwiched between a copper disk radiating element and the ground plane. Several analysis techniques are available [22-25] to calculate the radiation characteristics. One of the simpler methods models the volume under the disk and above the ground plane as a resonant cavity. The cavity is bounded at the top and bottom by an electric field wall (the tangential field must satisfy the boundary conditions and thus is 0) and along the edge by a magnetic wall (radial current on disk equals 0 along periphery). Since the z-directed electric field in the dielectric is assumed to be constant, the field generated outside the cavity will be composed of the transverse magnetic (TM_{nm}) modes. Bartia and Bahl have provided the solution to this model with no sources [26].

$$E_{\theta} = j^n \frac{V a k_o}{2} \frac{e^{-j k_o r}}{r} \cos(n\phi) [J_{n+1}(k_o a \sin\theta) - J_{n-1}(k_o a \sin\theta)] \quad (9)$$

$$E_{\phi} = j^n \frac{V a k_o}{2} \frac{e^{-j k_o r}}{r} \cos\theta \sin(n\phi) [J_{n+1}(k_o a \sin\theta) + J_{n-1}(k_o a \sin\theta)]$$

where

- V = hE_oJ_n(Ka) is the edge voltage
- h = substrate thickness
- a = disk radius
- n = mode number
- K_o = freespace wave number
- E_o = electric field across the disk gap
- J_n(x) = nth order bessel function of x

The dominant mode ($n=1$) of the above equations yields a pattern that best fits the radiation characteristics associated with a good reflector feed. The remaining higher order modes generate nulls at $\theta = 0$. In Fig. III-9, the first order mode approximation is plotted along with an ideal feed pattern (line 2) and an E-plane sketch of Kishk's [18] sinusiodally corrugated horn (line 3). The horn cross-polarization is below -28 dB ($\theta < 90$ deg.) and first sidelobe level is less than -34 db ($\theta = 135$ deg.). The approximation using the first order mode compares quite favourably to the design provided by Kishk. The radiation pattern rolls off a little too quickly at high values of θ , but hopefully this can be corrected by modifying the antenna geometry.

Based on the above modal analysis, the microstrip disk antenna will be modified and designed with respect to the paraboloid feed requirements. The following chapter will investigate the possibility of beam shaping the microstrip disk radiation pattern. IGAD-ROT2 will be used to perform all geometry modifications and plot generation. As well, the cross-polarization, gain factor, and reflector efficiencies will be optimized. Steps considered in the design process, and how they were implemented using IGAD-ROT2 will be discussed and then a final antenna design will be given.

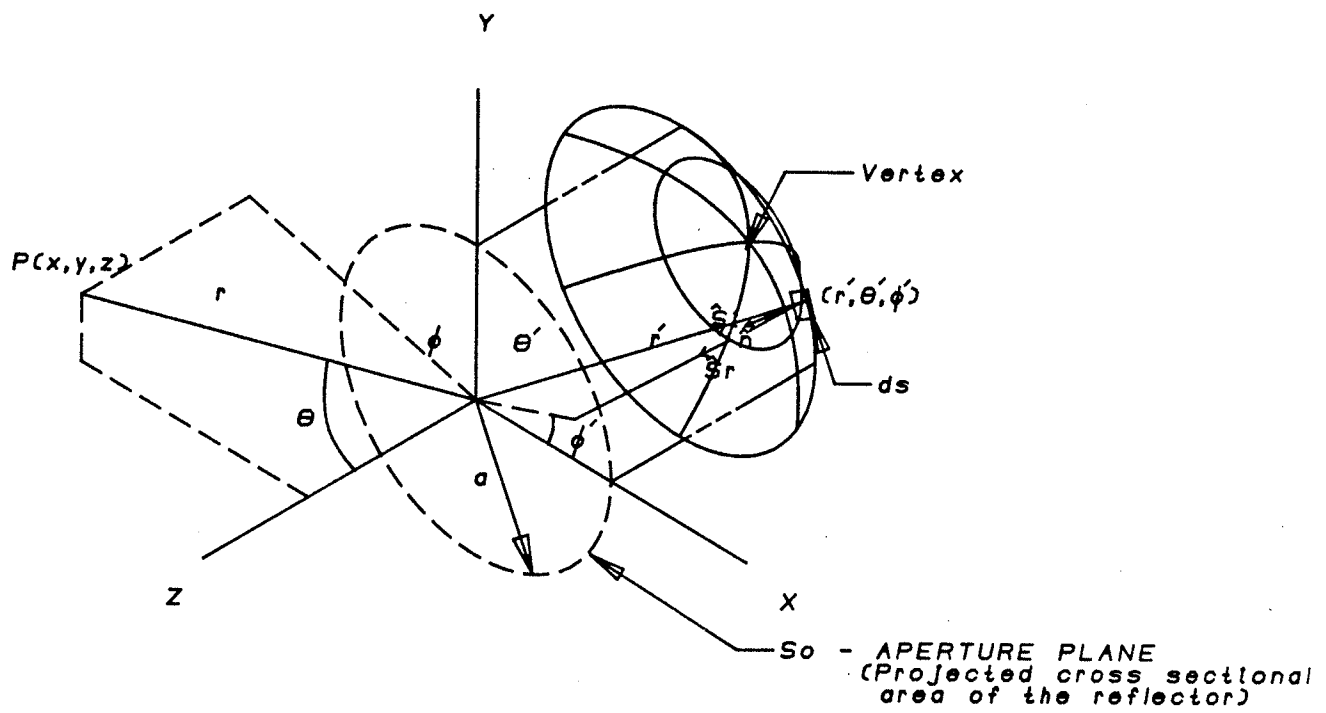


FIGURE III-1 Geometry of Paraboloid Reflector System

FAR FIELD AMPLITUDE PATTERN

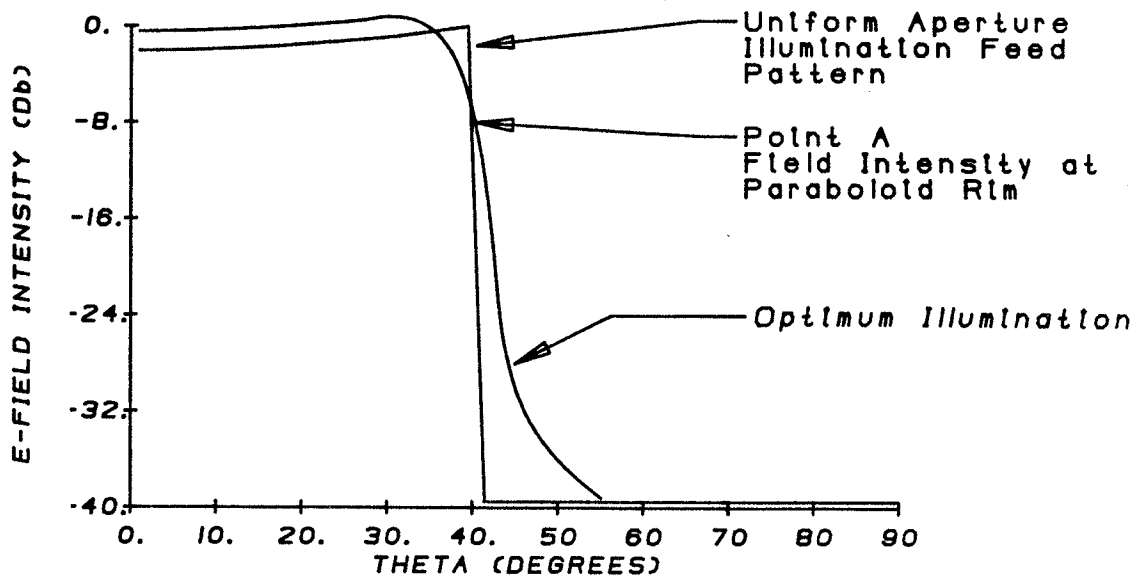


FIGURE II-2A Optimum Illumination Feed Pattern

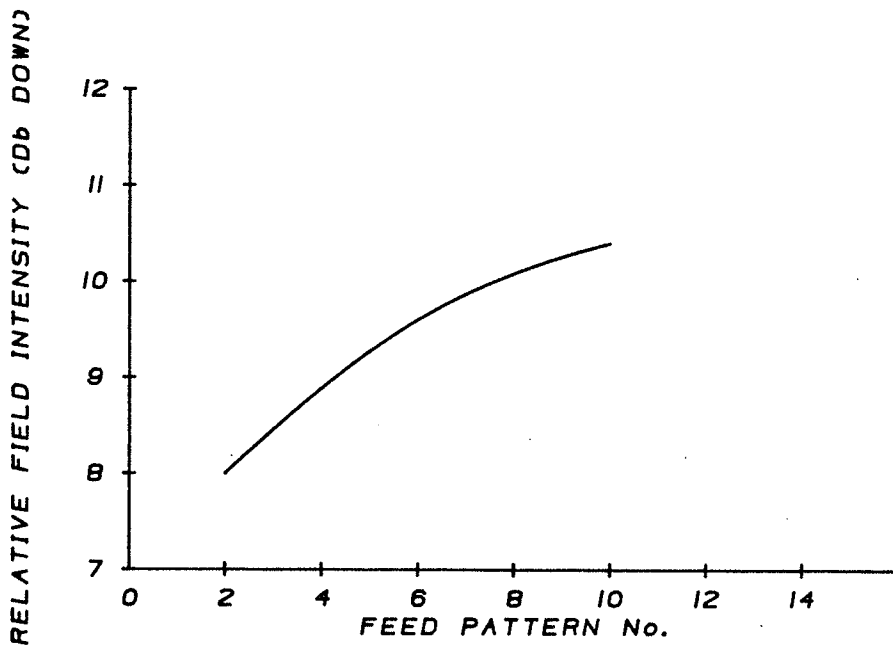


FIGURE III-2B Relative Field Intensity of Optimum Illumination at Paraboloid Rim for Differing Feed Pattern Nos.

SOURCE: S. Silver (ed.), "Microwave Antenna Theory and Design", MIT Radiation Lab, Series, vol. 12, McGraw-Hill, New York, 1949

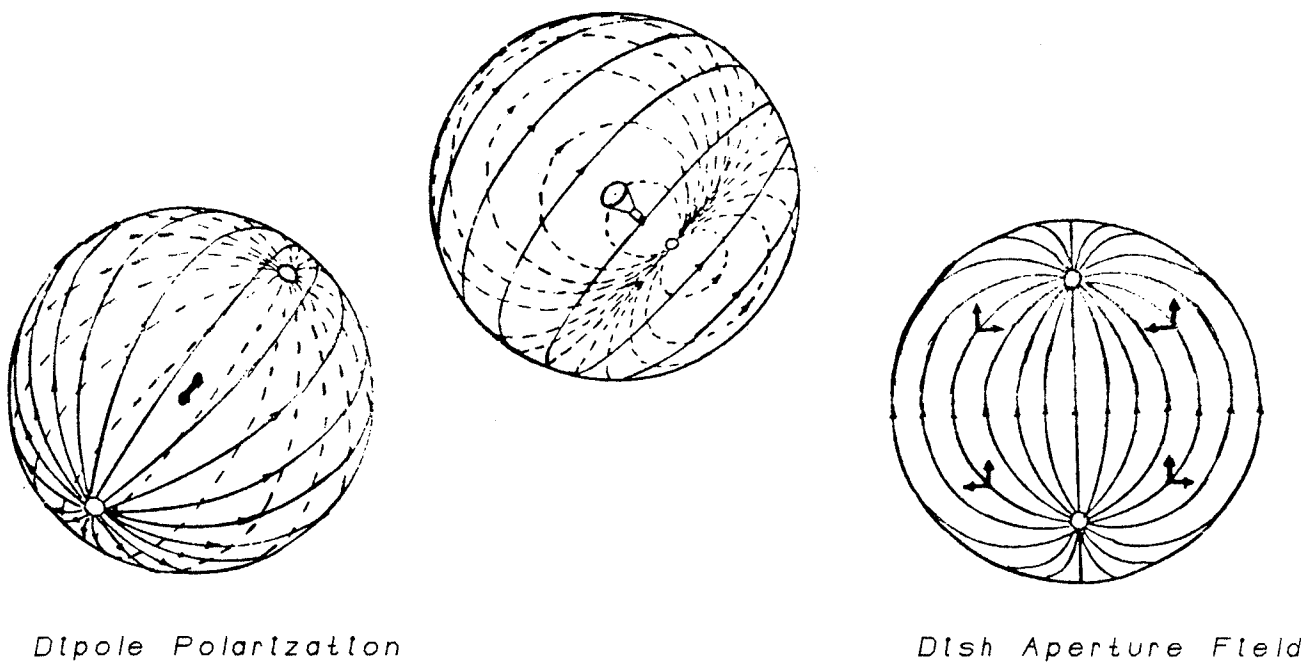


FIGURE III-3 Polarization Characteristics of Reflector Antennas

APERTURE FIELDS

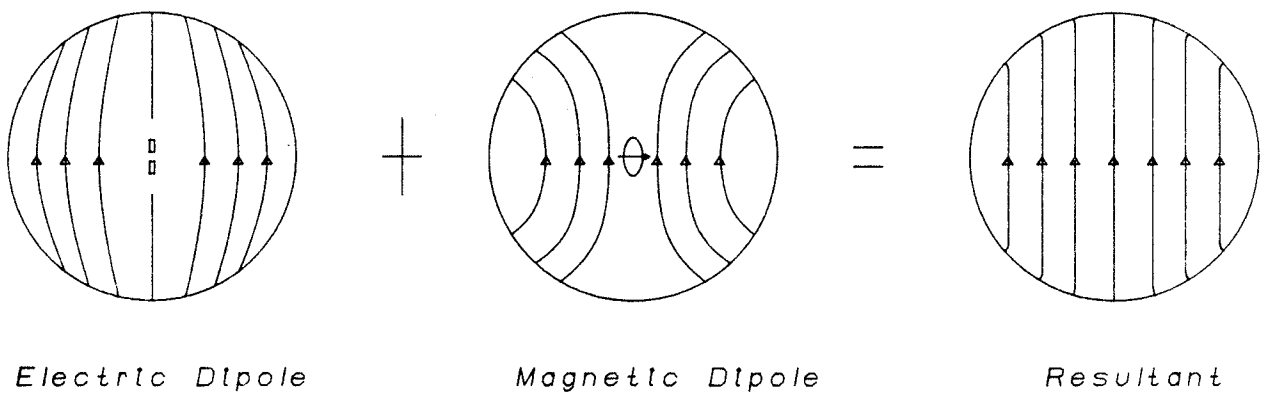


FIGURE III-4 Superimposed Magnetic and Electric Aperture Fields Produce Huygen's Source with Linear Polarization

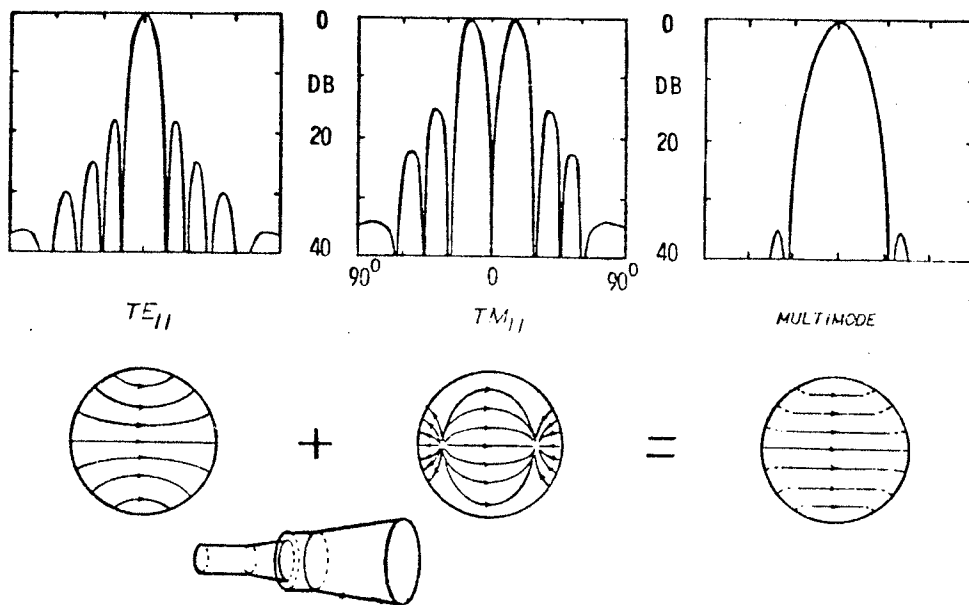


FIGURE III-5 The Dual Mode Conical Horn and Radiation Characteristics

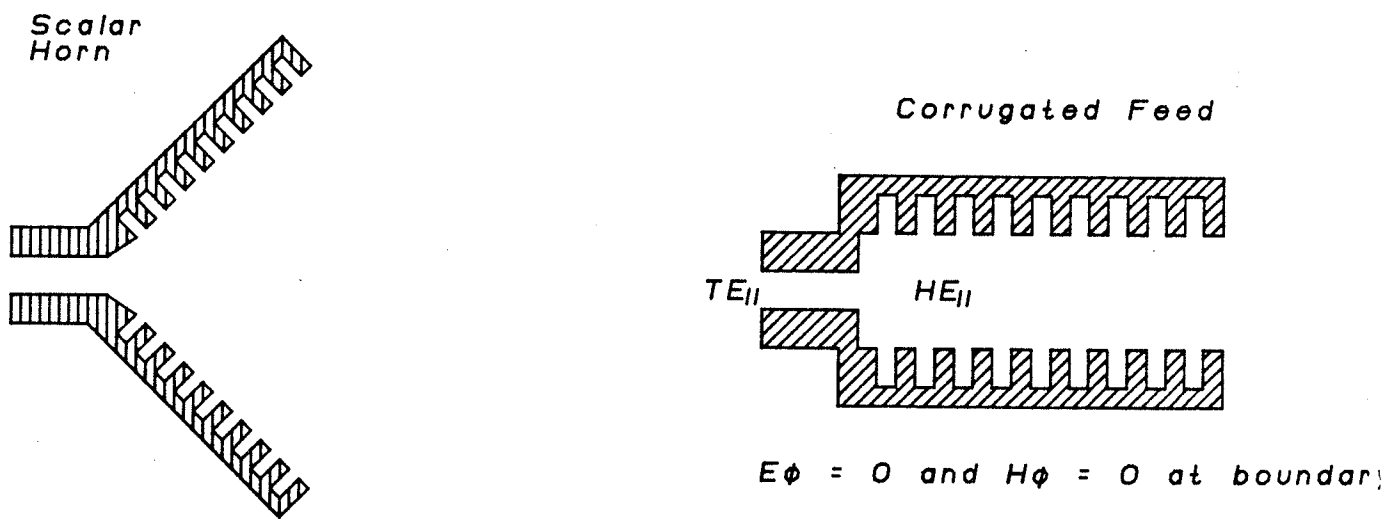


FIGURE III-6 The Scalar Horn and Corrugated Feed

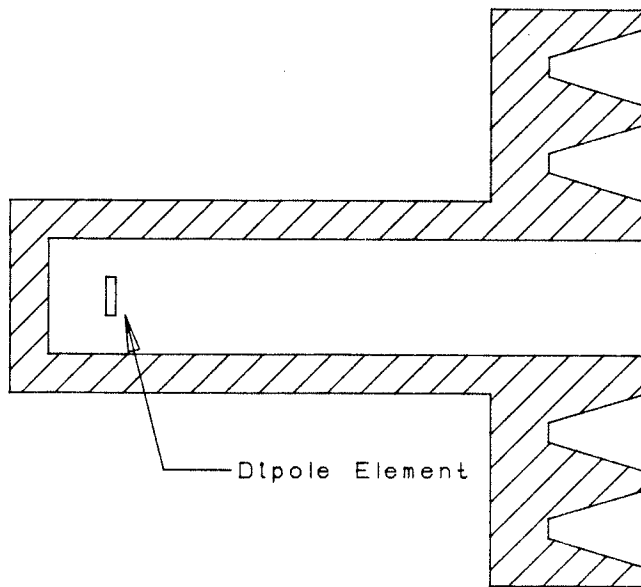


FIGURE III-7a Rotationally Symmetric Trapezoidally Corrugated Horn

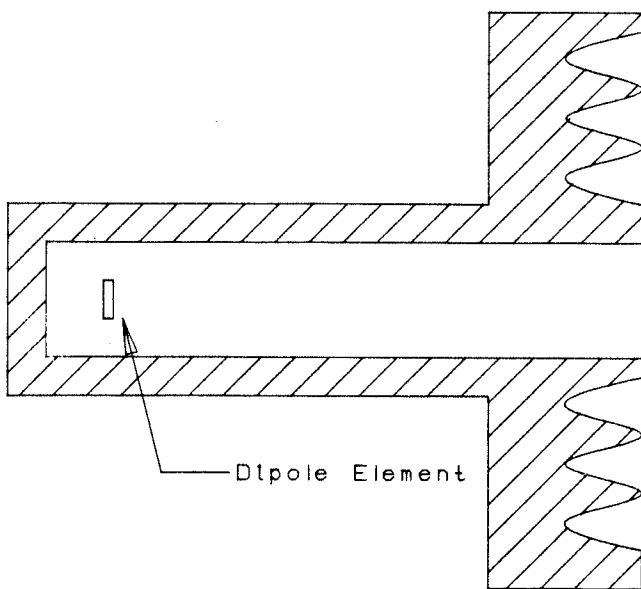


FIGURE III-7b Rotationally Symmetric Sinusoidally Corrugated Horn

Side View

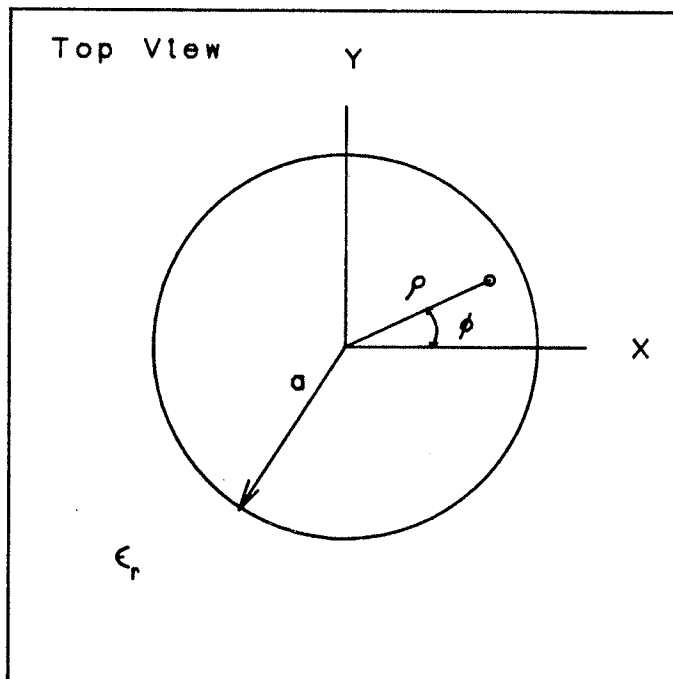
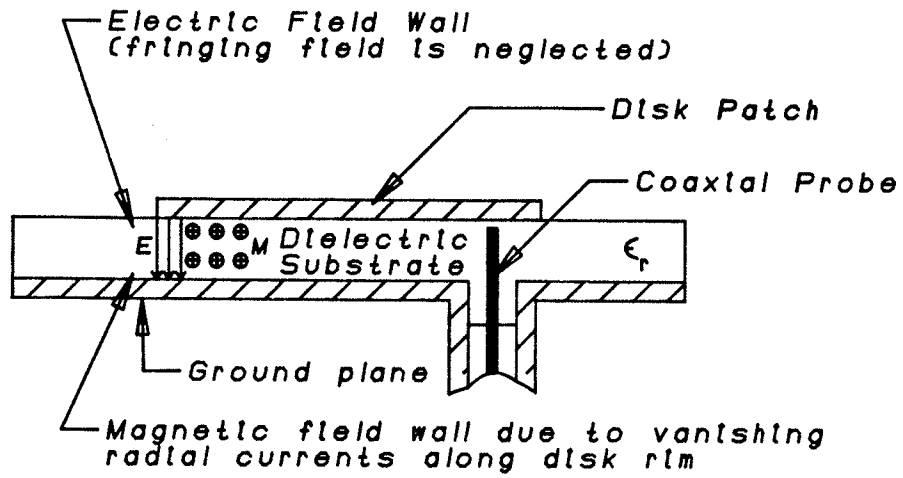
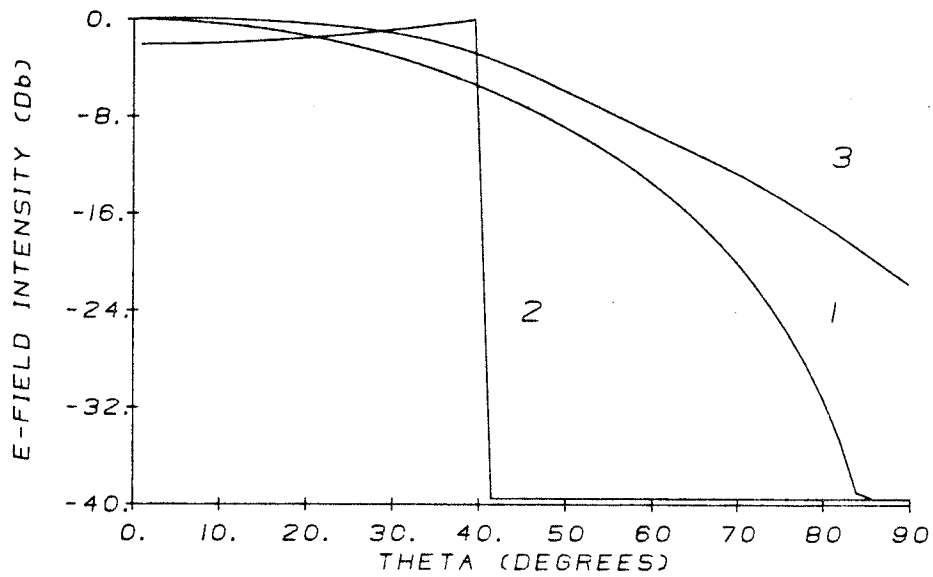


FIGURE III-B Microstrip Disk Geometry

FAR FIELD AMPLITUDE PATTERN



- 1 MICROSTRIP DISK FIRST ORDER MODE APPROX.
- 2 IDEAL FEED PATTERN
- 3 EXAMPLE OF A GOOD FEED PATTERN

FIGURE III-9 Comparison of First Order Mode Approximation with an Ideal Feed and a Good Feed

CHAPTER IV

DESIGN OF A SIMPLE PRIME FOCUS FEED

4.1) Introduction

The goals of this chapter are to: (1) introduce antenna design techniques using the graphic tools provided by IGAD-ROT2, and (2) produce an alternate antenna feed for front fed paraboloid reflectors. To accomplish both tasks, the steps associated with the antenna design process are elaborated on and related back to the graphics system whenever possible.

The design itself started as a disk antenna with poor feed characteristics. By using optimization techniques to shape the radiation pattern with respect to the gain factor and the cross-polarization, and by performing geometry modifications via IGAD-ROT2, it was possible to greatly improve the predicted feed performance. The following chapter presents the optimized disk antenna geometry and explains the search methods used. As well, several modifications to the optimized antenna geometry are illustrated utilizing the graphic techniques of IGAD-ROT2.

4.2) Initial Geometry

In the previous chapter, the microstrip disk antenna radiation characteristics were briefly investigated and determined to be suitable as a starting point for the design. Unfortunately ROT2 was not well equipped to handle all of the properties of microstrip design. The dielectric substrate of the disk patch could not be modelled using ROT2, it had to be represented as an air dielectric. In addition the dielectric constant of the substrate material was known to vary with prolonged exposure to the outside environment. This would have introduced unwanted alterations in the radiated field and degraded the system performance. The substrate layer was therefore dismissed when the analysis was carried out. Due to the lack of supporting substrate it was necessary to increase the ground plane and disk patch thicknesses to 0.1λ . Figure IV-1 illustrates the antenna geometry modelled by IGAD-ROT2. Each antenna surface was constructed from a cylinder of appropriate radius, z-axis location, length and angle subtended from the vertical. A total of six cylinders were required.

The excitation of the microstrip disk was restricted to the first order mode. Assuming the coaxial probe may be modelled as an infinitesimal dipole element, the field excited inside the cavity would be essentially an impulse function. The modes associated with the fourier expansion of the delta function

correspond to the propagation modes inside the cylindrical cavity. Excitation of these modes would occur if resonance was permitted by the antenna geometry. Introducing two dipoles, one on the x-axis, and the other the same distance away from the origin on the negative x-axis with an opposite and equal current distribution, would induce only the first order mode of the fourier cosine expansion. The remaining higher order modal components, and the 0 order mode cancelled due to the dual dipole symmetry. The dipoles were located along the scattering disk periphery. Figure IV-1 shows the coaxial probes modelled as dipole elements.

The transmit and receive frequencies of this feed were known to be 4 and 12 GHz respectively, thus the antenna had to be either broadband, or a narrowband device with two resonant frequencies. The analysis using ROT2 was carried out independant of the operating frequency because all spacial coordinates were measured as a function of the resonant wavelength

4.3) Optimizations of Antenna Geometry

The basic geometry of the antenna has been determined as shown in Fig. IV-1. The predicted radiation characteristics of this antenna are shown in Fig. IV-2. This figure reveals that three changes were initially required: (1) the circular symmetry had to be improved to reduce the cross polarization, (2) the radiation intensity had to be further collimated around the axis of rotation, and (3) the sidelobe levels had to be reduced. Controlled modification of the antenna geometry was the means to improve these patterns. Initially, modifying the scattering disk length and height above the ground plane was investigated (illustrated by A and B in Fig. IV-3). The ground plane was next distorted to improve the antenna performance. The bent ground plane flange (also shown in Fig. IV-3) introduced three new modification variables: C - the flange length, D - flange angle, and E - ground plane length. Other modifications (such as chokes) were implemented on the optimized geometry to help improve the antenna radiation characteristics.

Optimization of the above disk and flanged antennas was carried out with respect to the 5 search variables described above. The optimization program structure is shown in Fig. IV-4. The search function subroutine consists of four parts: writing the ROT2 input file, predicting the radiation characteristics via ROT2, calculating the cross-polar and the gain factor data, and

determining the optimization function value by properly weighting the above data. Unfortunately optimization techniques have not, as yet, been integrated with IGAD-ROT2 and must be performed separately. Prior to the execution of ROT2, the optimization variables are passed to the function subroutine. The antenna geometry is calculated using this data. Following this, the antenna geometry is passed to the analysis routine input file. The radiation, cross-polar and gain factor calculations are carried out in the manner previously discussed in chapter 2. After the routine has completed a search, the optimized radiation data is passed back to the CAD and plotted in the normal fashion.

The processor time necessary to perform 1 optimization function evaluation is between 3 and 10 minutes, depending on the complexity of the antenna geometry. This severely restricts the maximum number of function evaluations possible per optimization and hence limits the number of search variables to 2 or 3. The search variables previously discussed can not all be incorporated together within the same optimization, but rather must be treated in smaller groups to make efficient use of the computing resources. Past experience with different search techniques led to the selection of the Simplex Minimization method. Sequential methods such as Sequential Unconstrained Minimization Technique (SUMT) require too many function evaluations when handling inequality and equality constraints. Other multivariant search techniques optimize efficiently when the number of search

variables is large (> 4), but more than three variables is not required here. Therefore the simplex algorithm was selected to perform all optimizations.

4.3.1) Disk Scatterer Optimization

The first geometry item to be modified was the scattering disk. The height above the ground plane and length of the disk were varied to yield the optimum feed pattern. Constraints on the optimization variables were placed to ensure the disk and ground plane did not conflict. As well, the cross-polarization was restricted to a maximum of -20dB. The results of the optimization are given in Figure IV-5.

The initial disk antenna design results were encouraging but had several problem areas that had to be addressed. The backlobe, sidelobe and cross polarization maximums were too high and needed to be reduced. The E-plane and H-plane radiation intensities for $\theta < 90$ were similar, but the cross polarization was poor. This stemmed from the phase inequality between the two principal planes. To reduce the cross polarization it was necessary to bring the E and H-plane phase centers to the same location in space and make the magnitudes of both equal. The efficiency characteristics of the flat disk antenna were maximized to $\eta = 75.85\%$, spillover efficiency = 87.5%, illumination efficiency =

87.5% at a paraboloid aperture angle = 64 degrees or $f/d = .40$ (where f = focal length and d = dish diameter). The gain factor value was about 5% too low for paraboloid feeds. To achieve the additional 5% efficiency, it was necessary to reduce the back and sidelobe levels and increase the intensity rolloff in the $50 < \theta < 90$ degree range. Bending all or part of the ground plane was used to increase the axial radiation and help reduce the side and backlobes.

A scattering disk radius of .1348 wavelengths resulted from the above optimization. This yielded a 3.48 mm radius when translated to actual size at 12 GHz and was somewhat small for practical applications. Therefore the above optimization was resubmitted and the disk was restricted to a radius greater than 0.25 wavelengths and a height greater than 0.1 wavelengths above the ground plane. The results of this search are plotted in Fig. IV-6. This search ended at the disk constraints. The cross-polarization, efficiency parameters, and sidelobes were all degraded to a significant degree, but this model was selected as the base for the next optimization stage due to its increased disk size.

4.3.2) Flange Optimization

The second optimization was performed with respect to the flange length, flange angle, and ground plane length of the antenna (refer to Fig. IV-3). Again constraints were placed on the geometry to keep the flange length less than 1 wavelength and the flange angle within a 0-90 degree range. A ceiling constraint at -20dB was used for the maximum cross-polarization level. The results of the search are shown in Fig. IV-7.

The flanged ground plane collimated the radiation intensity about the axis of symmetry, but failed to improve the gain factor to any significant degree over the initial optimization value. The reason for this became evident upon investigation of the radiation intensity. The contribution to the gain factor from the significantly reduced sidelobe levels (-26 dB) was offset by the rapidly descending radiation pattern in the $20 < \theta < 90$ degree range. The radiation pattern had digressed from the uniform aperture field distribution given in equation 2-4 in this region, and hence lowered the gain factor. This was also evident by noting that the efficiency maximum occurred at an aperture angle of 56 degrees rather than the previous 64 degrees. An attempt to solve this problem was initiated by modifying the antenna geometry to increase the radiation intensity for $20 < \theta < 40$ degrees and reduce the backlobe levels. These modifications are discussed in the following sections.

The cross-polarization was reduced significantly to a maximum of -40dB for the flanged disk antenna. This value was much better than expected. The antenna shown in Fig. IV-7 is the basic optimized geometry and all remaining changes are effected only on this antenna.

4.4) Modifications to Flanged Disk Antenna

Several modifications were implemented on the flanged disk antenna in an attempt to increase the axial gain factor to a value of 80% or higher while maintaining the low cross-polarization and sidelobe levels. The two geometry changes detailed below include: (1) perturbation of the scattering disk contour to increase the radiation intensity near the origin and improve the gain factor and, (2) the addition of a $\lambda/4$ choke on the flange rim to reduce the side and backlobe levels.

4.4.1) Disk Modifications

The first modification performed on the antenna geometry was the distortion of the disk contour into a shape that would hopefully improve the feed characteristics. The flat top surface of the disk back scatterer was converted into the conic surface shown in Fig. IV-8a. The height (D) of the triangular peak was varied to five different values and the radiation characteristics were predicted for each.

IGAD-ROT2 was used to accomplish all geometry modifications. For the first conic scatterer type, five antenna submodels consisting of a flanged ground plane, the dipoles, and the desired far field calculations were created simultaneously using the submodel feature. Conic scattering elements of different heights

were then created independently for each antenna submodel. After all five submodels were complete, the translation program was invoked and the radiation characteristics were calculated and plotted. The design procedure described above illustrates how the submodel commands incorporated within IGAD-ROT2 may be used to significantly reduce the antenna model creation time.

The efficiency parameters, -3dB beamwidth, cross-polarization and sidelobe levels for each conic backscatterer are presented in Table I and the radiation patterns are given in Figs. IV-8a to IV-8c. It was anticipated that the current on the back side of the conic scattering element would increase the field intensity near the origin, but this was not the case. Instead, the H-plane pattern remained unchanged (for $\theta < 90$) and the height alteration served to change only the E-plane pattern. The cross-polarization was therefore easily modified by using the conic piece, but the antenna efficiency remained within 1% of the base antenna value. As well, sidelobe levels were not affected to a significant degree.

The backscatterer was next modified to have the conic point directed toward the ground plane as shown in Fig IV-9a. It was hoped this would distort the radiation characteristics associated with the cylindrical cavity and alter the far fields in a controlled manner. Pattern optimization with respect to the cone size would then be possible. The five submodels created with the first conic backscatterer were again used and modified to fit the

new cone requirements. IGAD-ROT2 provides two methods of modifying cylinder contours. The first method allows the designer to modify any number of the cylinder geometric and deviation parameters. The cylinder in question and the connecting cylinders are reconstructed and the storage text-data items automatically updated. In the second method, cylinders to be modified are deleted, thus breaking the contour connectivity. New contours are inserted into the resulting hole with the connectivity again established. The latter method was used to reconstruct each submodel backscatter such that the conic section was directed toward the ground plane. With this simple procedure it took only minutes to prepare the 5 submodels for resubmission to the analysis routine.

Again the efficiency parameters, -3dB beamwidth, cross-polarization and sidelobe levels are presented in tabular form (refer to Table II). These modifications, illustrated in Figs. IV-9a to IV-9c, had the most pronounced effect on the H-plane field. The radiation intensity was degraded with the increased cone height. The sidelobe levels were more pronounced, and the cross-polarization and efficiency were increased. These parameters became worse as the scatterer deviated from its original disk shape.

The cylinder modify command was used again on the 5 submodels to reconstruct the disk backscatterers with a post extruding away from the ground plane (see Fig. IV-10a). Attaching the post to a central arm extending from the vertex to the focal of a paraboloid dish provides a useful means of supporting the feed. Table III presents the performance characteristics of the antenna with respect to the different post sizes and the radiation patterns are given in Figs. IV-10a to IV-10c. The added post was effective in controlling the cross-polarization but as with the first set of model modifications, it didn't have an appreciable effect on the H-plane pattern, and thus had little effect on the gain factor.

An additional disk was added to the basic optimized geometry 0.1λ above the disk scatterer. IGAD-ROT2 was used to modify the previously described conic scattering elements into disks of varied radius. The extra disk altered the cross-polarization much like the extruded post geometry, but did not significantly change the remaining feed parameters.

Cone Height	-3 dB Beamwidth	Max Cross Pol. Level (dB)	Max. Side lobe level (dB)	Axial Gain Factor	Optimum Aperture Angle	F/D	Spillover Efficiency	Illumination Efficiency
0.05	57.6°	-32.2	-23.4	74.92%	56.0°	0.47	88.39%	87.76%
0.1	57.2°	-32.5	-23.5	75.08%	52.0°	0.51	85.48%	87.83%
0.15	56.8°	-32.8	-23.5	75.26%	52.0°	0.51	85.87%	87.64%
0.2	56.4°	-33.0	-23.5	75.42%	52.0°	0.51	86.21%	87.48%
0.25	56.0°	-32.9	-23.5	75.59%	52.0°	0.51	86.60%	87.28%

Table I - Conic Scatterer Modification Results (pointed towards ground plane)

Cone Height	-3 dB Beamwidth	Max Cross Pol. Level (dB)	Max. Side lobe level (dB)	Axial Gain Factor	Optimum Aperture Angle	F/D	Spillover Efficiency	Illumination Efficiency
0.05	57.6°	-33.4	-24.6	74.90%	56.0°	0.47	88.38%	84.74%
0.1	56.4°	-34.0	-26.5	75.02%	52.0°	0.51	86.00%	87.33%
0.15	53.6°	-26.0	-24.9	74.48%	52.0°	0.51	86.44%	86.15%
0.2	54.8°	-21.5	-19.8	73.16%	48.0°	0.56	83.07%	88.03%
0.25	55.2°	-18.6	-17.4	71.39%	48.0°	0.56	82.36%	86.41%

Table II - Conic Scatterer Modification Results (pointed away from ground plane)

Post Dimensions	-3 dB Beamwidth	Max Cross Pol. Level (dB)	Max. Side lobe level (dB)	Axial Gain Factor	Optimum Aperture Angle	F/D	Spillover Efficiency	Illumination Efficiency
.1x.2 [*]	64.2°	-29.2	-17.9	75.64%	60.0°	0.43	88.97%	85.01%
.1x.3	54.2°	-29.0	-22.3	75.93%	52.0°	0.51	87.52%	86.71%
.05x.2	57.0°	-35.0	-26.5	75.48%	52.0°	0.51	86.03%	87.73%
.05x.3	52.4°	-33.6	-25.5	75.51%	52.0°	0.51	86.16%	87.64%
.05x.5	56.2°	-30.0	-23.6	75.21%	52.0°	0.51	85.72%	87.73%

* Post Radius x Post Height

Table III - Disk Scatterer with External Post Modification Results

4.4.2) Choke Modifications

Four different choke modifications were applied to the flanged disk antenna in order to further reduce the back and sidelobe levels. By introducing an infinite impedance to the flange surface currents, the choke would have reduced the current on the back side of the ground plane and correspondingly cut the backplane radiation intensity. The choke slit width, slit depth, choke wall thickness, and external choke slit thickness are shown in Figure IV-11 and were varied to 5 different lengths. The radiation pattern plots for each submodel have not been included but Tables IV to VII display the performance characteristics associated with each modification type.

The added chokes were less successful than the disk changes. It was anticipated that the choke structure would lower the sidelobe levels up to 10 dB, but this was not the case. The sidelobe levels were either unaffected or degraded from the base flanged disk antenna. The chokes did alter the E-plane pattern in many cases, but not the H-plane pattern. Consequently the maximum cross-polarization was variable but the antenna efficiency remained virtually unchanged.

Choke Wall Width	-3 dB Beamwidth	Max Cross Pol. Level (dB)	Max. Side lobe level (dB)	Axial Gain Factor	Optimum Aperture Angle	F/D	Spillover Efficiency	Illumination Efficiency
0.05	58.2°	-31.9	-24.7	75.38%	52.0°	0.51	85.73%	87.92%
0.025	66.0°	-29.3	-24.3	74.74%	56.0°	0.47	88.20%	84.75%
0.1	68.0°	-31.8	-25.3	75.60%	52.0°	0.51	85.70%	88.21%
0.15	58.0°	-16.8	-23.8	67.25%	68.0°	0.37	79.94%	83.06%

Table IV - Choke Wall Width Modification Results

Choke Silt Width	-3 dB Beamwidth	Max Cross Pol. Level (dB)	Max. Side lobe level (dB)	Axial Gain Factor	Optimum Aperture Angle	F/D	Spillover Efficiency	Illumination Efficiency
0.05	58.2°	-31.9	-24.7	75.38%	52.0°	0.51	85.73%	87.92%
0.1	56.6°	-30.0	-25.7	75.58%	52.0°	0.51	85.94%	87.94%
0.15	53.6°	-24.9	-24.1	75.43%	56.0°	0.47	88.44%	85.14%
0.2	56.0°	-29.3	-24.2	76.32%	56.0°	0.47	89.29%	85.44%

Table V - Choke Silt Width Modification Results

Choke Silt Depth	-3 dB Beamwidth	Max Cross Pol. Level (dB)	Max. Side lobe level (dB)	Axial Gain Factor	Optimum Aperture Angle	F/D	Spillover Efficiency	Illumination Efficiency
0.25	58.2°	-31.9	-24.7	75.38%	52.0°	0.51	85.73%	87.92%
0.1	61.0°	-34.0	-24.1	75.66%	56.0°	0.47	88.14%	85.81%
0.2	64.8°	-27.3	-19.3	74.33%	56.0°	0.47	85.53%	86.85%
0.3	56.6°	-28.3	-24.9	75.44%	56.0°	0.47	88.83%	84.92%
0.4	59.6°	-36.6	-24.8	75.73%	56.0°	0.47	88.92%	85.15%

Table IV - Choke Silt Depth Modification Results

External Choke Silt Width	-3 dB Beamwidth	Max Cross Pol. Level (dB)	Max. Side lobe level (dB)	Axial Gain Factor	Optimum Aperture Angle	F/D	Spillover Efficiency	Illumination Efficiency
0.1	54.0°	-27.0	-25.8	75.45%	52.0°	0.51	86.21%	87.48%
0.05	56.0°	-30.4	-25.8	75.37%	52.0°	0.51	86.27%	87.37%
0.075	56.8°	-29.4	-25.3	75.46%	52.0°	0.51	86.37%	87.26%
0.15	54.2°	-26.2	-25.3	75.75%	52.0°	0.51	86.18%	87.77%
0.3	54.6°	-26.2	-25.8	76.10%	52.0°	0.51	86.11%	88.29%

Table VII - External Choke Silt Width Modification Results

4.5) Flanged Disk Antenna with Maximized Gain Factor

The following section gives one additional geometry optimization that was performed to try and increase the antenna efficiency to 80%. The flange was again optimized with respect to its length, angle, and ground plane length, but this time the level of cross-polarization was not restricted. The resultant radiation patterns and efficiency parameters are given in Fig. IV-12. Although the maximum efficiency was significantly increased to 78.67% at an aperture angle of 52.0 degrees, the circular symmetry and sidelobe levels are unacceptable.

A $0.05 \times 0.3 \lambda$ post extruding from the disk geometry away from the ground plane was utilized previously and improved the cross-polar field component of the base flanged disk antenna. Using IGAD-ROT2 once again to modify the disk geometry to include the additional rod, the radiation patterns were again calculated as shown in Figure IV-13. The post helped reduce the cross-polar field and the sidelobe intensities at the expense of a 0.42% efficiency. The maximum gain factor now corresponds to an aperture angle of 48 degrees. This is too low for commercial applications since most receive only dishes require the feed aperture angle to fall in the 58-62 degree range.

4.6) Modifying the Feed Structure

To excite only the first order mode inside the cylindrical cavity of the flanged disk antenna, two symmetric dipoles were placed inside the cavity with opposite current distributions. There are a couple of drawbacks associated with this feeding method. The cost of the two probes and broadband phase shifters is excessive, and the implementation of such a structure is difficult. For these reasons an alternate feed structure using only 1 coaxial probe was examined.

Figures IV-14a and IV-14b illustrate the geometry and radiation characteristics of the single probe excited, flanged disk antenna. The radius of the disk scattering element was calculated using microstrip disk formulations to permit only the dominant mode to propagate. The predicted radiation characteristics (shown in Figure IV-14b) indicate the dominant mode is generated, but the equality and circular symmetry of the E and H-planes is degraded by the excitation of alternate modes. The H-plane pattern in the figure seems to be void of these excess modal components. By altering the E-plane pattern to improve the cross-polarization, it was possible to obtain patterns that were similar to the dual dipole results.

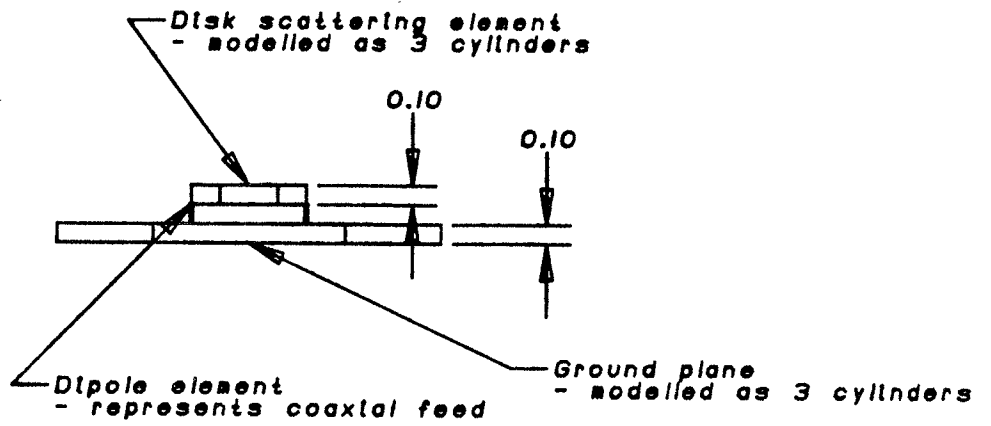
The .05 x .3 wavelength post was again added to the disk scatterer to improve the cross-polarization. Figures IV-15a and IV-15b show the geometry and radiation characteristics of this antenna. The symmetry of the two principal patterns was greatly improved and the cross-polarization reduced by the post. Approximately 1% of the antenna efficiency was lost by the reduction of the E-plane field in the $0 < \theta < 60$ degree range. The results of this modification show that the performance of the single dipole feed may approach those of the dual dipole feed, but further study in this area must be undertaken to determine the true optimum antenna feeding structure.

4.7) Summary of Geometry Modifications

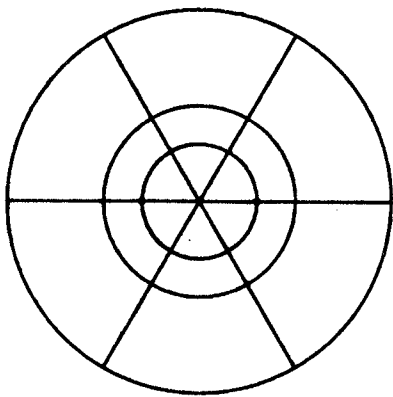
It may be generally concluded that the geometry changes given above were unsuccessful in significantly improving the antenna radiation characteristics. Little effect was noted on the gain factor or sidelobe levels and the -3dB beamwidth was relatively constant. The main reason for this stemmed from the inability of the geometry changes to alter the H-plane pattern. The H-plane pattern remained rigidly constant in the $\theta < 90$ degree region for almost all cases. Since circular symmetry is desired, the radiation and efficiency characteristics were constrained by the H-plane values and could not be altered. However, the E-plane pattern was dependent on many of the modifications and as a result the cross-polarization was easily varied.

The geometry changes may have been unsuccessful in improving the feed performance, but they were useful in illustrating the advantages associated with graphic antenna design techniques. Model modifications were performed in a very efficient manner and the results were quickly and easily interpreted. The results of the above changes ruled out many search variables that may have led to ineffective optimizations.

Front View



Top View



Isometric View

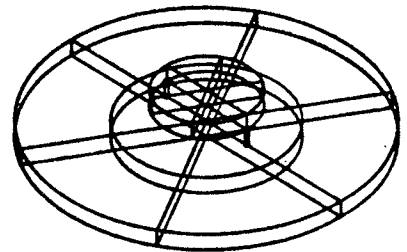
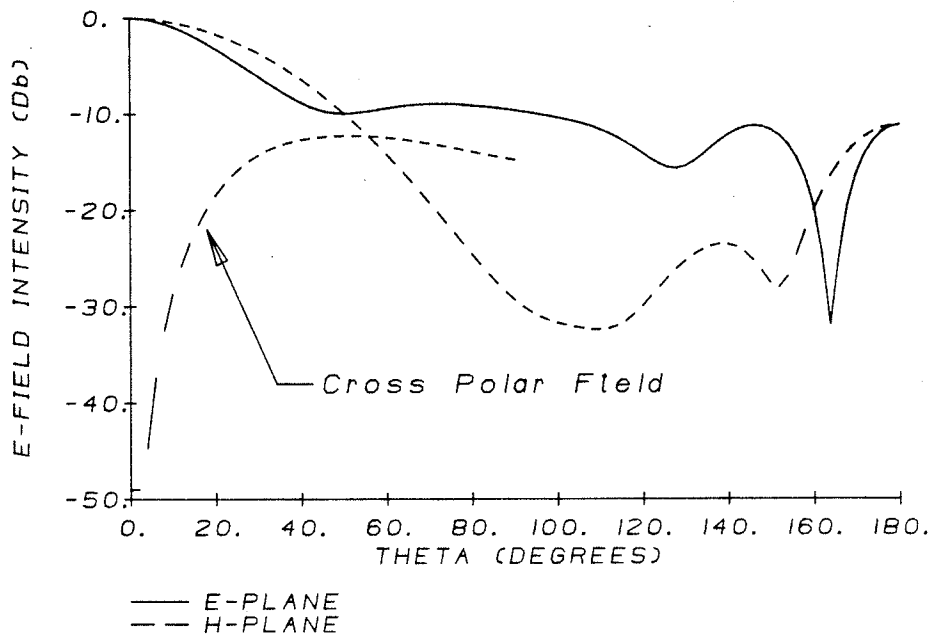


FIGURE IV-1 Disk Antenna modelled Using IGAD-ROT2

FAR FIELD AMPLITUDE PATTERN



PARABOLIC REFLECTOR EFFICIENCY AND GAIN FACTOR

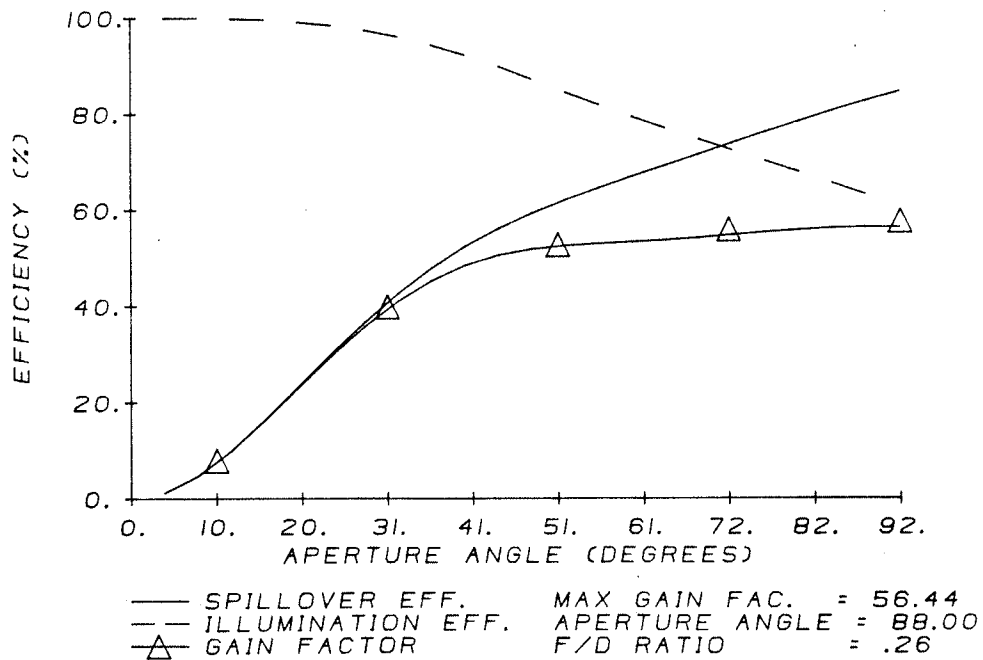
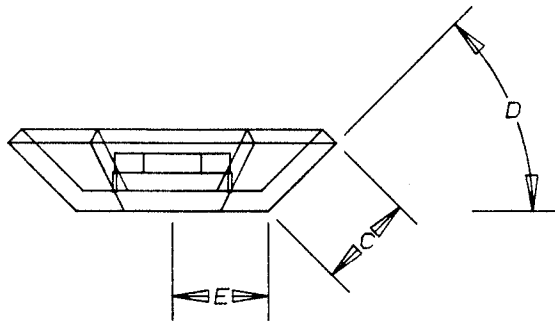
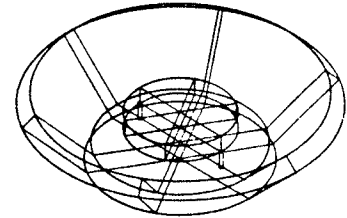


FIGURE IV-2 Radiation Efficiency Characteristics of Disk Antenna (Refer to FIGURE IV-1)

Front View



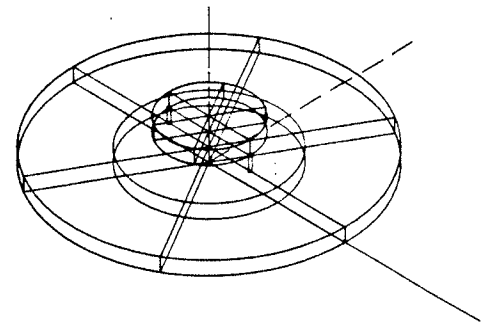
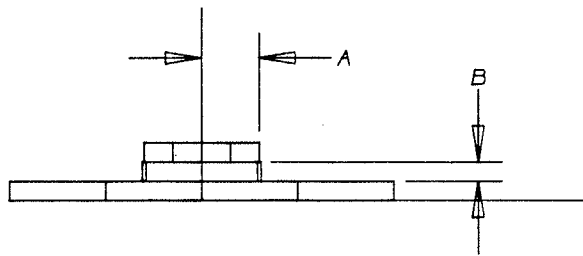
Isometric View



Flanged Disk Antenna

- A = Disk Radius
- B = Disk Height
(above ground plane)
- C = Flange Length
- D = Flange Angle
- E = Ground Plane Radius

- All geometry dimensions are specified with respect to the operating frequency wavelength



Non-Flanged Disk Antenna

FIGURE IV-3 Optimization Variables for Disk Antennas

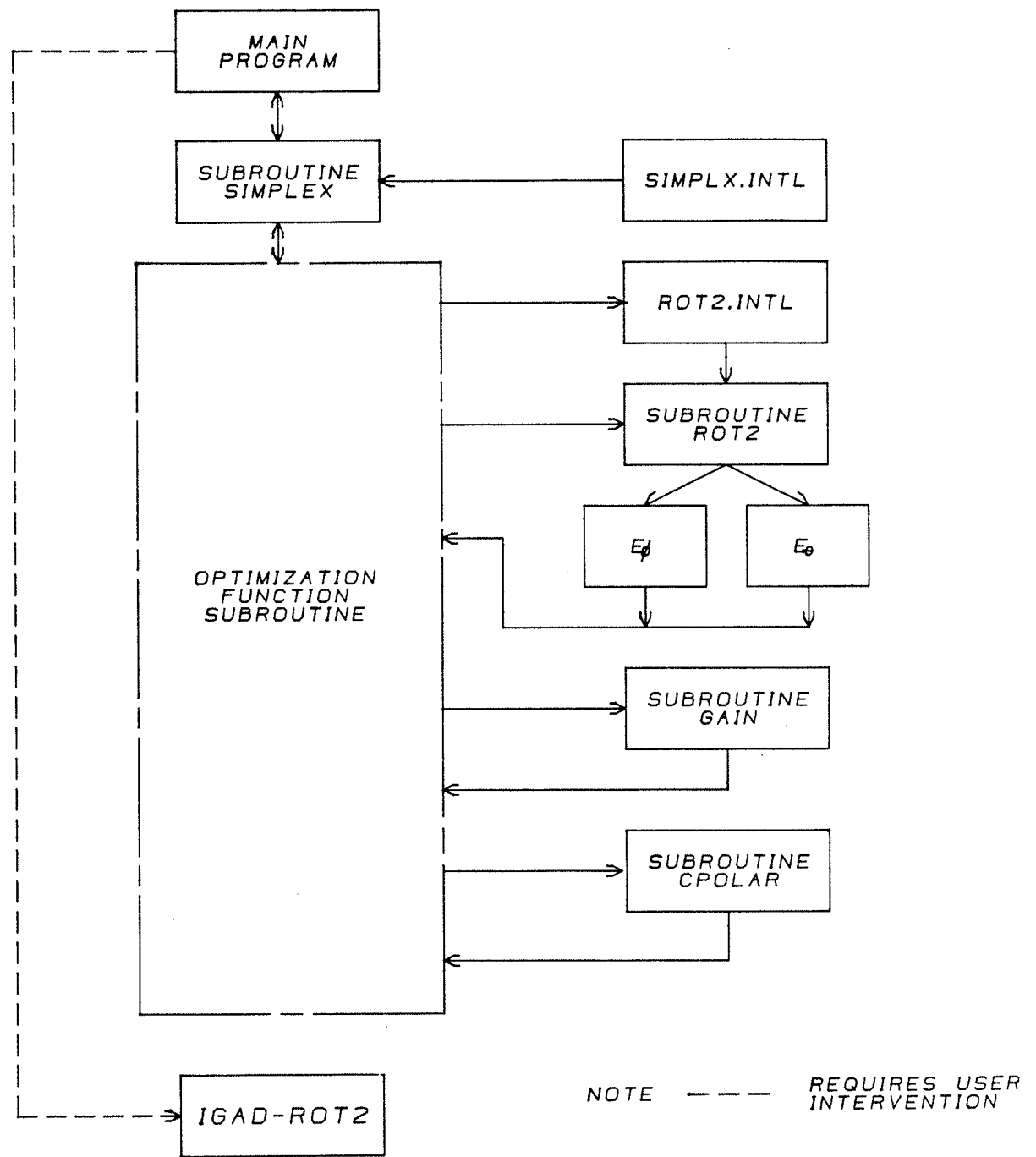
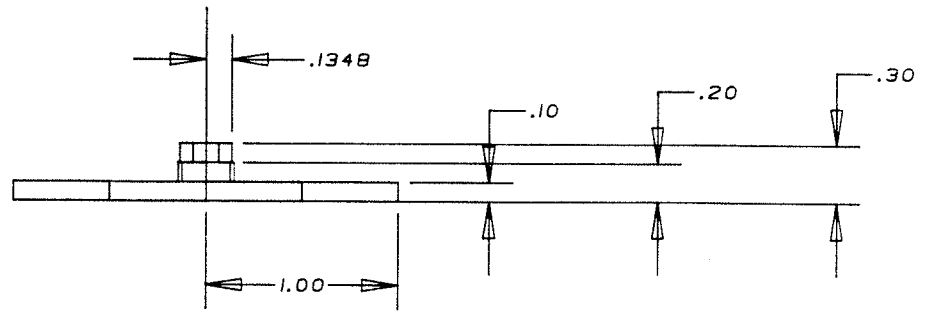


FIGURE IV-4 Optimization Program Structure

Front View



Isometric View

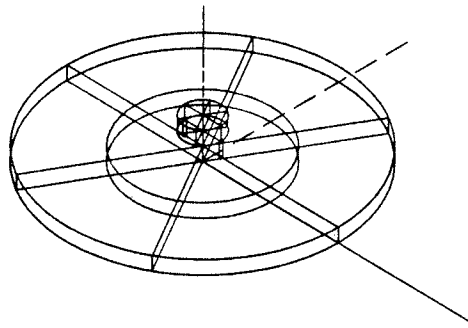
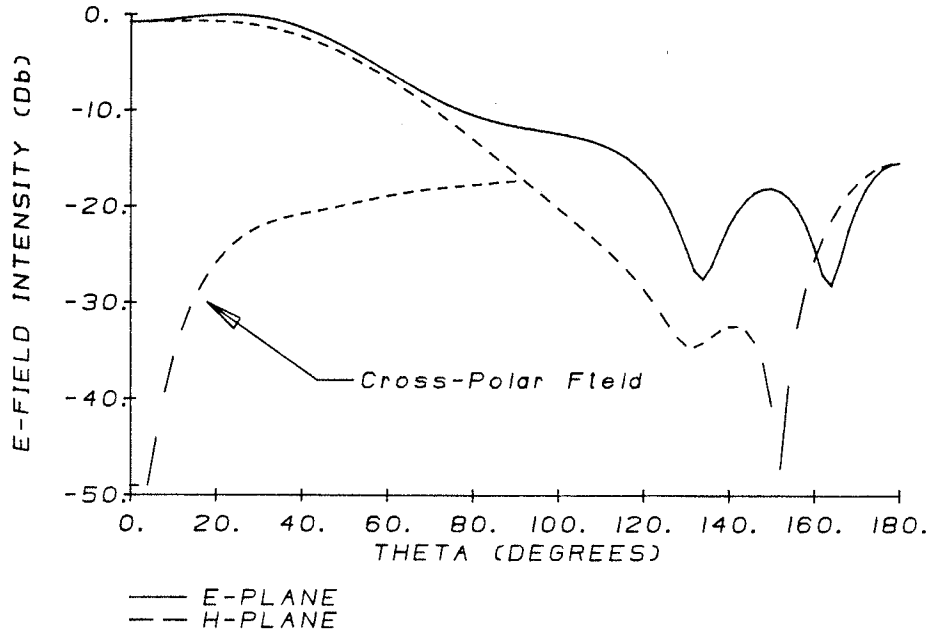


FIGURE IV-5a Constrained Optimization of Non-Flanged Disk Antenna
Cross Polarization $\leq -20\text{dB}$, Disk Height > 0.1

FAR FIELD AMPLITUDE PATTERN



PARABOLIC REFLECTOR EFFICIENCY AND GAIN FACTOR

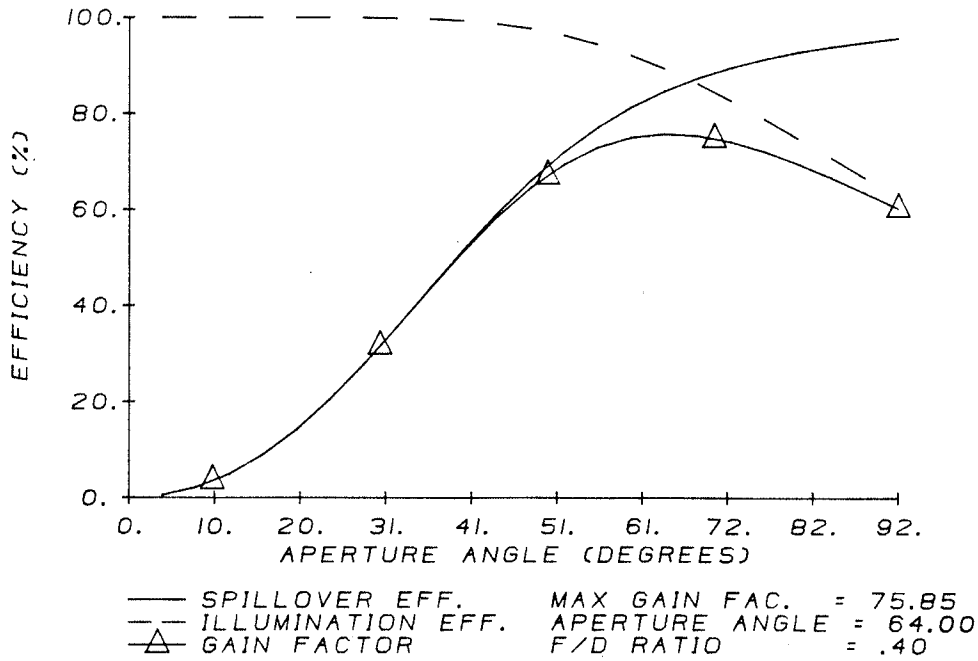
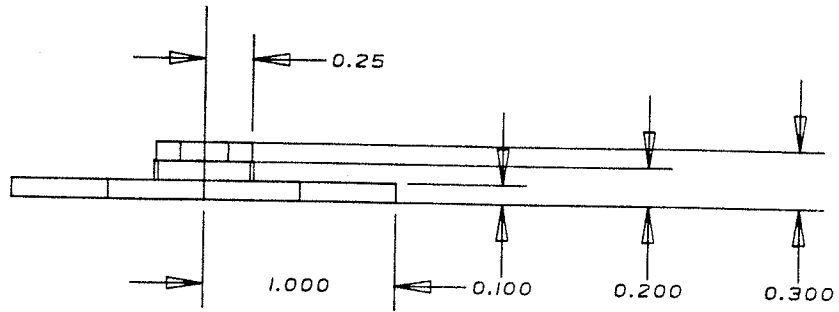


FIGURE IV-5b Constrained Optimization of Non-Flanged Disk Antenna Radiation and Efficiency Characteristics Cross Polarization <-20dB, Disk Height >0.1

Front View



Isometric View

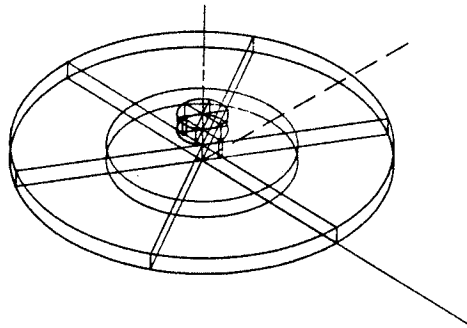
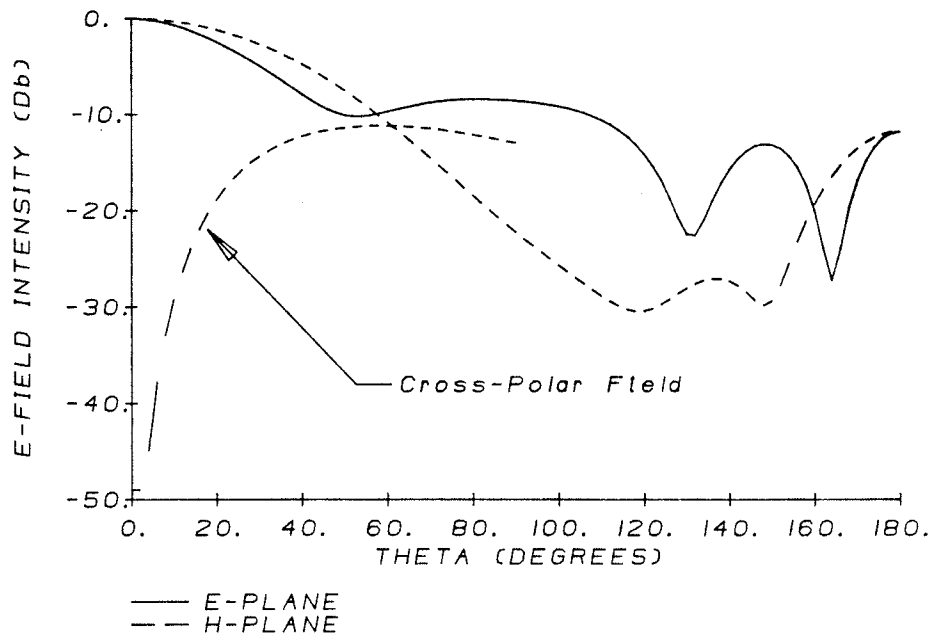


FIGURE IV-6a Constrained Optimization of Non-Flanged Disk Antenna
Cross Polarization ≤ -20 dB, Disk Height > 0.1
Disk Radius > 0.25

FAR FIELD AMPLITUDE PATTERN



PARABOLIC REFLECTOR EFFICIENCY AND GAIN FACTOR

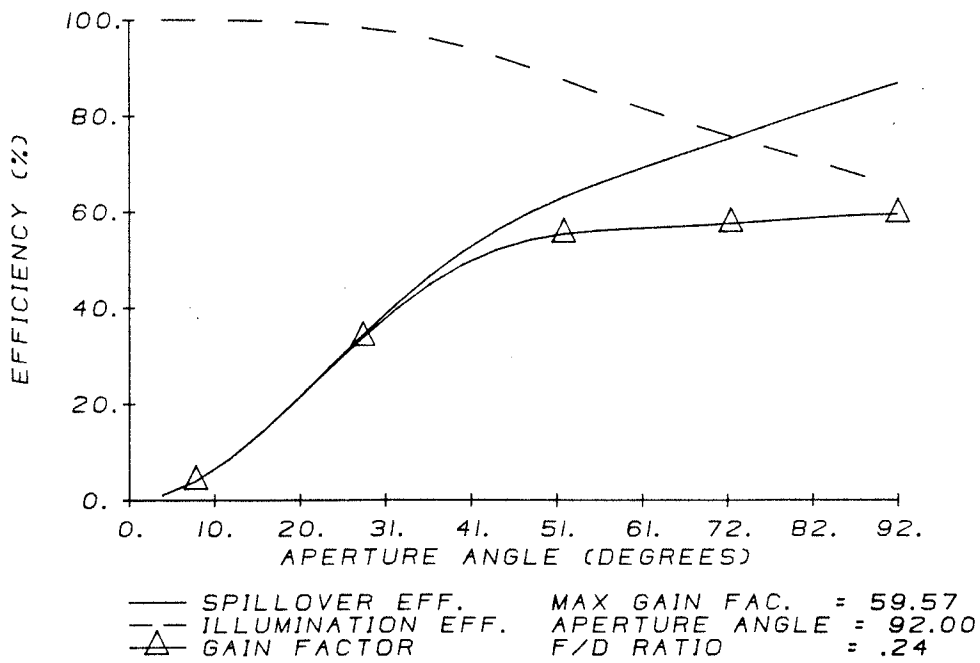
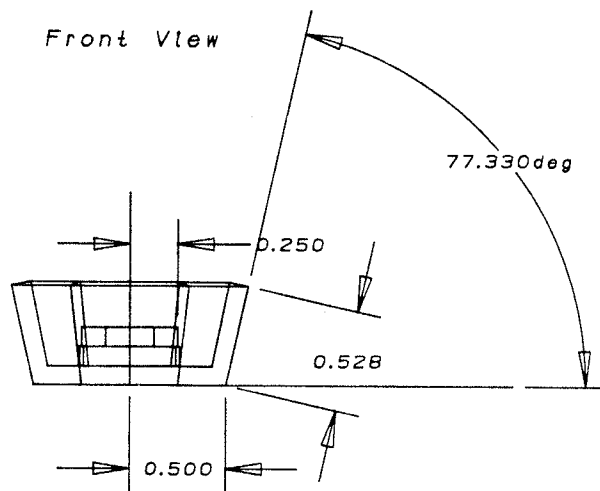


FIGURE IV-6b Constrained Optimization of Non-Flanged Disk Antenna Radiation and Efficiency Characteristics
 Cross Polarization <-20Db, Disk Radius >0.25, Disk Height >0.1



Isometric View

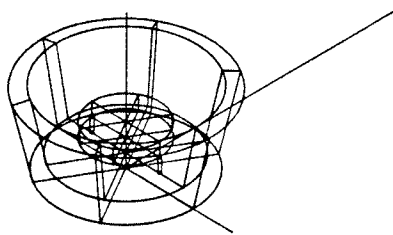
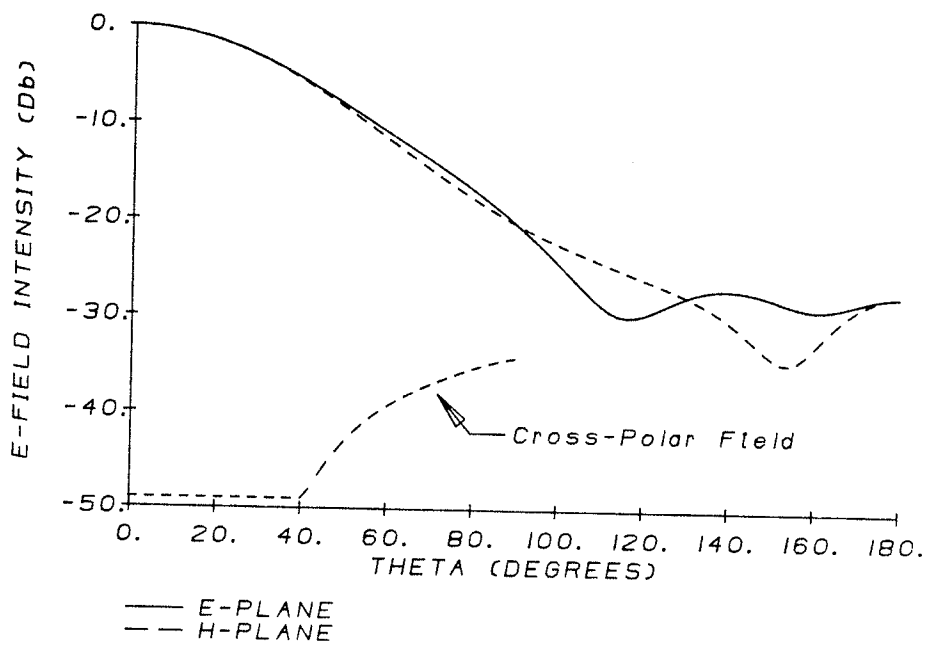


FIGURE IV-7a Constrained Optimization of the Flanged Disk Antenna
 Cross Polarization $\leq -20\text{dB}$, Flange Length ≤ 1.0
 Disk Radius > 0.25 , Disk Height > 0.1

FAR FIELD AMPLITUDE PATTERN



PARABOLIC REFLECTOR EFFICIENCY AND GAIN FACTOR

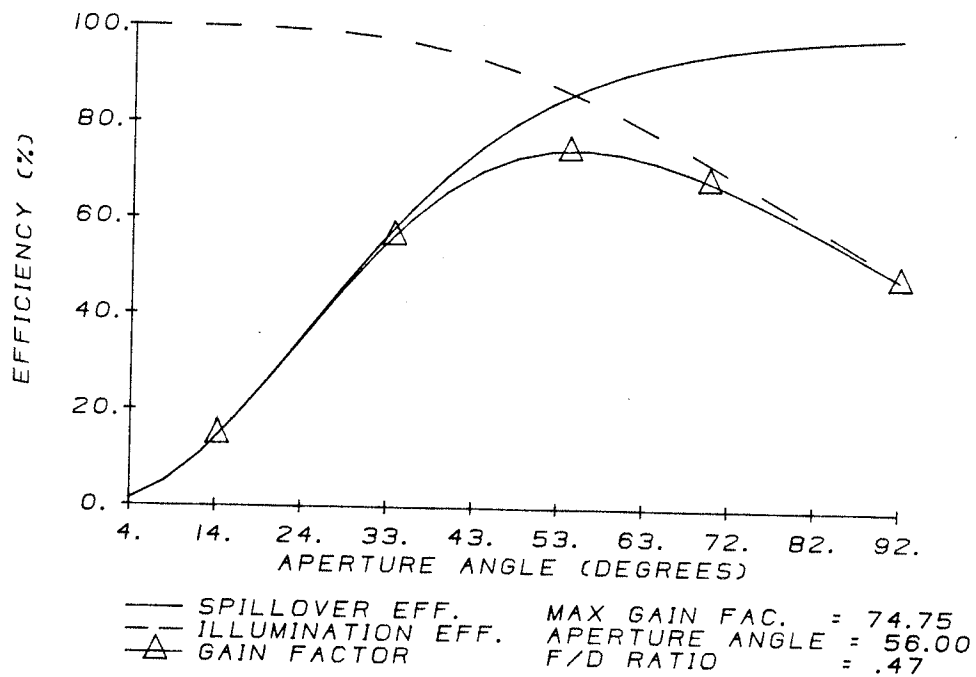
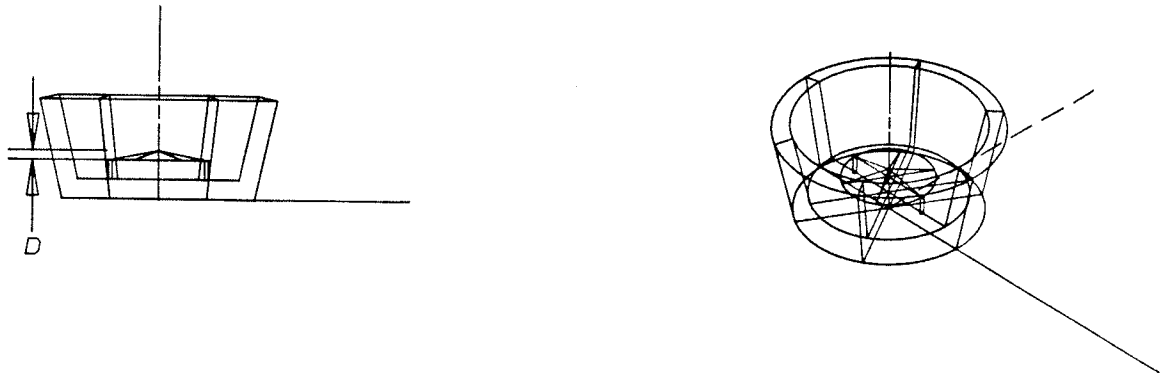


FIGURE IV-7b Constrained Optimization of the Flanged Disk Antenna Radiation and Efficiency Characteristics
 Cross Polarization <-20dB, Flange Length <1.0
 Disk Radius >0.25, Disk Height >0.1



FAR FIELD AMPLITUDE PATTERN

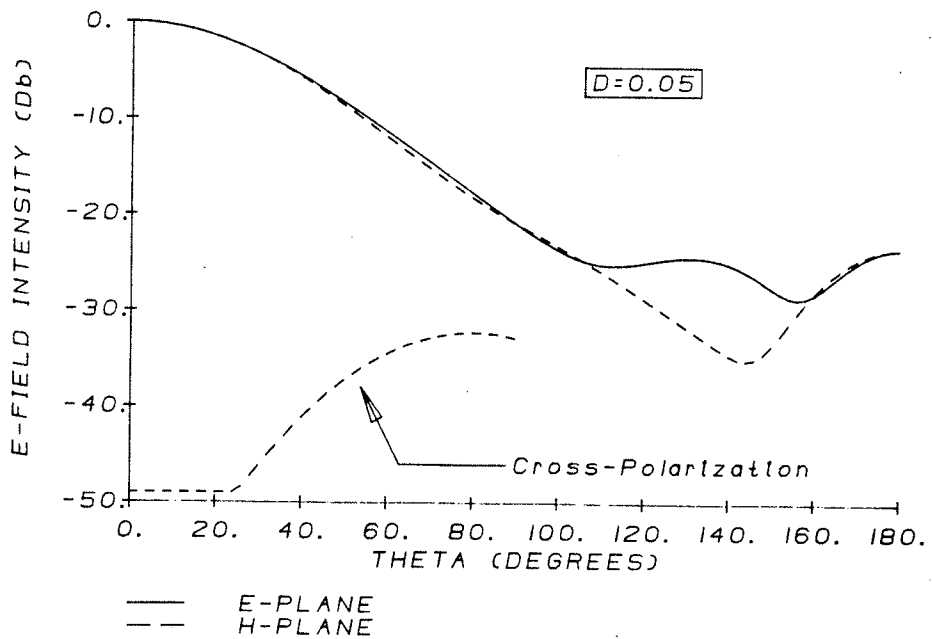
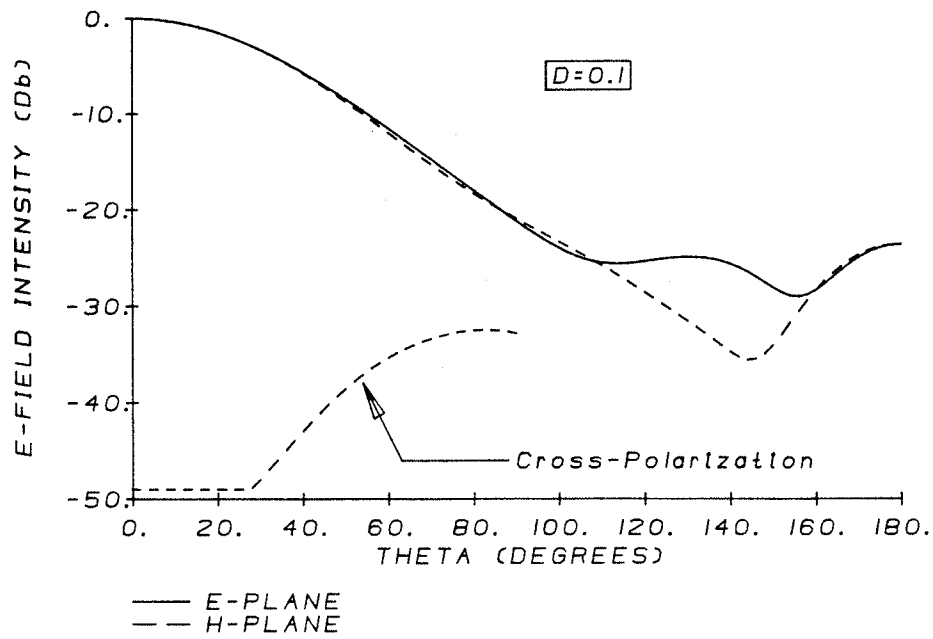


FIGURE IV-8a Conic Disk Antenna Radiation Characteristics
Cone Peak Away from Ground Plane

FAR FIELD AMPLITUDE PATTERN



FAR FIELD AMPLITUDE PATTERN

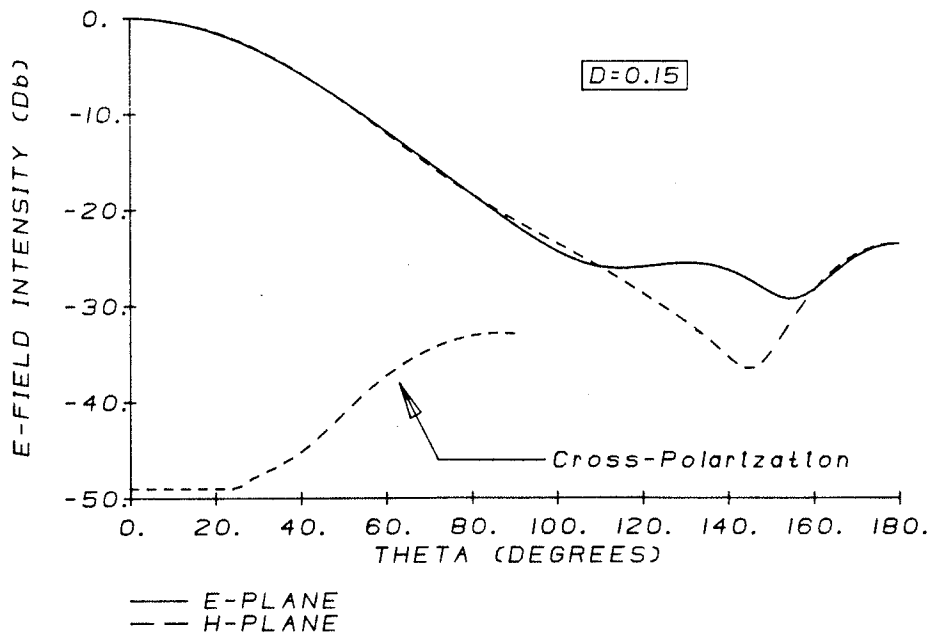
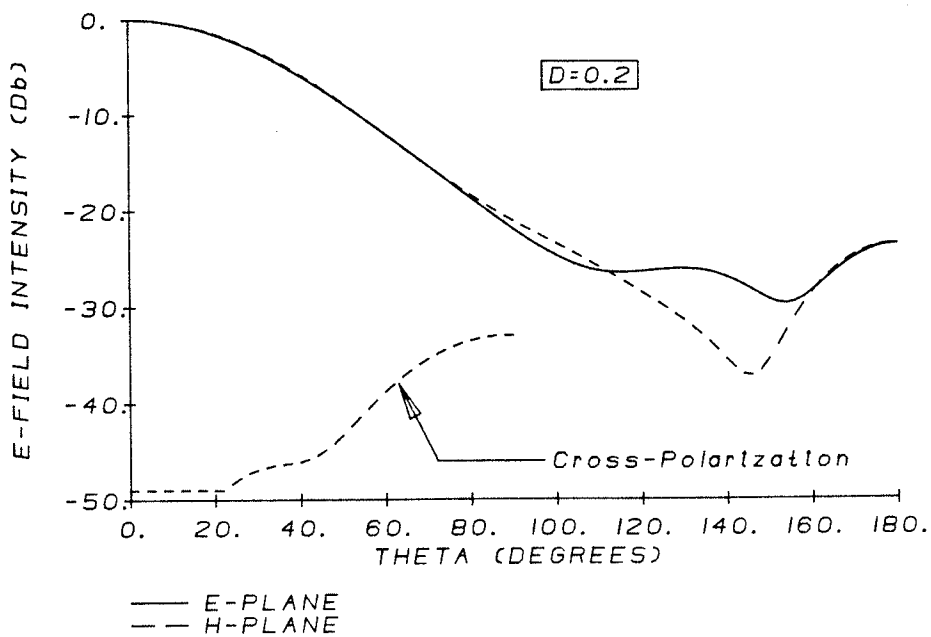


FIGURE IV-Bb Conic Disk Antenna Radiation Characteristics
Cone Peak Away from Ground Plane
(Refer to FIGURE IV-8a)

FAR FIELD AMPLITUDE PATTERN



FAR FIELD AMPLITUDE PATTERN

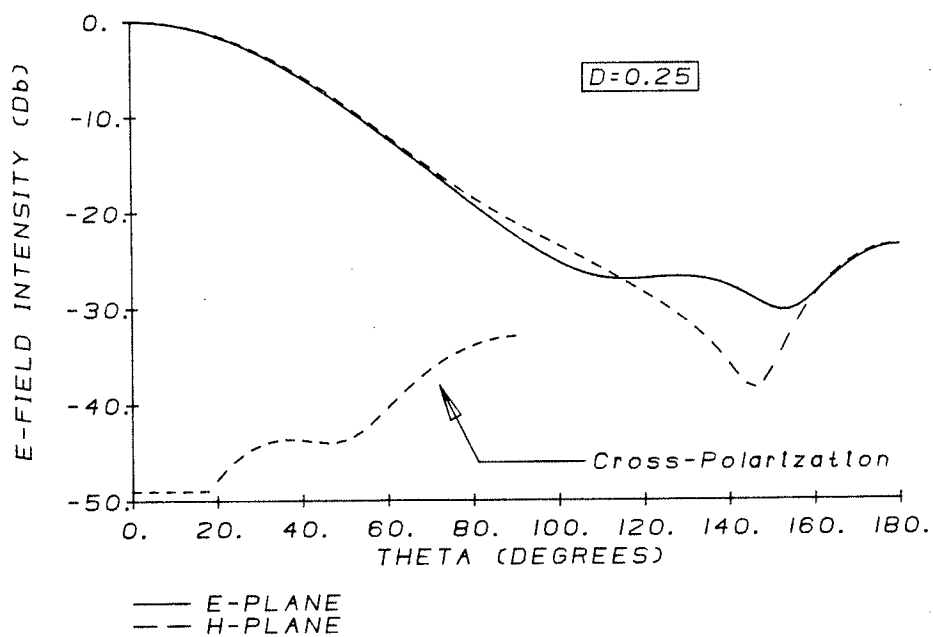
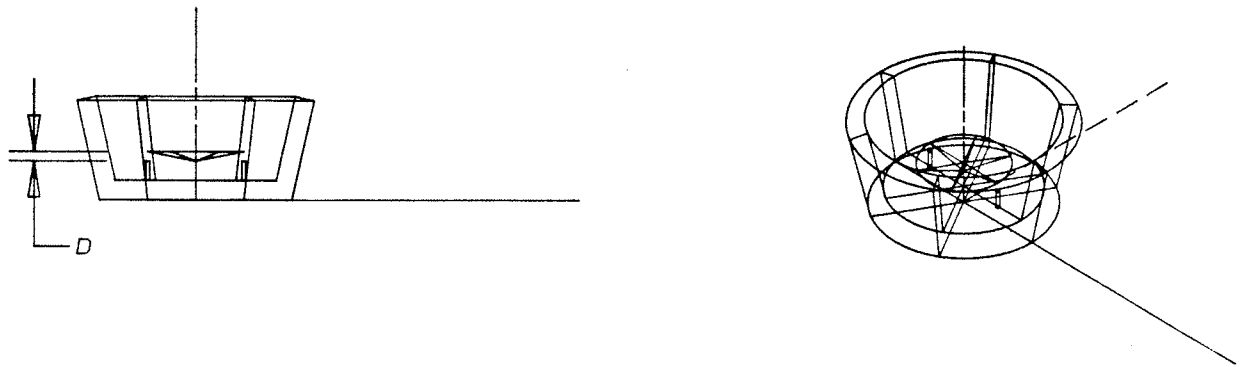


FIGURE IV-8c Conic Disk Antenna Radiation Characteristics
Cone Peak Away from Ground Plane
(Refer to FIGURE IV-8a)



FAR FIELD AMPLITUDE PATTERN

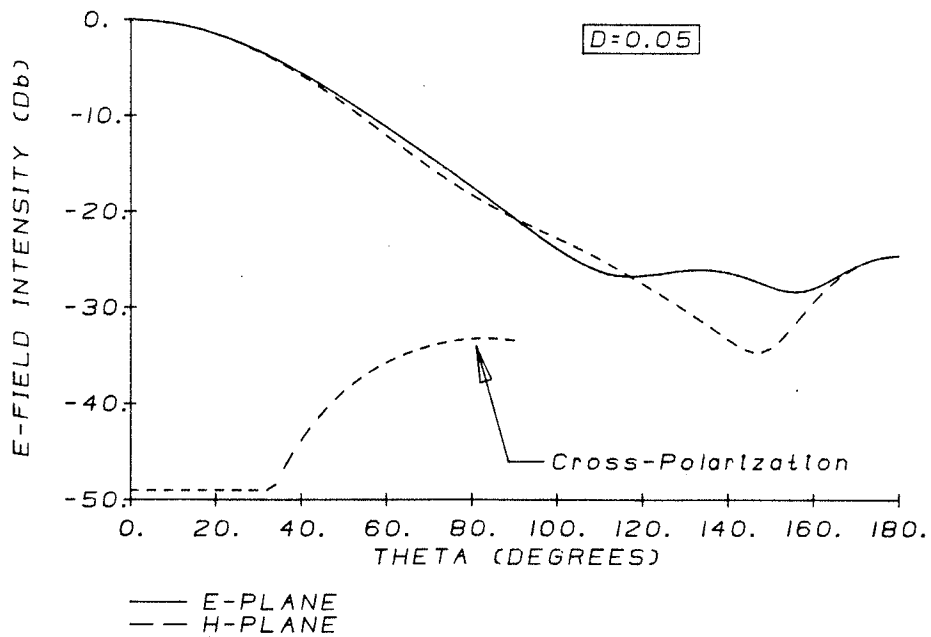
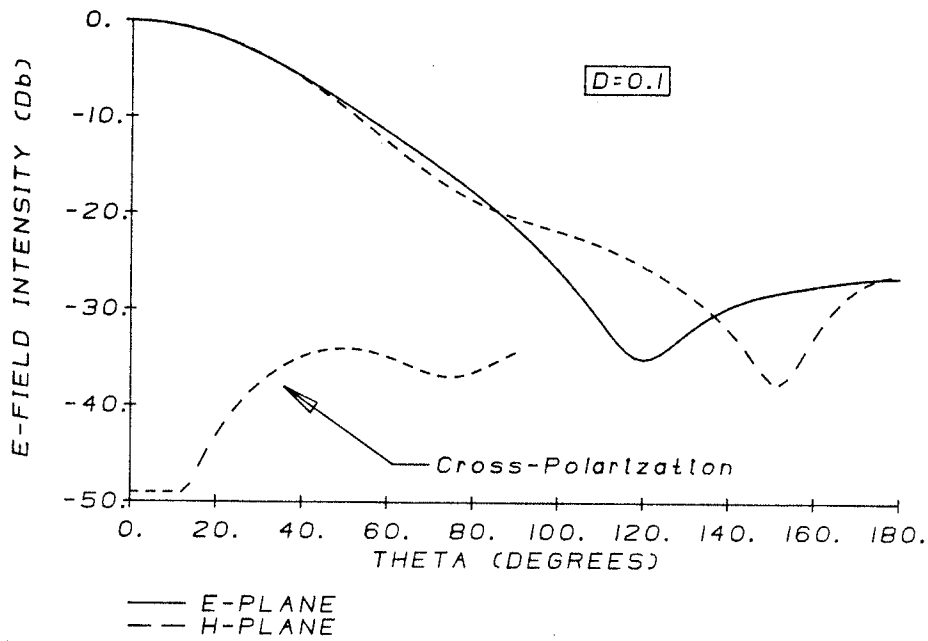


FIGURE IV-9a Conic Disk Antenna Radiation Characteristics
Conic Peak Towards the Ground Plane

FAR FIELD AMPLITUDE PATTERN



FAR FIELD AMPLITUDE PATTERN

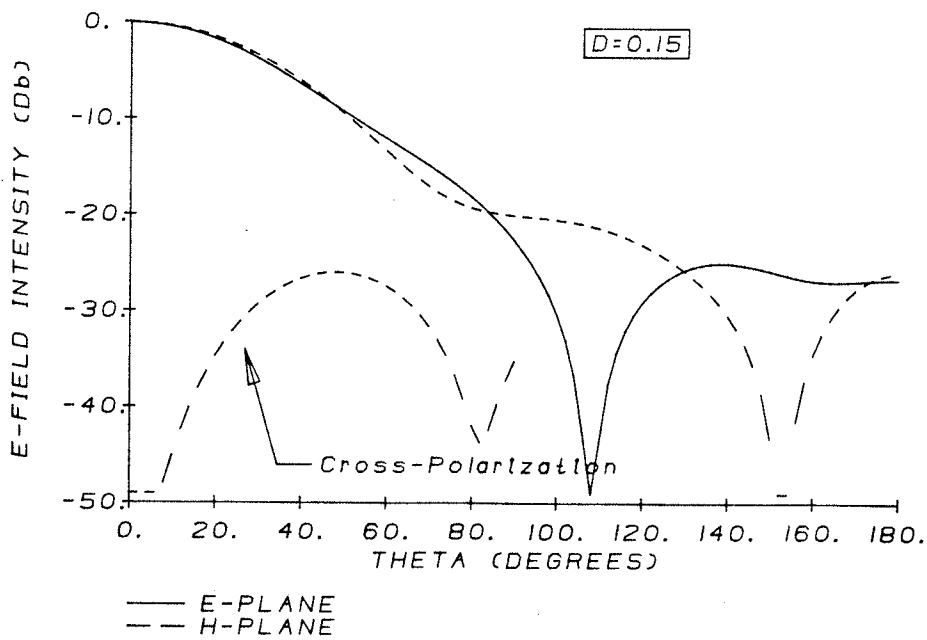
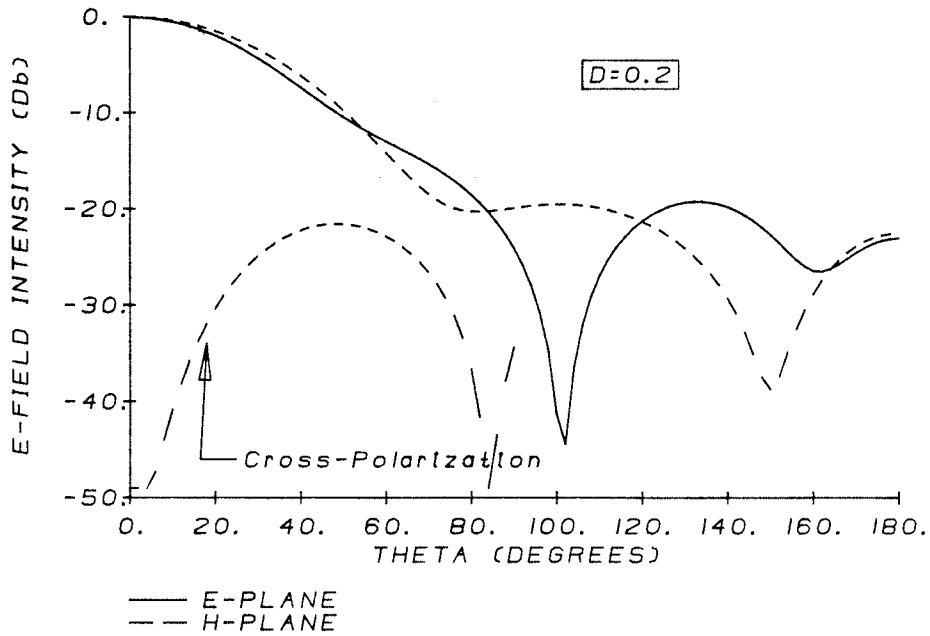


FIGURE IV-9b Conic Disk Antenna Radiation Characteristics
Conic Peak Towards the Ground Plane
(Refer to FIGURE IV-9a)

FAR FIELD AMPLITUDE PATTERN



FAR FIELD AMPLITUDE PATTERN

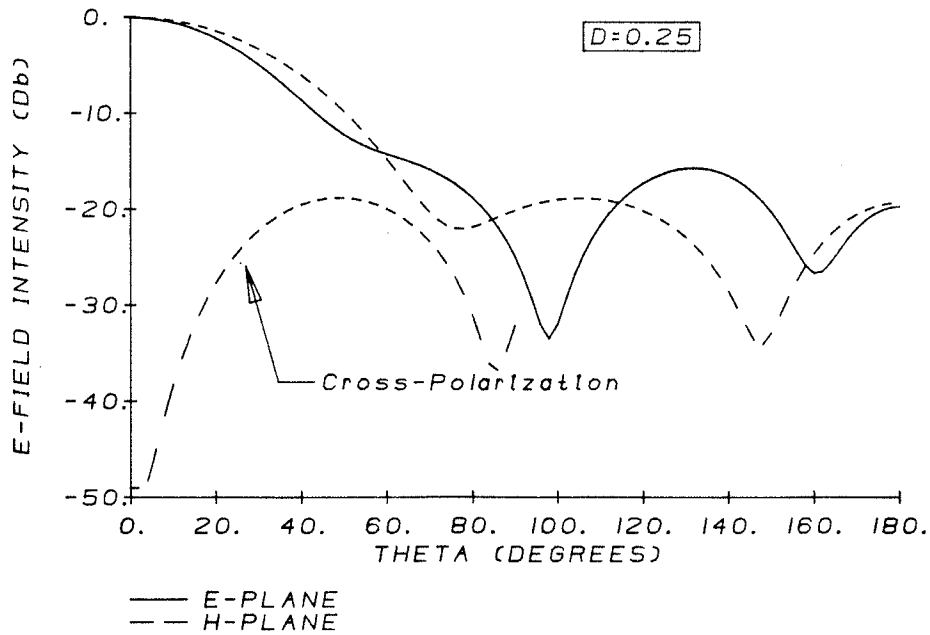
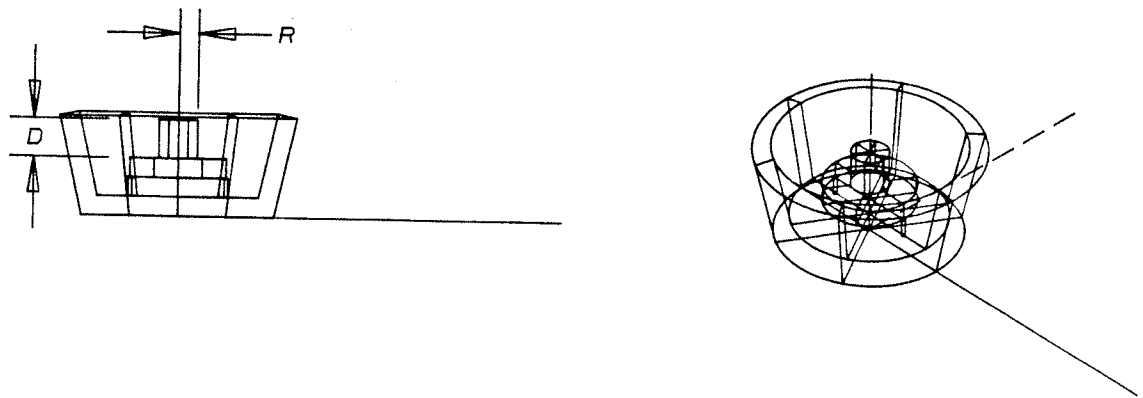


FIGURE IV-9c Conic Disk Antenna Radiation Characteristics
Conic Peak Towards the Ground Plane
(Refer to FIGURE IV-9a)



FAR FIELD AMPLITUDE PATTERN

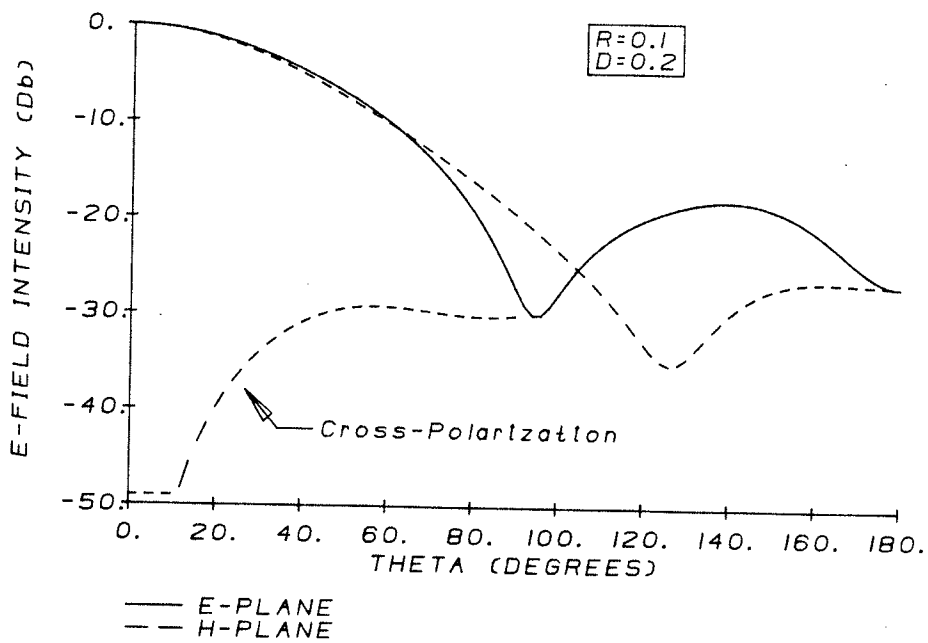
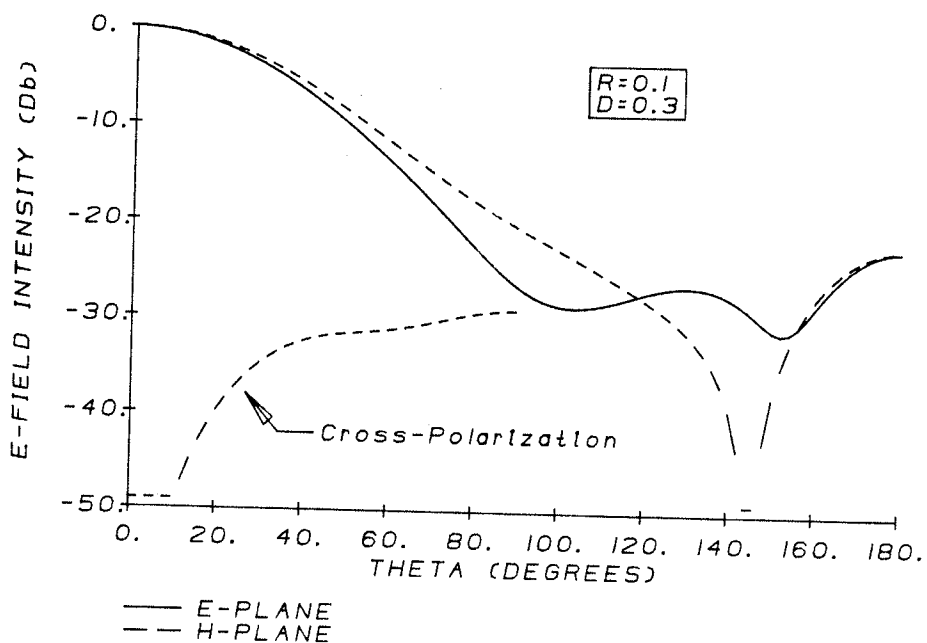


FIGURE IV-10a Disk Antenna with External Post Radiation Characteristics

FAR FIELD AMPLITUDE PATTERN



FAR FIELD AMPLITUDE PATTERN

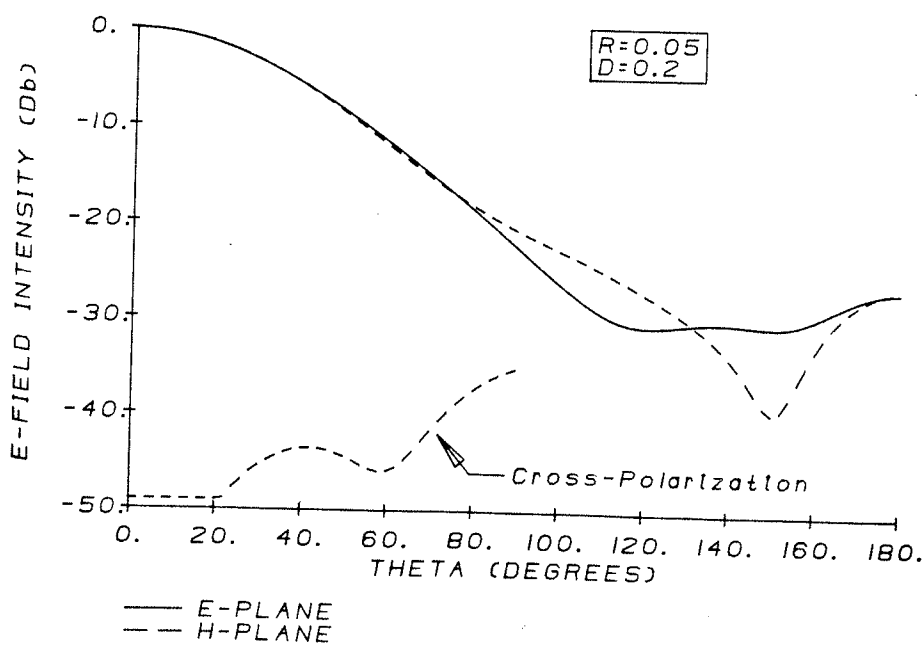
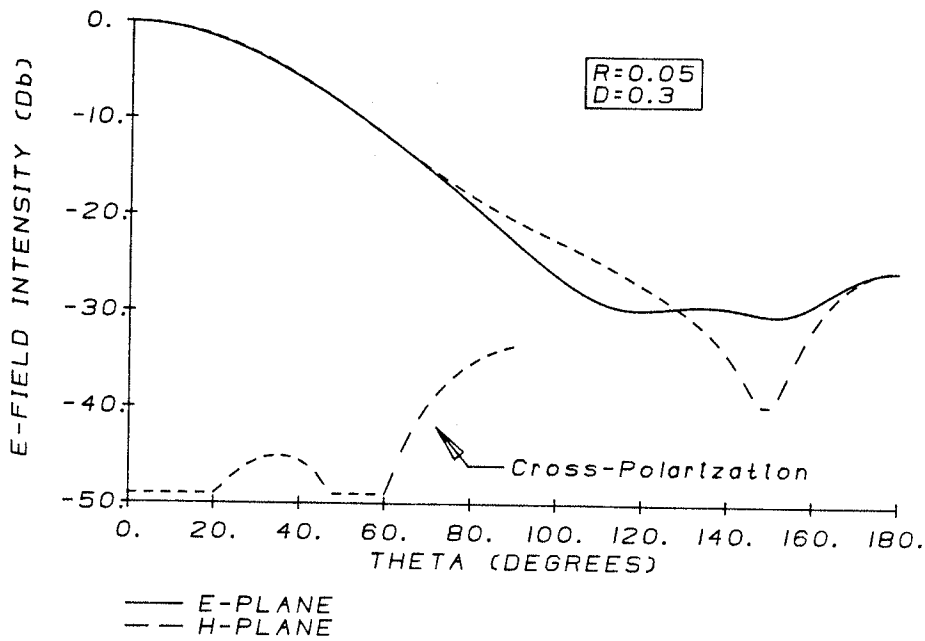


FIGURE IV-10b Disk Antenna with External Post Radiation Characteristics (Refer to FIGURE IV-10a)

FAR FIELD AMPLITUDE PATTERN



FAR FIELD AMPLITUDE PATTERN

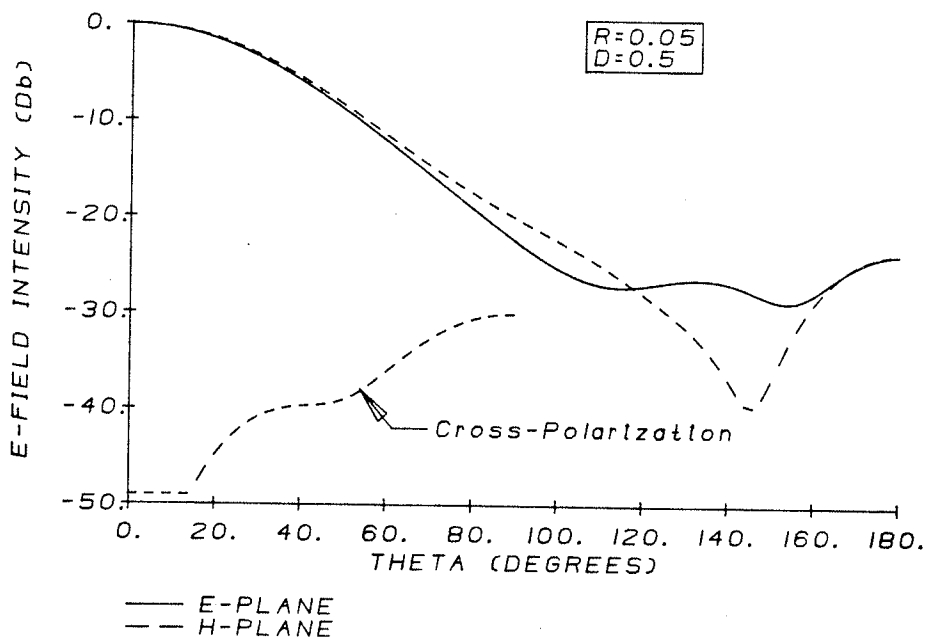
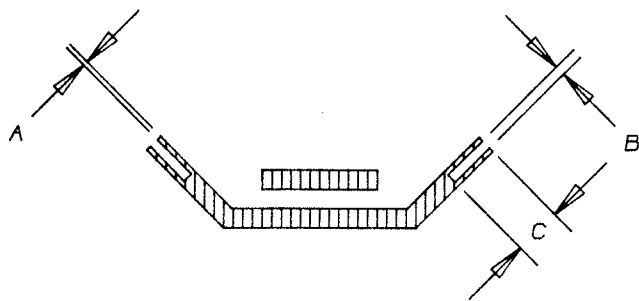


FIGURE IV-10c Disk Antenna with External Post Radiation Characteristics (Refer to FIGURE IV-10a)

Choke on Flange Rlm



- A = Choke Wall Width
- B = Choke Silt Width
- C = Choke Silt Depth
- D = External Choke Silt Width

External Choke on Flanged Rlm

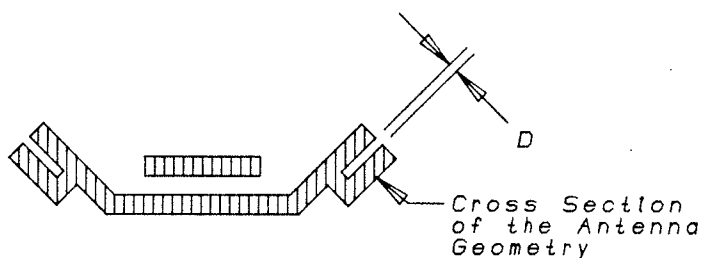
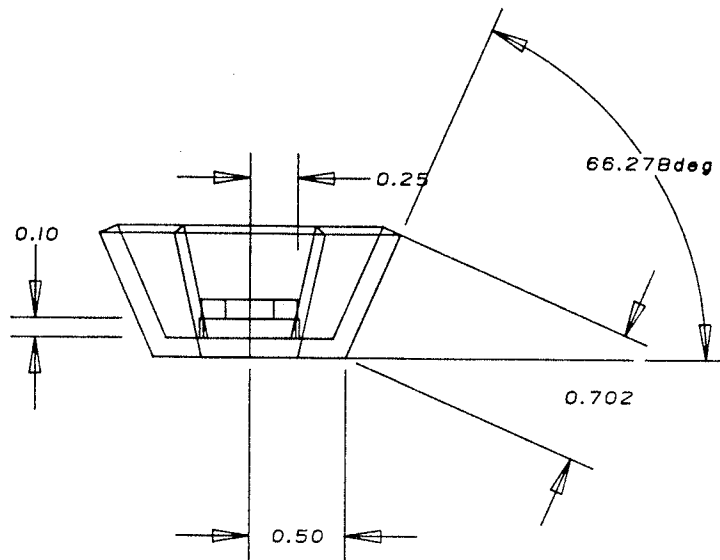


FIGURE IV-II Modification Parameters for the Normal and External Choke Types

Front View



Isometric View

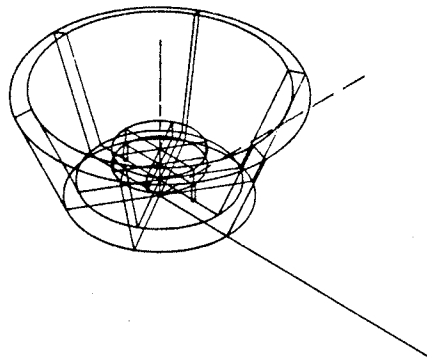
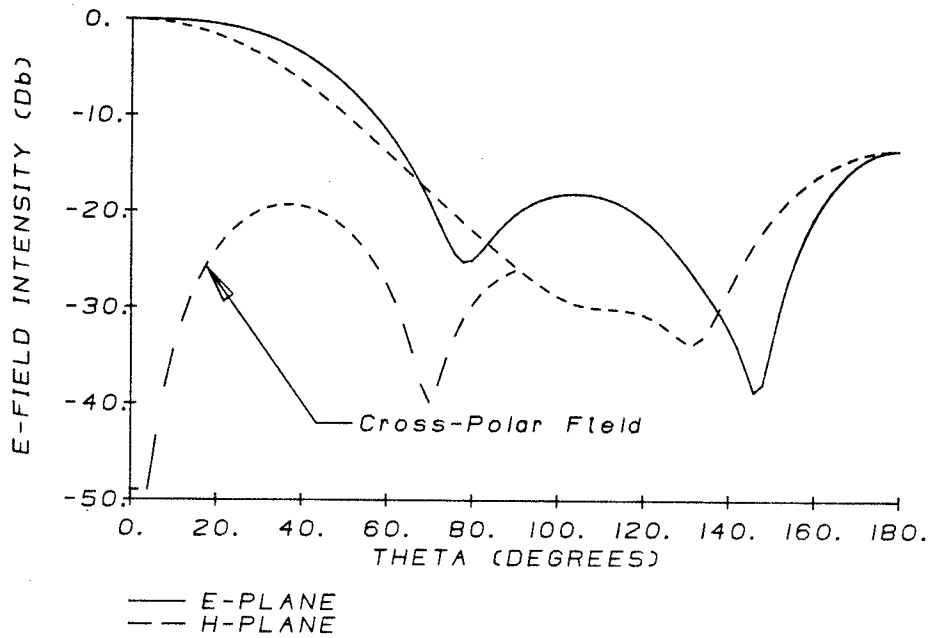


FIGURE IV-12a Constrained Optimization of the Flanged Disk Antenna
Flange Length >1.0 , Disk Length <0.25 ,
Disk Height >0.1

FAR FIELD AMPLITUDE PATTERN



PARABOLIC REFLECTOR EFFICIENCY AND GAIN FACTOR

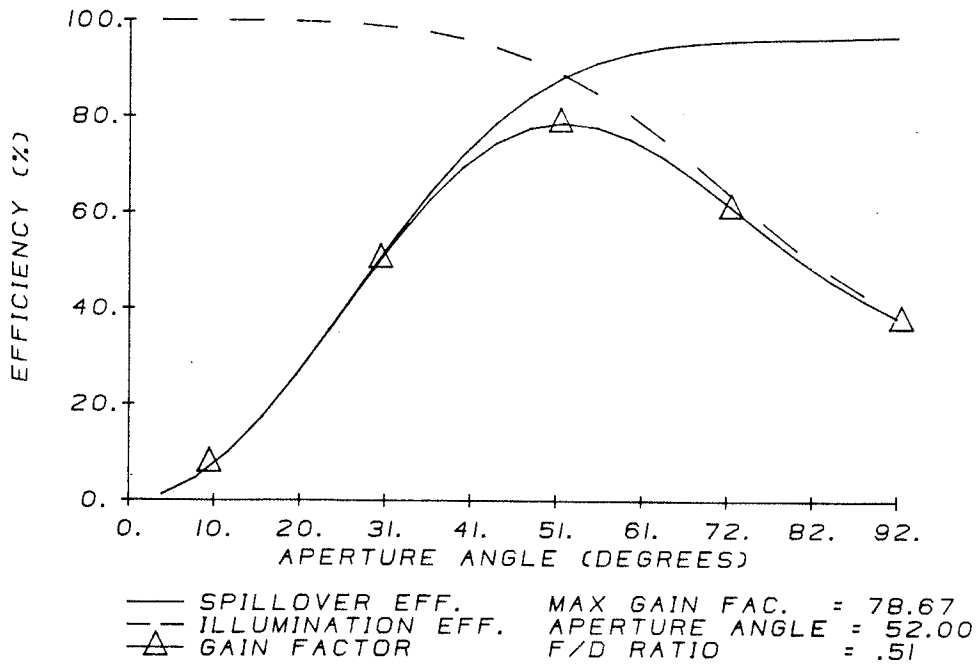
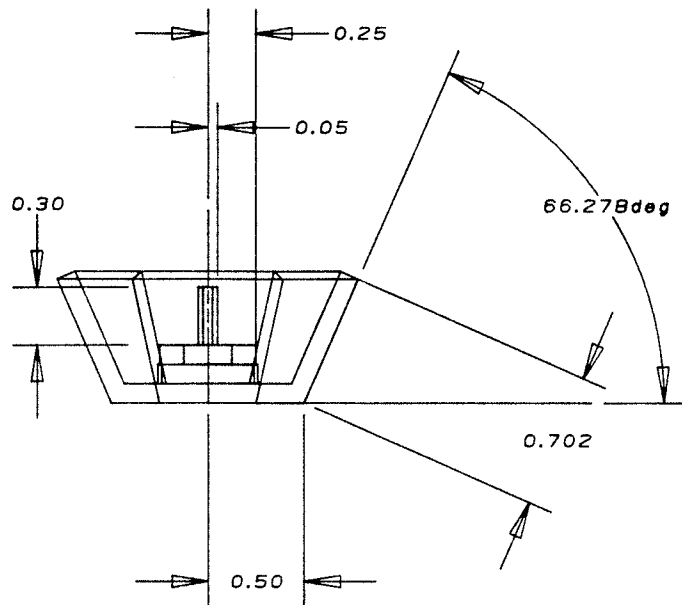


FIGURE IV-12b Constrained Optimization of the Flanged Disk Antenna Radiation and Efficiency Characteristics
 Flange Length > 1 , Disk Length $< .25$,
 Disk Height $> .1$

Front View



Isometric View

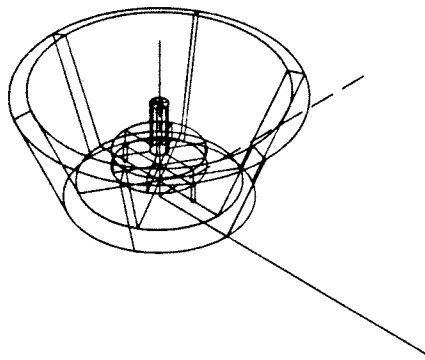
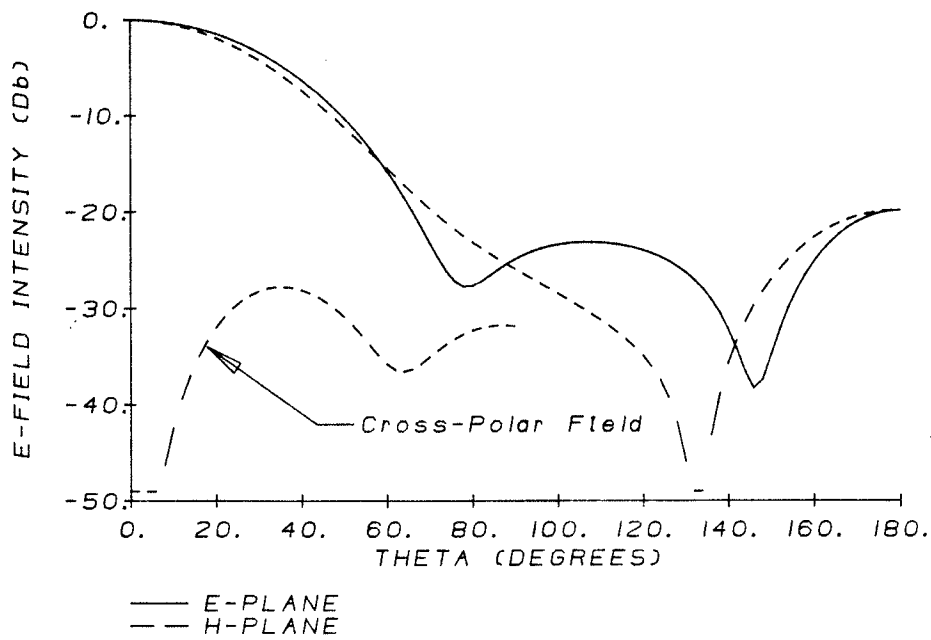


FIGURE IV-13a Flanged Disk Antenna with External Post

FAR FIELD AMPLITUDE PATTERN



PARABOLIC REFLECTOR EFFICIENCY AND GAIN FACTOR

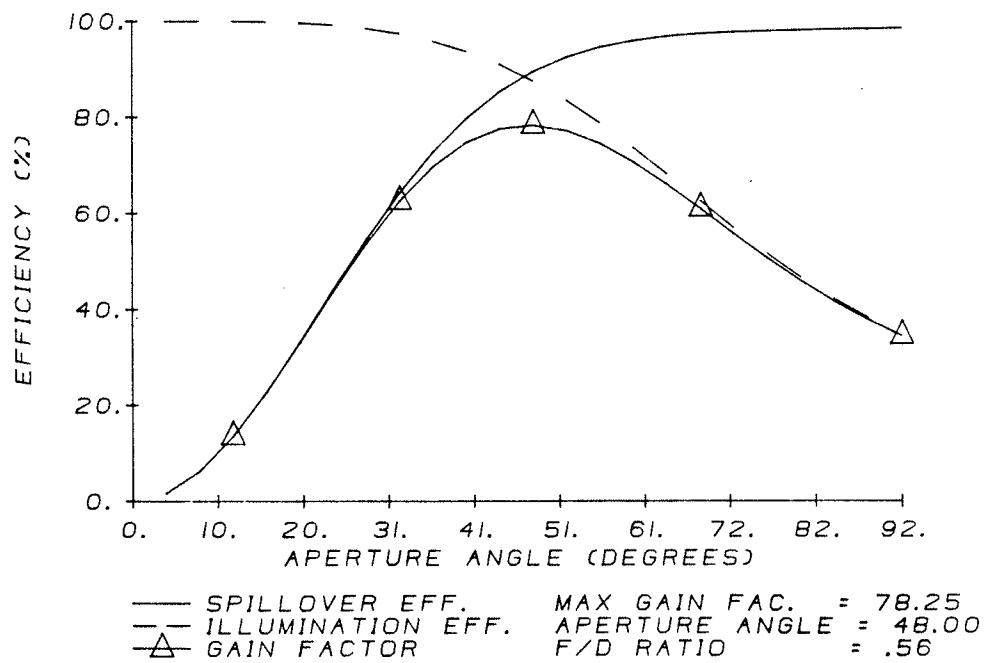
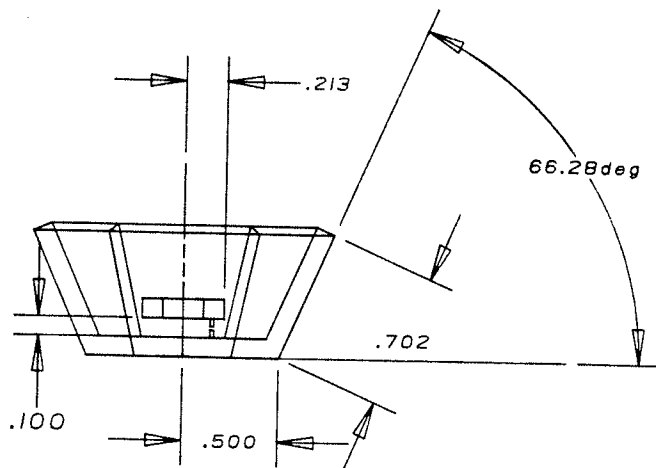


FIGURE IV-13b Flanged Disk Antenna with External Post Radiation and Efficiency Characteristics (Refer to FIGURE IV-13a)

Front View



Isometric View

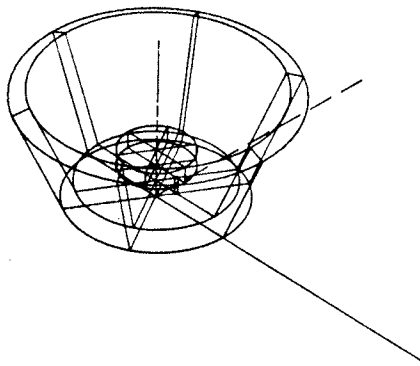
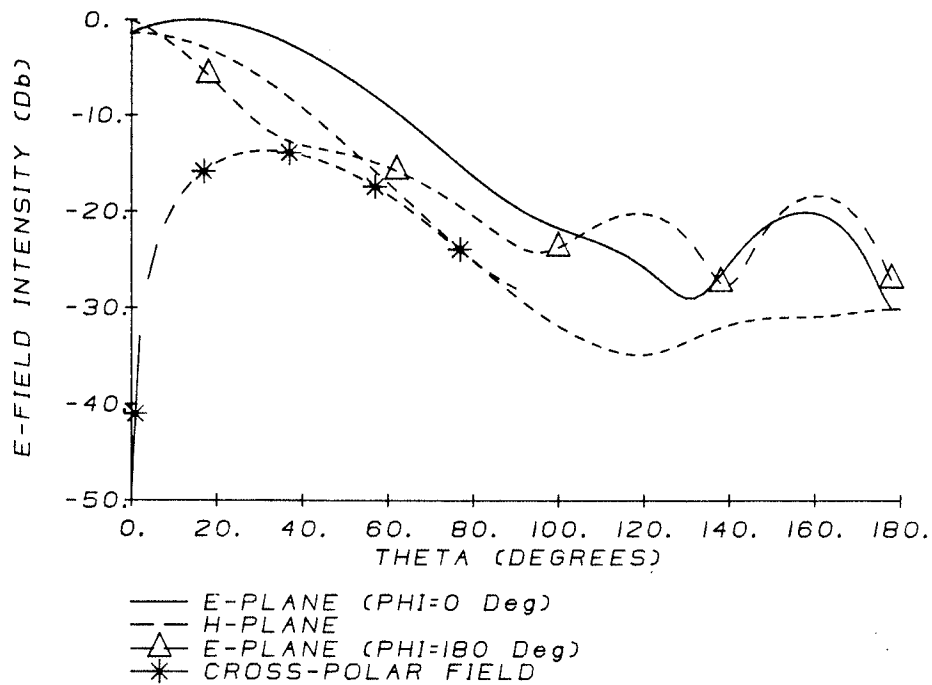


FIGURE IV-14a Single Dipole Fed Flanged Disk Antenna

FAR FIELD AMPLITUDE PATTERN



PARABOLIC REFLECTOR EFFICIENCY AND GAIN FACTOR

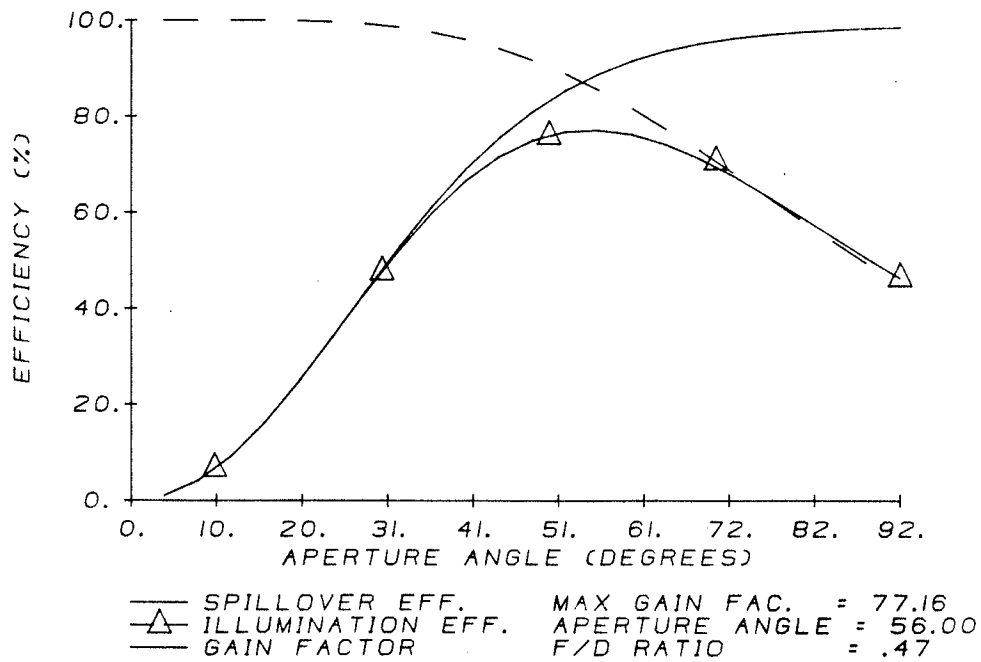
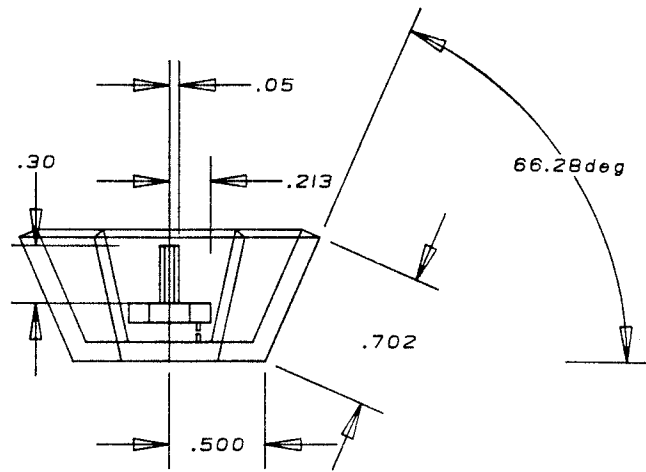


FIGURE IV-14b Single Dipole Fed Flanged Disk Antenna Radiation and Efficiency Characteristics (Refer to FIGURE IV-14a)

Front View



Isometric View

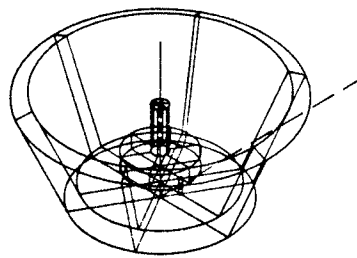
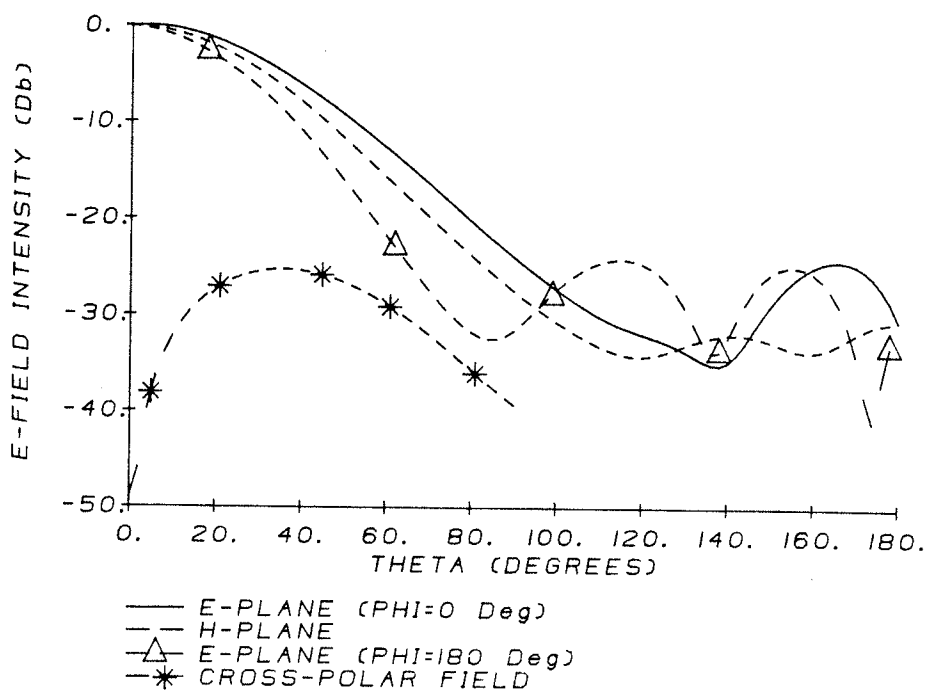


FIGURE IV-15a Single Dipole Fed Flanged Disk Antenna with External Post

FAR FIELD AMPLITUDE PATTERN



PARABOLIC REFLECTOR EFFICIENCY AND GAIN FACTOR

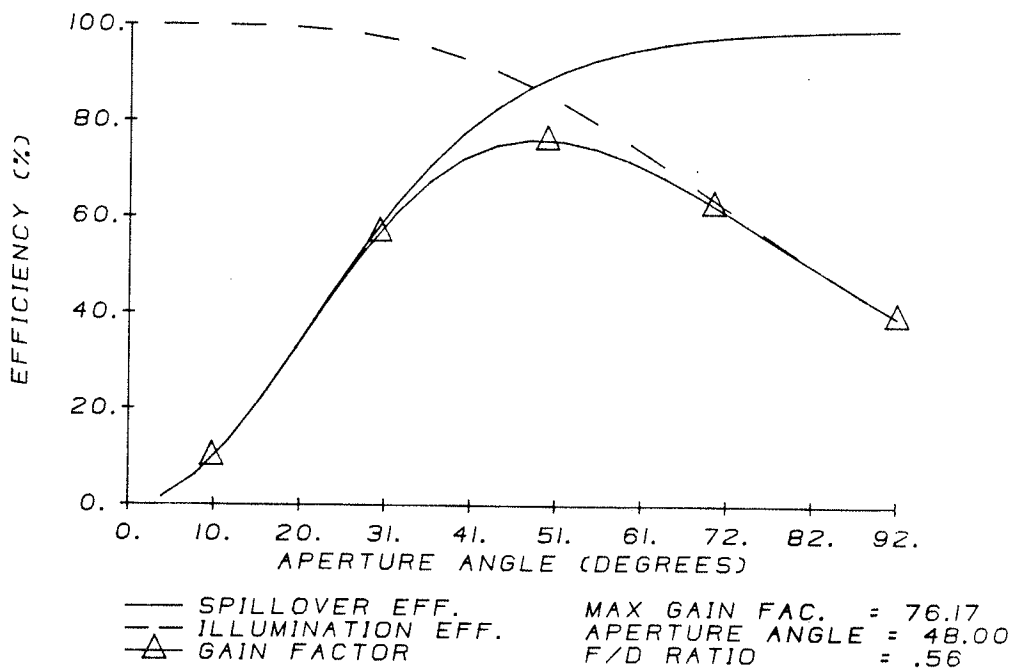


FIGURE IV-15b Single Dipole Fed Flanged Disk Antenna with External Post Radiation and Efficiency Characteristics (Refer to FIGURE IV-15a)

CHAPTER V

CONCLUDING REMARKS AND FUTURE DEVELOPMENTS

5.1) IGAD-ROT2

Presented in this paper is the Interactive Graphic Antenna Design package and its application to paraboloid reflector feed design. The IGAD-ROT2 system was developed as a graphic pre and post processor for ROT2 to accomplish the following:

- Relieve the menial chores associated with computer assisted antenna modelling and editing.
- Visually present the antenna and its radiation characteristics.
- Be used as a learning aid.
- Heighten the understanding of antenna fundamentals.
- Provide a database for future development of an antenna structural analysis system.
- Produce high quality production drawings.

The attributes of the system were examined using a prime focus feed as an example. Aside from the advantages of CAD listed above, the graphic system also made possible a couple of

enhancements not found in ROT2. The submodel option enables the designer to work concurrently with several models. As a result, a reduction of storage requirements, and model creation, editing, and file handling time is realized. The required user knowledge of IGAD-ROT2 is reduced by the connectivity data associated with each geometrical shape. This data ensures each contour is properly created. Any violations are brought to the designers attention.

A user oriented on-screen menu of graphic symbols and names is used to enter all commands and numeric data. Two menus are provided, one for the construction mode, and the other for the plot mode. Although the basic pre and post processing functions of ROT2 are handled by IGAD-ROT2, several areas of software development must be addressed to complete the package. A list of the future developments are given below

- 1) Add modification subroutines to enable editing of all commands
- 2) Add radial and three dimensional plots.
- 3) Add predefined multiple contour commands such as ground planes, cones, and feed horns and have the modification commands affect the entire scatter.
- 4) Integrate interactive optimization techniques.
- 5) Merge IGAD database with structural analysis software.

5.2) Disk Antenna

The IGAD-ROT2 package was used to design a unique paraboloid feed antenna. The flanged disk antenna resulted from modifications to the circular metal ground plane of a simple disk antenna. Because of its simple geometry, this antenna lends itself to mass production techniques such as stamping. The disk antenna was conceived using the electromagnetic fundamentals of the printed microstrip disk antennas. Two different antenna geometries resulted. Unfortunately neither design satisfied the prime focus feed requirements that have been established by corrugated horns. A comparison of the two antenna radiation and efficiency characteristics is presented below with some expected results.

TABLE IV-1 Comparison of Flanged Antennas

	Antenna 1	Antenna 2	Expected Results
Max.Gain Factor	74.75%	78.25%	80.0%
Aperture Angle	56.0 deg	48.0 deg	60.0 deg
Cross-Pol.	-33.0 dB	-28.2 dB	-30.0 db
Sidelobe Level	-27.1 db	-20.0 dB	-30.0 dB

Note - Antenna 1 = Flanged disk antenna optimized with respect to the gain factor and cross-polarization
- Antenna 2 = Flanged disk antenna optimized with respect to the gain factor only

From the above table, it can be seen that both antennas fell short of the 80% efficiency mark and exhibited high sidelobe levels. The maximum cross-polarization level of Antenna 1 was better than anticipated. The inability to meet the above design parameters stemmed from the rigid nature of the H-plane field. Few of the modifications performed were able to alter the H-plane radiation intensity significantly and the ones that did, degraded the antenna performance. This made it difficult to increase the efficiency above 78%. The aperture angles (that correspond to a maximum gain factor) of the above examples were about 10 degrees too low for the majority of commercial dishes.

Future work on these designs should involve geometry modifications to fit the H-plane radiation pattern to the prime focus feed requirements. In addition, the bandwidth and input impedance of the structure must be determined. The bandwidth will be limited by the gap size between the ground plane and the circular disk. A wide bandwidth (via a large gap) or the use of dual operating frequencies should be investigated. The input impedance is believed to vary with respect to dipole locations. This holds true for microstrip disk patches. Consequently, it should not be a difficult task to match the antenna. Finding an alternate means of exciting the antenna with a single dipole feed was briefly investigated to increase the ease of manufacturing and reduce the cost. It was found that the single dipole feed performance was comparable to its dual dipole counterpart, but

further work in this area was required to substantiate and optimize the findings.

In summary, the IGAD-ROT2 package has shown it can effectively lessen the time and knowledge needed to produce quality antenna designs. This system was used to produce a unique paraboloid antenna feed. Unfortunately the design modifications performed failed to produce field patterns that matched those of established prime focus feeds.

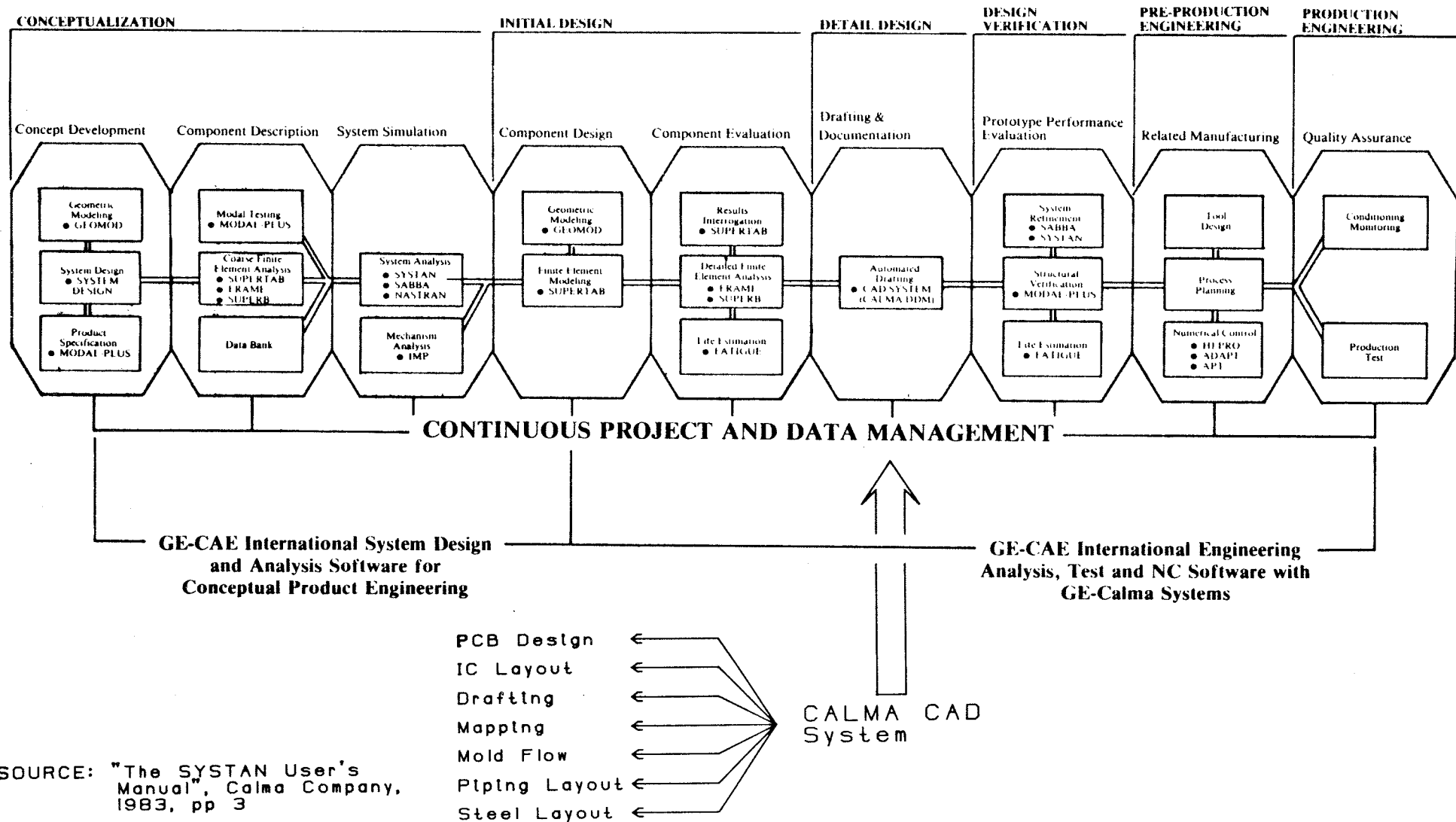
REFERENCES

- 1) Rydahl, O., "ROT2 User Guide," Electromagnetics Institute, Denmark, 1974, pp 1-10
- 2) Burke G. J., A. J. Poggio, "NEC Users Guide," Naval Ocean System Centre, San Diego, California, 1977
- 3) Jorgensen, R., "Manual for COBRA Synthesis," 1982
- 4) Gott, B., "Why can't we manage CAD," Mechanical Engineering Conference Publication, 1980, pp 1-7
- 5) Greene, E.F., "Why not Interactive Graphics for PCB Design," Autofac IV Proceedings, pp 268-270
- 6) "User Manual for SYSTAN," General Electric - CAE International, 1983, pp 3
- 7) "DAL Users Manual," Calma Company, 1983
- 8) "System Reference Manual for DDM and Dimension III," Calma Company, 1983
- 9) "DDM and Dimension III Guide to DAL/Fortran," Calma Company, 1983
- 10) Rydahl, O., "Scattering from Small Bodies," Master's Thesis, Electromagnetics Institute, Copenhagen, Denmark, 1974, pp 1-5, 43-47
- 11) Ludwig, A.C., "The Definition of Cross-Polarization", IEEE Trans. Antennas and Propag., Vol. AP21, pp. 116-119, 1973
- 12) Balanis C., "Antenna Theory Analysis and Design", pp 608-631
- 13) Jansky, K.G., "Electrical Disturbances Apparently of Extraterrestrial Origin," Proc. IRE, Vol. 21(10), 1933, pp 1387-1388
- 14) Reber, G., "Cosmic Static," Astrophys. Journal, Vol. 100(3), pp 279-287
- 15) Cutler, C.C., "Parabola Antenna Design for Microwaves," Proc. IRE, Vol. 35(11), 1947, pp 1284-1294
- 16) Jones, E.M.T., "Paraboloid Reflector and Hyperboloidal Lens," Trans. on Antennas and Propagat., Vol. ap-2(4), 1954, pp 119-127

- 17) Potter, P.D., "A New Horn Antenna with Suppressed Sidelobes and Equal Beamwidths," Microwave Journal, Vol. 6(6), 1963, pp 71-78
- 18) Potter, P.D. and A.C. Ludwig, "Beamshaping by Higher Order Modes in Conical Horns," NEREM record 1963, Vol. 5, pp 92-93, Northeast Electronics Research and Engineer Meeting, Boston, Mass.
- 19) Minnet H.C. and B.MacA. Thomas, "A Method of Synthesizing Radiation Patterns with Axial Symmetry," IEEE Trans. Antennas and Propagat., Vol. AP-14(5), 1966, pp 654-656
- 20) Kay A.F., "The Scalar Feed," AFCRL Report No. 64-347 (AD No. 601609), 42 pp., Air Force Cambridge Research Laboratories, Hanscom AFB, Mass.
- 21) Kishk, A.A., "Design and Investigation of Simple Prime Focus Feeds For Paraboloid Reflectors," MSc. Thesis, Dept of Electrical Eng., University of Manitoba, 1983, pp 53-91
- 22) Watkins, J., "Circular Resonant Structures in Microstrip," Electron. Lett., vol 5, 1969, pp 524-525
- 23) Long, S.A., L.C. Shen and P.B. Morel, "Theory of the Circular Disc Printed-Circuit Antenna," Proc. IEE, Vol. 125, 1978, pp 925-928
- 24) Derneryd, A.G., "Analysis of the Microstrip Disk Antenna Element," IEEE Trans. on Antennas and Propagat., Vol. AP-27, 1979, pp. 660-664
- 25) Carver, K.R. and E.L. Coffey, "Theoretical Investigation of the Microstrip Antenna," Technical Report PT-00929, Physical Science Laboratory, New Mexico State University, Las Cruces (New Mexico), Jan. 1979
- 26) Bahl, I.J and P. Bartia, "Microstrip Antennas", Artech House, 198?, pp 85-106

Appendix A

GE ENGINEERING SYSTEM



SOURCE: "The SYSTAN User's Manual", Calma Company, 1983, pp 3

APPENDIX B - LIST OF IGAD-ROT2 SUBROUTINES

Program Name	Program Description
CONSTRUCTION MODE SUBROUTINES	
CORRUG.DA	- Corrugated horn command.
CREDIP.DA	- Constructs a dipole on the graphics screen and stores the data as a text-data item.
CREFFI.DA	- Stores far field calculation parameters as a text data item.
CREGEOM.DA	- Controls the creation of geometry contours.
CYLADD.DA	- Retrieves information required to create a cylinder.
CYLMOD.DA	- Cylinder modification routine.
CYLPRP.DA	- Creates a cylinder perpendicular to an existing one.
DEV.DA	- Retrieves contour deviation parameters
DIP.DA	- Dipole creation command.
DSKADD.DA	- Retrieves information required to create a disk.
DSKMOD.DA	- Disk modification routine.
ELIADD.DA	- Retrieves information required to create a ellipsoid.
FFI.DA	- Determines the far field calculation parameters (with and without near field approximations)
GEODAT.DA	- Returns data associated with a contour selected by the user.
GEOM.DA	- Controlling program for contour addition, deletion and modification.
HYPADD.DA	- Retrieves information required to create a hyperboloid.
LISTFL.DA	- Lists on alpha-numeric screen the parameters associated with one far field calculation.

- MON.DA - Monopole creation command.
- PARADD.DA - Retrieves information required to create a paraboloid.
- PERMDIP.DA - Displays a dipole on the graphics screen.
- PERMCYL.DA - Displays cylinder on the graphics screen.
- PERMDSK.DA - Displays disk on the graphics screen.
- PERMELI.DA - Displays ellipsoid on the graphics screen.
- PERMHYP.DA - Displays hyperboloid on the graphics screen.
- PERMMON.DA - Displays a monopole on the graphics screen.
- PERMPAR.DA - Displays paraboloid on the graphics screen.
- PERMSPH.DA - Displays sphere section on the graphics screen.
- PLW.DA - Plane-wave creation command.
- REXEC.DA - Translation program. Converts data stored as command text-data items into ROT2 input program.
- SPHADD.DA - Retrieves information required to create a sphere.

PLOT MODE SUBROUTINES

- AXIS.DA - Creates plot axes, includes hash marks and labels.
- DRAW.DA - Sets up the drawing mode to enable paper plots of the radiation characteristics and antenna geometry.
- GENOTE.DA - Write text notes (called general notes) on the graphics screen.
- GRAPH.DA - Sets up graph parameters and plots the scaled radiation data on the graphics screen.
- PLOT2.DA - Retrieves all plot information from user (including plot type) and scales data.
- RLINE.DA - Draws the plot line on the graphics screen.
- SCALE1.DA - Scales on set of plot data.
- SCALE2.DA - Scales two sets of plot data simultaneously.

SLOSWTCH.DA - Toggles between the plot and construction screen layouts.

DRAWING MODE SUBROUTINES

DRAWMOD.DA - Handles drawing creation functions.

HPPLOT.DA - Submits a drawing to the HP plotter.

PLTDRAW.DA - Maintains drawing and window editing functions.

GENERAL FUNCTION SUBROUTINES

EXIT.DA - Exits IGAD-ROT2 back to DDM.

IGADROT2.DA - Initializes the IGAD-ROT2 package.

GETGLIST.DA - Retrieves the working submodel numbers and the construction submodel (the model displayed on the screen).

LOAD.DA - Loads a new or existing antenna model.

NEW.DA - Adds new submodels (up to 10 in total) to existing antenna model(s).

SAVE.DA - Saves the current antenna model.

MODEL DISPLAY SUBROUTINES

GNUMOD.DA - Alters the current geometry, incident field and calculation identification numbers.

COLR.DA - Alters the color of subsequently created geometry

GRID.DA - Adds, deletes, or alters the screen grid

RPT - The DAL function Repaint (refreshes the graphics screen)

VERF.DA - Displays command parameters associated with an item of geometry.

ZOM.DA - Magnifies the display to the model extents, performs zoom in and zoom out functions.

DIMENSIONING/TEXT SUBROUTINES

- ACC.DA - Alters the number of decimal places displayed in dimensioning text.
- BDH - DAL function Base Line Dimension Horizontal
- BDP - DAL function Base Line Dimension Parallel
- BDV - DAL function Base Line Dimension Vertical
- DMH - DAL function Dimension Horizontal
- DMP - DAL function Dimension Parallel
- DMV - DAL function Dimension Vertical
- DAL - DAL function Dimension Angular
- PIC - DAL function Picture (turns on 2-d picture mode in the selected viewport)
- TED - DAL function Text Edit (allows editing of screen general notes)

DAL/FORTRAN SUBROUTINES

- UCMPLST.FOR - Compare two lists.
- UCPOL.FOR - Calculate cross and co-polar field data.
- UDDFIT.FOR - Scale data to fit within plot axes.
- UDHPTLST.FOR - Create point list for a rectangular plot.
- UDLOGX.FOR - Convert input array to logarithms.
- UDNORM.FOR - Normalize input array to specified value.
- UDRPTLST.FOR - Create a point list for a radial plot (note this has not been integrated with graphic software yet).
- UDSCALE.FOR - Inspects input array and returns maximum and minimum values.
- UDTMAX.FOR - Truncate input array to given maximum.
- UDTMIN.FOR - Truncate input array to given minimum.
- UGAIN.FOR - Calculate gain parameters for ideal paraboloid reflector feed.
- UGETD.FOR - Retrieve plot data from ROT2 data file (VMS) and pass to DAL antenna model.

NOTE - Some of the routines listed above were developed in conjunction with or by Gordon Neilson - an Electrical Engineer at the University of Manitoba.

APPENDIX C - CALCULATION OF THE PARABOLOID APERTURE EFFICIENCIES

The formulations used to calculate the spillover and illumination efficiencies are given below:

$$\eta_s = \frac{\int_0^{\theta_0} G_f(\theta) \sin\theta \cdot d\theta}{\int_0^{\pi} G_f(\theta) \sin\theta \cdot d\theta} \quad (\text{B-1})$$

$$\eta_I = 32 \left(\frac{f}{d} \right)^2 \frac{\left| \int_0^{\theta_0} \sqrt{G_f(\theta)} \tan\left(\frac{\theta}{2}\right) d\theta \right|^2}{\int_0^{\theta_0} G_f(\theta) \sin\theta \cdot d\theta} \quad (\text{B-2})$$